INFSO-ICT-247733 EARTH

Deliverable D4.2

Green Radio Technologies

Contractual Date of Delivery: December 31, 2011

Actual Date of Delivery: January 30, 2012

Editor(s): Main Editor: Serge Bories (CEA), Chapter Editors: Jean-Marie Retrouvey (NXPFR), Björn Debaillie (IMEC), Custódio Peixeiro (IST), Rodolfo Torrea(IMEC), Anton Ambrosy (ALUD), Mona Hashemi (EAB), Sven Pettersson(EAB), Jouko Leinonen (UOULU)

Author(s): Dieter Ferling, Anton Ambrosy (ALUD), Sven Petersson, Mona Hashemi, Per Burström (EAB), Aykut Erdem, Philippe Maugars, Jean-Marie Retrouvey (NXPFR) , Shinji Mizuta, Guido Dietl (DOCOMO), Mauro Boldi (TI), Alexandre Giry, Serge Bories (CEA), Björn Debaillie, Rodolfo Torrea (IMEC), Filipe Cardoso, Custódio Peixeiro (IST), Jouko Leinonen (UOULU), Yolanda Fernandez (TTI)

Participant(s): ALUD, NXPFR, TI, CEA, IMEC, TTI, DOCOMO, UOULU, EAB, IST

Work package: WP4

Estimated person months: 60 PM

Security: Public

Version: 1.0

Keyword list: Mobile communications, ecological impact, Green Radios, energy efficiency, radio node, base station, MIMO, macro-cell, small-cell, beamforming, radio interface technologies, transceiver components, power saving, adaptability.

Abstract:

This deliverable is an intermediate report on energy efficiency improvements expected on base stations radio technologies due to the energy efficiency enablers selected for the project as the most promising tracks. These results are achieved by innovative solutions on radio transmission techniques, on hardware components, and their combination through adequate interface techniques, with contribution from all WP4 tasks. Concepts, solutions and expected results are analysed in terms of energy efficiency potential and adaptability to dynamic systems for macro- and small-cells. Moreover, each solution is analyzed for specific deployment scenarios, operating conditions, optimization time scale, and traffic load. Thereby, these technology bricks associated with their operating conditions will be exploited to build and evaluate the "Integrated Solutions" which provide the global results of the project.

Authors

Partner	Name	Email and Phone
Alcatel-Lucent Deutschland AG (ALUD)	Dieter FERLING Anton AMBROSY	dieter.ferling@alcatel-lucent.com +49 711 82142992 anton.ambrosy@alcatel-lucent.com +49 711 82145631
Ericsson AB (EAB)	Sven PETERSSON Per BURSTRÖM Mona HASHEMI	sven.petersson@ericsson.com +46 10 71 23583 per.burstrom@ericsson.com +46 10 71 44556 mona.hashemi@ericsson.com +46 10 71 39107
NXP Semiconductors France (NXPFR)	Aykut ERDEM Philippe MAUGARS Jean-Marie RETROUVEY	aykut.erdem@nxp.com +33 2 31 45 63 96 philippe.maugars@nxp.com +33 2 31 45 64 67 jean-marie.retrouvey@nxp.com +33 2 31 45 64 13
DOCOMO Communications Laboratories Europe GmbH (DOCOMO)	Shinji MIZUTA Guido DIETL	mizuta@docomolab-euro.com +49 89 56824 229 dietl@docomolab-euro.com +49 89 56824 245
Telecom Italia S.p.A. (TI)	Mauro BOLDI	mauro.boldi@telecomitalia.it +390112287771
Commissariat à l'Energie Atomique (CEA)	Alexandre GIRY Serge BORIES	alexandre.giry@cea.fr +33438783965 serge.bories@cea.fr +33 4387851863
Interuniversitair Micro-Electronica Centrum vzw (IMEC)	Björn DEBAILLIE Rodolfo TORREA	debailli@imec.be +3216281851 torrea@imec.be +32 16288220
Instituto Superior Tecnico (IST)	Filipe CARDOSO Custódio PEIXEIRO	filipe.cardoso@estsetubal.ips.pt +351265790000 custodio.peixeiro@lx.it.pt +351 218 418 478
University of UOULU (UOULU)	Jouko LEINONEN	jouko@ee.oulu.fi +358 8 553 2968

Partner	Name	Email and Phone
TTI Norte, SL (TTI)	Yolanda FERNANDEZ	yfernandez@ttinorte.es +34 942 29 12 12

Executive Summary

This deliverable “Green Radio Technologies” presents the intermediate results on energy efficiency improvements provided by the different green radio technologies selected as most promising tracks in the EARTH project. All these radio technologies are focused on base station (BS) applications for 4G broadband cellular networks (LTE). The proposed solutions deal with several domains like hardware components and equipment, radio transmission techniques (including multiple antenna techniques) and adequate interface technologies. Each of them is quantitatively analysed in terms of energy efficiency potential and/or adaptability to dynamic systems for macro- and small-cells. Consequently, each result is analyzed for specific deployment scenario, operating condition, optimization time scale and traffic load.

The first three proposed solutions investigate the BS radio equipment aspects. A distinction is done between components for macro-cell and small-cell BS depending on their respective contribution to the power consumption. For macro-cell BS, the application of a signal load adaptive transceiver achieves significant energy savings for medium and low loads according to the optimization of operating points and the deactivation of certain components. For small-cell BS, all the components from baseband engine to antenna interface have been designed and optimized to be energy efficient and/or energy flexible. Concerning the printed antenna array BS equipment, the use of a low loss foam substrate is studied for improving energy efficiency.

A second group of solutions deals with radio interface technologies that exploit the interaction between higher protocol layers and the hardware to improve the energy efficiency. The adaptability to system dynamics solution allows selecting the most power-efficient modulation as a function of the fast changing channel quality. Discontinuous transmission, bandwidth adaptation, and their combination show important energy savings according to the studied scenario.

The last group of radio technologies deals with multiple antennas solutions. By controlling the radiation pattern and so the spatial filter, beamforming active antennas can focus the energy in the direction of interest. MIMO solutions exploiting the channel properties to improve the throughput are investigated from an energy efficiency point of view.

The presentation of each radio technology details the motivation, the solution concept, the expected benefits and its positive or negative impact on other EARTH project solutions. Thereby, these technology bricks associated with their operating conditions will be exploited to build and evaluate the “Integrated Solutions” which provide the global results of the project.

Table of Contents

List of Figures

List of Tables

Acronyms and Abbreviations

AA	Active Antenna
AMC	Adaptive Modulation and Coding
ANT	Antenna
ASIP	Application Specific Instruction Processors
BAW	Bulk Acoustic Wave filter
BCH	Broadcast Channel
BB	Baseband
BS	Base Station
CDF	Cumulative Distribution Function
CoMP	Coordinated Multi-Point
CQI	Channel Quality Indicator
CSI	Channel State Information
CSRS	Cell Specific Reference Signal
DC	Direct Current
DL	Downlink
DoA	Direction of Arrival
DPD	Digital Pre Distortion
DTX	Discontinuous Transmission
E^3F	Energy Efficiency Evaluation Framework
EARTH	Energy Aware Radio and neTwork tecHnologies
ECI	Energy Consumption Index
EDF	Earliest Deadline First
EE	Energy Efficiency
EIRP	Equivalent Isotropic Radiated Power
EPA	Extended Pedestrian A
ETU	Extended Typical Urban
EVA	Extended Vehicular A
EVM	Error Vector Magnitude
FAMUP	Frequency Adaptive Multi-User Priority
FDD	Frequency Division Duplexing
FDPS	Frequency Dependent Packet Scheduling
FBAR	Film Bulk Acoustic Resonator
FPGA	Field Programmable Gate Array
GPIO	General Purpose Input/Output
GSM	Global System for Mobile communications
HARQ	Hybrid Automatic Repeat Request
HSPA	High Speed Packet Access
IQ	Real and Imaginary
LNA	Low Noise Amplifier
LTE	Long Term Evolution
MCS	Modulation and Coding Scheme
MCI	Maximum Channel to Interference ratio
MIMO	Multiple-Input-Multiple-Output
MN	Matching Network
NACK	Negative ACKnowledge
OFDMA	Orthogonal Frequency Division Multiple Access
PA	Power Amplifier

PAPR	Peak-to-Average Power Ratio
PBCH	Physical Broadcast CHannel
PDCCH	Physical Downlink Control Channel
PER	Packet Error Rate
PMI	Precoding Matrix Indicator
PF	Proportional Fair
PHY	PHYsical
PRB	Physical Resource Block
PSS	Primary Synchronization Signals
RAN	Radio Access Network
RF	Radio Frequency
RI	Rank Indicator
RoF	Radio over Fiber
Rx	Receive
QoS	Quality-of-Service
SAW	Surface Acoustic Wave filter
SDM	Spatial Division Multiplexing
SiNAD	Signal-to-Noise And Distortion ratio
SINR	Signal-to-Interference-plus-Noise Ratio
SOTA	State-Of-The-Art
SPI	Serial Peripheral Interface Bus
SRS	Sounding Reference Signal
SS	Small Signal
SSS	Secondary Synchronization Signals
SU	Single User
TDD	Time Division Duplexing
TRX	Transceiver
Tx	Transmit
UE	User Equipment
UL	UpLink
UMa	Urban Macro
UMi	Urban Micro
VM	Vector Modulator

1. INTRODUCTION

The EARTH project aims to address the global environmental challenge by investigating and proposing effective mechanisms to drastically reduce energy consumption of mobile broadband communication systems by a factor of at least 50% compared with the current ones, without compromising users' perceived quality of service and system capacity [EARTH-Leaf].

Most of the equipment of the current systems have static configuration that can support the maximum traffic load. However it has been shown [EARTH-D2.3] that in average the equipment is operating significantly below their full capacity, leading to a significant potential on reducing the power consumption for medium and low traffic load periods. 'Adaptability' is the key concept met in most of the solutions for Green Radios presented in this document. This means that hardware or software solutions can decide and adjust their configuration from external data in order to improve their energy efficiency. Consequently the analysis of the track performances may become more complex while it depends on the traffic load, the channel quality, the end-users density or their angular direction, or component impedance load. Each of the proposed adaptive solutions acts with different time scale that ranges from milliseconds to months.

This document contains the intermediate results on energy efficiency improvements provided by the different green radio technologies selected as "Most Promising Tracks" in the EARTH project. All these radio technologies focus on the base station for 4G broadband cellular network (LTE). The proposed solutions deal with several domains like hardware components and equipment, radio transmission or adequate interface technologies and multiple antennas techniques. But all of them are quantitatively analysed as regards their energy efficiency potentials and/or their adaptability to dynamic systems for macro- and small-cell base stations. Consequently for each solution, the areas of application and application conditions are depicted according to deployment scenarios, optimization time scale and traffic load.

A first group of solutions investigate the BS radio equipment aspects. A distinction is done between components for macro-cell and small-cell BS due to the different origins and their relative weight of power consumption. For macro-cell BS, the application of a signal load adaptive transceiver achieves significant energy saving for medium and low loads according to the optimization of operating points and the deactivation of certain components. For small cell BS, all the components from baseband engine to antenna interface have been designed and optimized to be energy efficient and/or energy flexible. Considering the printed antenna array BS equipment, the use of a low loss foam substrate is studied for improving energy efficiency.

A second group of solutions deals with radio interface technologies that exploit the interaction between higher protocol layers and the hardware to improve the energy efficiency. The adaptability to system dynamics solution allows selecting the less consuming modulation as regard the fast changing channel quality. Bandwidth adaptation, discontinuous transmission and their combination show important energy savings according to the studied scenario.

The last group of radio technologies concerns the multiple antennas solutions. By controlling the radiation pattern and so the spatial filter, the beamforming in active antenna can focus the energy only where needed. The MIMO solutions that use the channel properties to support high throughput, are investigated from an energy efficiency point of view.

Each presented radio technology is structured to express the motivation, the solution concept, the expected benefits and its positive or negative impact on other EARTH solutions. Thereby these results are clearly associated with their applications scenario and conditions to be used for identifying the "Integrated Solution" [EARTH-D6.2b].

2. TRANSCEIVERS FOR MACRO-CELL BASE STATIONS

The power consumed by macro-cell base stations shows a continuously decrease due to the technological evolution observed over the years and due to the aim of minimizing the power consumption for maximum signal load (instantaneous level of the transmitted signal related to the maximum RF output power defined for transmission). But there is additional potential on power reduction due to non-uniform load distribution over the day and due to short-term characteristics of transmitted signals.

The significant traffic load variation is shown in FIGURE 1. It is based on 15 minutes average and is part of the reference scenario defined in the project [EARTH-D2.3] for performance evaluations. The maximum traffic load values in the evening hours differ due to the deployment achieving for example 60% in dense urban or only 30% in suburban scenarios. This shows that in average the equipment is operating significantly below its capacity leading to a huge potential on reducing the power consumption.

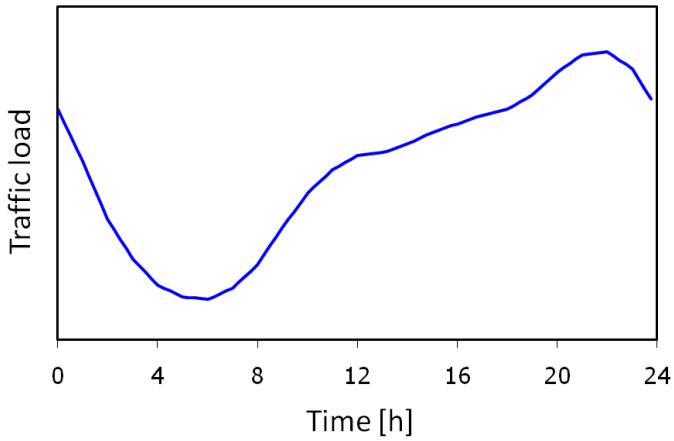

FIGURE 1. 24 hours traffic load profile.

In the EARTH project, LTE signals are considered as reference for defining concepts and solutions to increase the energy efficiency in wireless mobile communication systems. The short-term characteristic of LTE signals show time slots of data transmission at maximum (100%) signal load or even at lower signal level (FIGURE 2). During data transmission, user information and physical signals and channels (CSRS, PSS, SSS and BCH) are scheduled. In time slots of no data, only signalling (physical signals and channels) is transmitted consisting by symbols of different levels below 100% (i.e. 27% for CSRS-BCH, 17% for CSRS only, and 12% for PSS|SSS signals or BCH channel, in 10MHz configuration) and even empty symbols (0% signal load). Their level depends on the bandwidth configuration.

In particular, LTE standard enables high reductions in the DC consumption according to the presented frame structure. The empty symbols open the opportunity of deactivating components in the equipment during these short time slots providing a certain reduction of the power consumed during operation. The different signal levels below 100% gives the possibility of applying a further solution to reduce the power consumption by adapting the operating points of some components for optimizing the energy efficiency.

In macro-cell base stations the transceiver and especially the power amplifier are the components with the largest power consumption showing their maximum power efficiency at 100% signal level which is decreasing significantly with the decrease of the instantaneous signal level respectively the average traffic load.

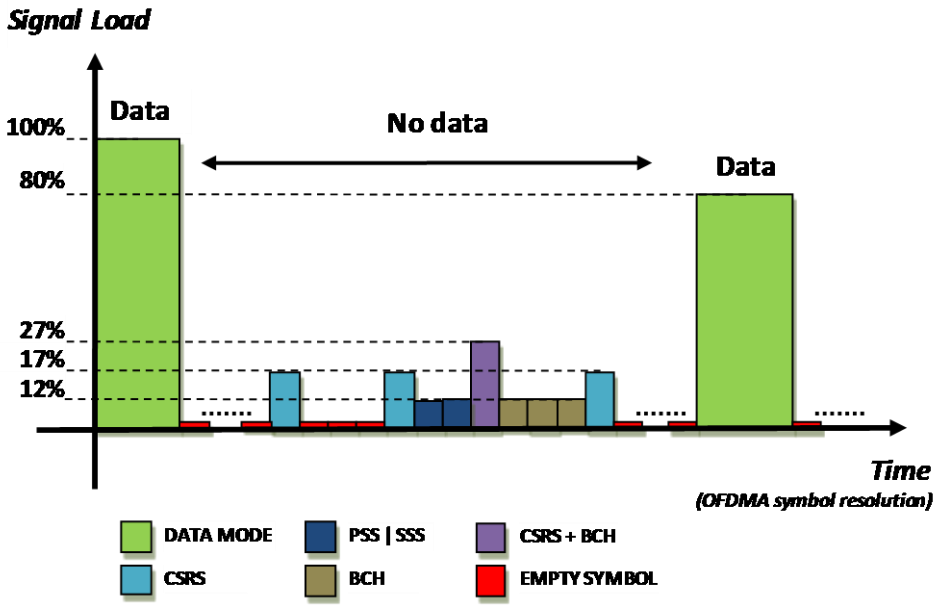

FIGURE 2. Relative RF output power level according to the LTE frame structure.

For exploiting the potential to reduce the power consumed in low and medium load situation, new techniques for reducing the energy consumption have been defined and evaluated for different transceiver components. Such solutions acting at component level show key features of power efficient transceiver systems [FeBBWP10], and can be used for different wireless standards by applying them in specific ways. They take benefit from the signal characteristics described above and are presented in the following sections.

2.1. SIGNAL LOAD ADAPTIVE TRANSCEIVER SYSTEM FOR MACRO BASE STATION

The new techniques for reducing the energy consumption in macro base station transceivers for medium and low load situations are addressing different components proposed for defining the Signal Load Adaptive Transceiver System (SLA-TRX) which integrates the following transceiver blocks:

- The *Digital Signal Processing and Control* (DSPC) unit shows a digital interface to the baseband (BB) for receiving and transmitting BB-signals and a system control interface (SC) to layer 1 and 2 of the base station. The DSPC provides signal processing required to assure the quality of signals to meet the specification (e.g. digital pre-distortion to meet the spectrum emission mask), and control signals (CS) for configuring the analogue components (e.g. to define the RF transmission or reception).
- The *Small Signal RF-TRX* (SS RF-TRX) does the signal conversions between the digital and analogue domains and the frequency conversions between BB and RF frequencies.
- The *Adaptive Energy Efficient Power Amplifier* (AEEPA) amplifies the signal to be transmitted and provides the output power level requested for the sector to be operated.
- The *Adaptive Power Supply Unit* (APSU) delivers the supply voltages and currents required by the TRX system.

FIGURE 3 shows the different transceiver blocks building up the SLA-TRX.

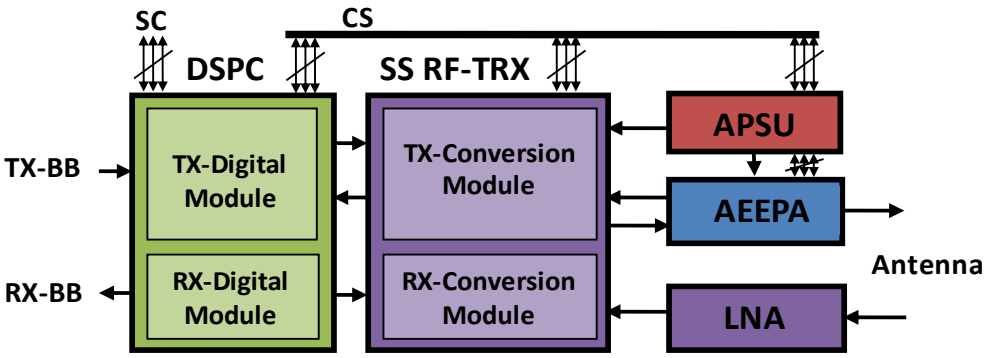

FIGURE 3. Block diagram of a transceiver system for macro-cell base stations

The main concept of the SLA-TRX is to adapt the operation of the analogue hardware components for minimum power consumption in the following way:

- Adjustment of the operating points, basically of power amplifier and power supply unit, when signal loads do not reach the maximum. This feature is called in this document Operating Point Adjustment (OPA).
- Fast deactivation and reactivation of components, specifically the PA and certain blocks of SS RF-TRX, when empty symbols. This feature is called Component Deactivation (CD).

For realising these features, the DSPC block is receiving control signal information from layer 1 and 2 of the BS and is analysing the required characteristics of the BB signals in order to adapt the signal processing and to control the adaptation process of analogue hardware components mentioned above. The appropriate concepts for DSPC, SS RF-TRX, AEEPA and APSU will be defined and presented in the following sections of this document.

The power performance of the SLA-TRX system is defined by a power characteristic showing the consumed power related to the signal load. The comparison of this characteristic with a state-of-the-art characteristic, which does not consider the proposed concepts, will show the benefit on energy consumption for instantaneous operation. The power characteristic serves as input for the power consumption model of the whole BS, and can thus be used for providing a basis to evaluate the impact on energy efficiency on node and on system level as outlined in [EARTH-D2.3].

2.2. DSPC - SOLUTIONS FOR SIGNAL LOAD ADAPTIVE TRANSCEIVERS

The fundamental role or the transmit part in the DSPC (the digital transceiver) is to adapt the signals for transmission to the properties of SS RF-TRX and PA assuring the quality of signals to meet the specifications. Such features are typically signal synthesis for multicarrier applications, digital predistortion (DPD) and crest factor reduction for enabling a higher maximum power efficiency of the PA, and IQ imbalance compensation to support direct frequency conversion architectures. A typical DSPC block is presented in [EARTH-D4.1].

Following the SLA-TRX concept presented above, the DSPC has to provide additional functionality by controlling the component reconfiguration of the other transceiver blocks, by adapting the signal conditioning algorithms to the reconfiguration procedures and by assuring the quality of transmitted signals which can be impacted by imperfections of the reconfigured analogue components.

The main DSPC features required for SLA-TRX are to be included in the signal conditioning and control (SCC) block and are provided basically by three functional blocks (FIGURE 4):

- The sample based signal scan (SBS) executes the required analysis of the received BB signals. The information is used in conjunction with the corresponding layer 1 or 2 information for defining the appropriate action to adapt the transceiver operation to the instantaneous signal load for minimized power consumption. It assures a component reconfiguration synchronized to the signal stream.
- The adaptive clipping (ACLP) adapts the clipping threshold to the signal load. This leads to a reduction of peak values in correlation to the reduced average signal load allowing operating point adaptation of PAs for minimized power consumption.
- The signal quality check (SQC) is analysing the quality of the signal TXS prepared for transmission at the PA output, assuring that the transmitted signals meet the specification.

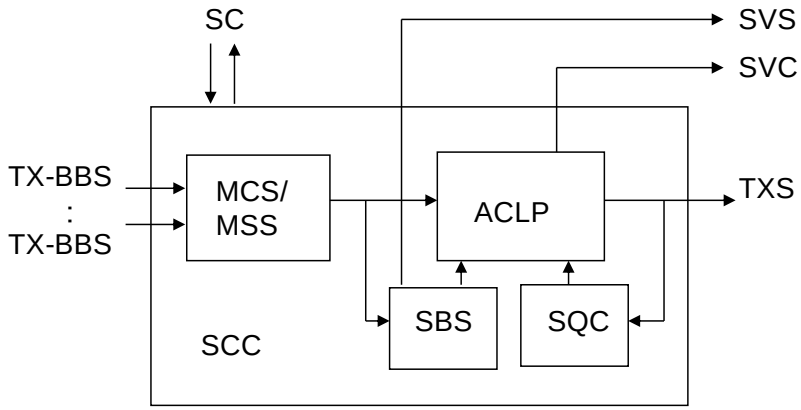

ACLP—Adaptive clipping
BBS—Baseband signal
MCS—Multicarrier signal synthesis
MSS—Multi-standard signal synthesis
PAPR—Peak-to-average power ratio
SBS—Sample based signal scan
SC—System control
SCC—Signal conditioning and control
SQC—Signal quality check
SVC—Supply voltage control
SVS—Supply voltage switch
TX—Transmitter
TXS—Tranmission signal, multicarrier and multi-standard, PAPR reduced (clipped)

FIGURE 4. Architecture of a SCC block of the digital transmit block for SLA-TRX solutions

The DSPC supports the two features defined for energy efficiency optimization in the SLA-TRX: the OPA of analogue components at medium and low signal loads and the CD in time periods without signal transmission.

For enabling the operating point adjustment, following DSPC operations are defined:

- The optimum clipping threshold is determined and applied for minimizing the peak values of the signal. This allows the optimal adjustment of the PA operating point for maximum power efficiency.
- Control information is provided to the components to be adjusted, which defines a set of positions of new operating parameters available for following reconfigurations.
- Reconfiguration signals are transmitted which initiate the reconfiguration, selects the position of the new operating parameters and synchronizes the adaptation procedure with the transmitted signal.

The deactivation of components is managed by the DSPC as following:

- The time periods without signal transmission are determined based on SC information and signal analysing.
- Control information is provided to components designated for deactivation and reactivation.

- Starting signals are transmitted for synchronizing the deactivation or reactivation procedure with the transmitted signal.

For providing the above operations, the DSPC provides control signals to the components designated for adaptation. Their reconfiguration will be executed by the components autonomously. The DSPC utilizes parameters defined by the hardware implementation as time delays and transition slopes to synchronize the adaptation procedures with the signal variation for avoiding an inacceptable impact on the signal quality.

By applying the features proposed for power reduction, some analogue components show discontinuous behaviour during adaptation procedures by changing their parameters for different operating points. As this impacts algorithms running in the DSPC block for mitigation of analogue imperfections, e.g. digital pre-distortion, these algorithms must by adapted for assuring their stable operation.

A significant impact on the signal quality can be caused by a gain variation of the power amplifier when changing the operating point. The gain variation during time slots of LTE symbols, caused by transitions times during OPA, leads to increased noise outside the signal band with the risk for violating the spectrum emission mask. This effect is shown in FIGURE 5 based on simulations with 40 ms LTE signals of 40% traffic load performed for baseband signals. The increase of spectral noise is significant and is violating the spectrum emission mask close to the signal band. For complying with the LTE specifications, a powerful compensation of the gain variation is to be implemented in the DSPC by allowing a residual gain variation in the range of 10%.

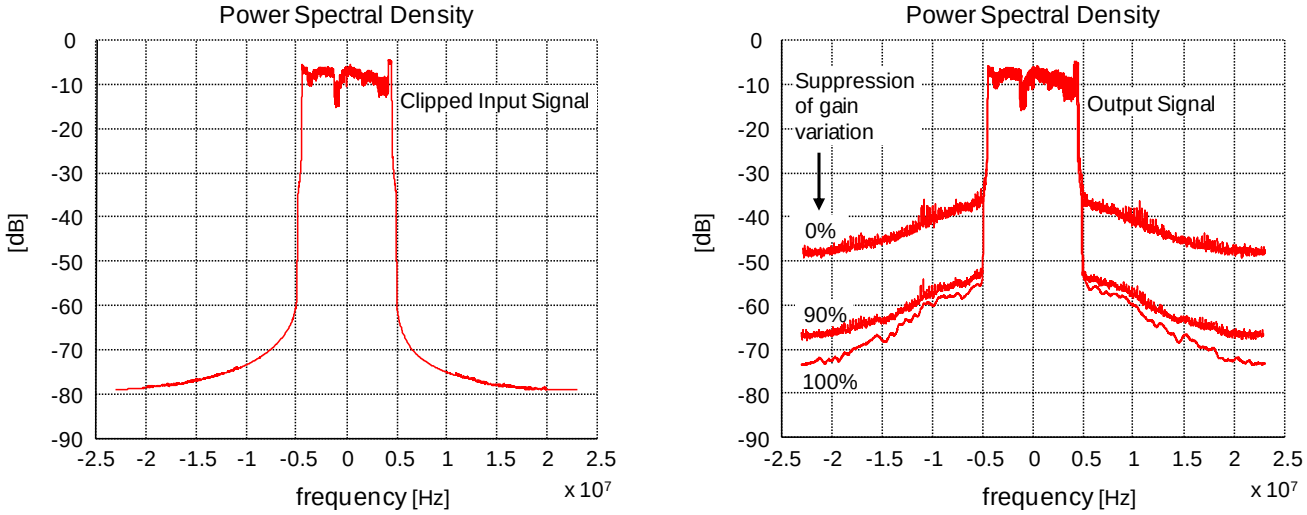

FIGURE 5. Impact on LTE signal spectrum (40 ms; 30% load) after passing the AEEPA

When modifying the PA operating point individually for successive LTE symbols, the gain variation in the transceiver implies a path loss variation for successive symbols in the user equipment leading to increased Error Vector Magnitude (EVM) values which can exceed 10% for the signal received by the mobile equipment. A compensation of these gain variation implemented in the DSPC as mentioned above, will minimize the impact on the EVM in the UE-receiver to acceptable values between 1 and 2%.

The presented DSPC solutions enable the realization of the SLA-TRX. The supported power efficiency improvement is assessed by the SLA-TRX system evaluation and presented in section 2.6

2.3. DUAL POWER MODE SMALL SIGNAL RF TRANSCEIVER

The small signal RF transceiver is composed of two main parts: The dual mode small signal RF transmitter and the receiver.

2.3.1. RECEIVER

The receiver chain amplifies and down converts the aerial signals to the baseband level in order to be processed by the DSPC properly. The most critical design parameters for a receiver, in order to guarantee the quality of service, are the followings:

- Input referred noise figure (NF) performance of the complete receive chain
- Linearity of the complete chain: Input 2nd and 3rd order intercept points (IIP2, IIP3) as well as the input 1dB compression point (ICP1)
- Receiver gain from antenna to the DSPC
- The spectral purity of the local oscillator used for the aerial signal down conversion

A simplified block diagram of the RF receiver designed for the SLA-TRX is depicted below (FIGURE 6). The receive chain has two channel receiver, and each receiver is constituted by a low noise amplifier (LNA) followed by a medium power amplifier (MPA). The amplified signal is filtered out by a band select (system select) filter and then down converted by a high isolation dual mixer having certain level of isolation between the two channels. The required local oscillator (LO) signal for the down conversion mechanism is generated by an onboard LO generator. Once the RF signal is down converted into an intermediate frequency (IF), it is further filtered out by a relatively narrower filter (IF filter) having a pass-band of the baseband signal. The same signal is amplified again by a gain controlled IF amplifier (VGA) followed by the final filtering before transforming the analogue IF signal to the digital domain by a dual ADC.

Having a RF interfacing via SMA connectors at the LNA inputs, the receiver referred in FIGURE 6 can easily be cascaded with additional front-end blocks like additional gain blocks or filters in front in order to get further amplification and/or filtering.

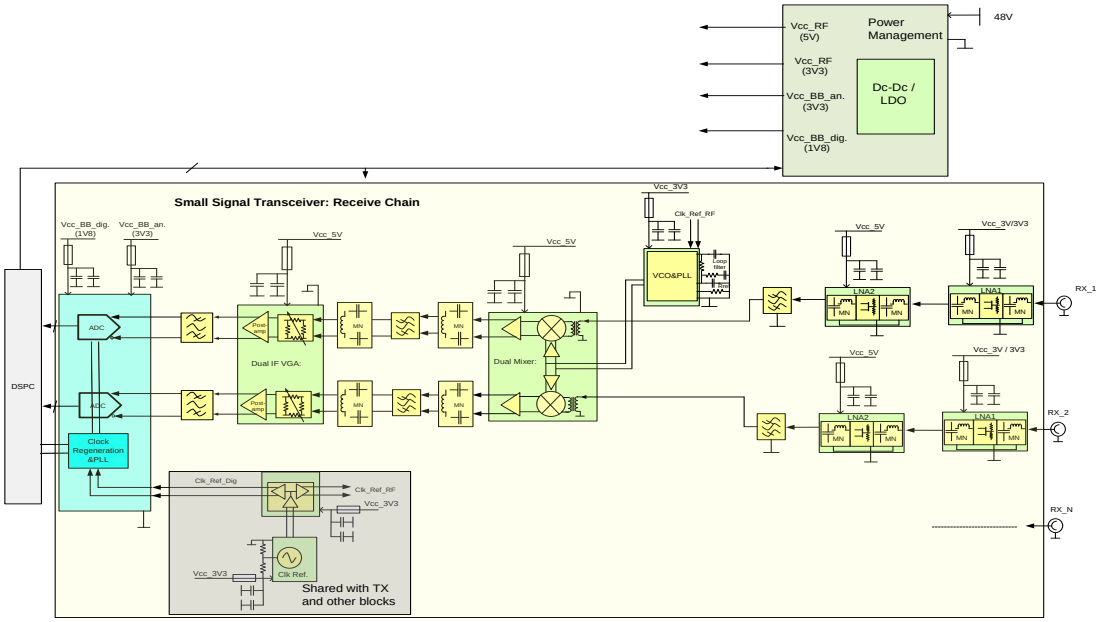

FIGURE 6. Block diagram of the heterodyne receiver proposed for the SLA-TRX

The breakdown of the different parameters of the receiver referred above is given in FIGURE 7. The lab evaluations show the similar results compared to the simplified link budget referred in this figure.

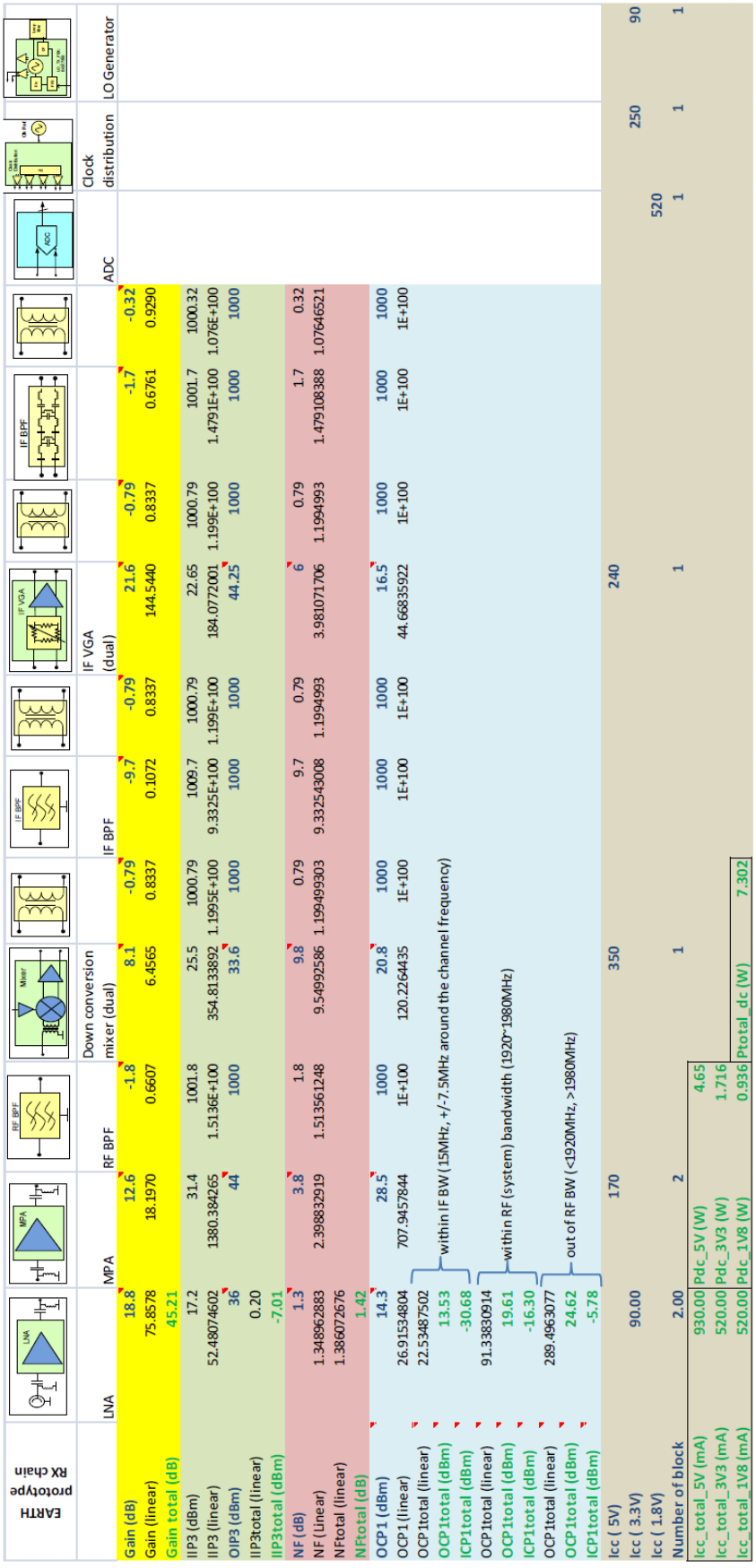

EARTH prototype RX chain	LNA	MPA	RF BPF	Down conversion mixer (dual)	IF BPF	IF VGA (dual)	IF BPF	IF BPF	ADC	Clock distribution	LO Generator
Gain (dB)	18.8	12.6	-1.8	8.1	-0.79	21.6	-0.79	-1.7	-0.32		
Gain (linear)	75.8578	18.1970	0.6607	6.4565	0.8337	144.5440	0.8337	0.6761	0.9290		
Gain total (dB)	45.21										
IIP3 (dBm)	17.2	31.4	1001.8	25.5	1000.79	22.65	1000.79	1001.7	1000.32		
IIP3 (linear)	52.48074602	1380.384265	1.5136E+100	354.8133892	1.1995E+100	184.0772001	1.199E+100	1.4791E+100	1.076E+100		
OIP3 (dBm)	36	44	1000	33.6	1000	44.25	1000	1000	1000		
IIP3total (linear)	0.20										
IIP3total (dBm)	-7.01										
NF (dB)	1.3	3.8	1.8	9.8	0.79	6	0.79	1.7	0.32		
NF (Linear)	1.348962883	2.398832919	1.513561248	9.54992586	1.199499303	3.981071706	1.1994993	1.479108388	1.07646521		
NFtotal (linear)	1.386072676										
NFtotal (dB)	1.42										
OCP1 (dBm)	14.3	28.5	1000	20.8	1000	16.5	1000	1000	1000		
OCP1 (linear)	26.91534804	707.9457844	1E+100	120.2264435	1E+100	44.66835922	1E+100	1E+100	1E+100		
OCP1total (linear)	22.53487502	within IF BW (15MHz, +/-7.5MHz around the channel frequency)									
OCP1total (dBm)	13.53										
ICP1total (dBm)	-30.68										
OCP1total (linear)	91.33830914	within RF (system) bandwidth (1920~1980MHz)									
OCP1total (dBm)	19.61										
ICP1total (dBm)	-16.30										
OCP1total (linear)	289.4963077	out of RF BW (<1920MHz, >1980MHz)									
OCP1total (dBm)	24.62										
ICP1total (dBm)	-5.78										
Icc (5V)		170		350		240				250	90
Icc (3.3V)	90.00								520		
Icc (1.8V)									1	1	1
Number of block	2.00	2		1		1					
Icc_total_5V (mA)	930.00	Pdc_5V (W)	4.65								
Icc_total_3V3 (mA)	520.00	Pdc_3V3 (W)	1.716								
Icc_total_1V8 (mA)	520.00	Pdc_1V8 (W)	0.936	Ptotal_dc (W)	7.302						

FIGURE 7. Performance and DC power consumption partitioning of the receiver

The transfer functions from RF to IF conversion of the receiver referred above can be seen in the figure below:

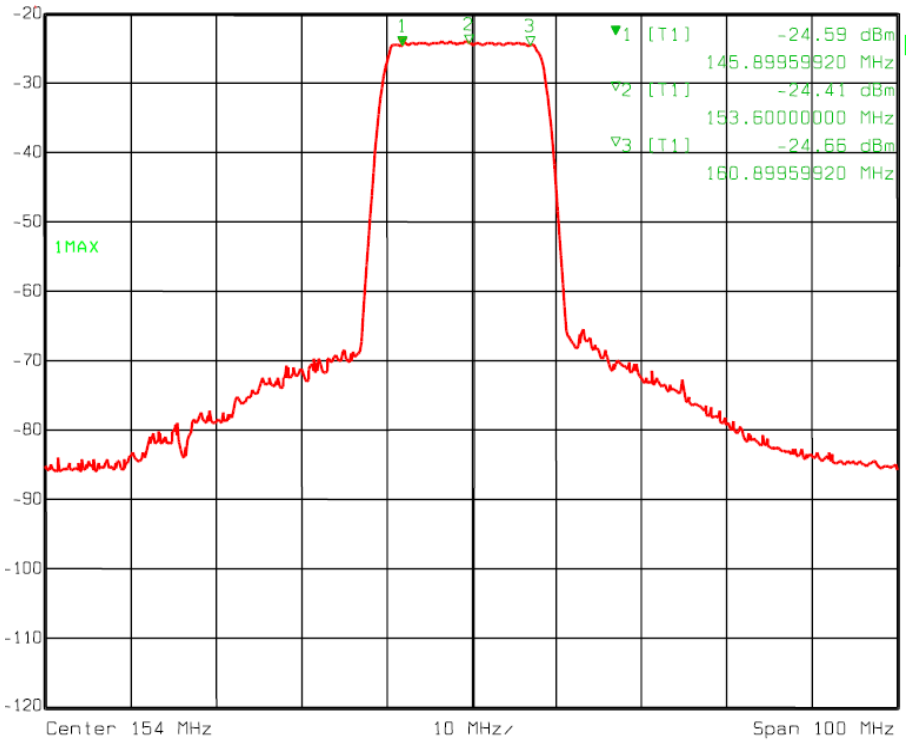

FIGURE 8. Performance of the RF to IF conversion of the receiver

2.3.2. DUAL MODE TRANSMITTER

The main functionality of the small signal transmitter (TX) is to convert the digital baseband signal provided by the DSPC into the modulated RF signal, then to amplify and filter-out the modulated analogue signal in order to drive the power amplifier with an appropriate signal in terms of power level and spectral purity.

Depending on the complete transmit architecture especially related to the linearity versus energy efficiency constraints the small signal implementation can also vary in order to be compatible with this architecture. For instance, the architecture of the small signal transmitter proposed for the SLA-TRX is a part of the digital pre-distortion (DPD) architecture as referred in the DSPC section above. Hence, the feedback path seen at the bottom of the block diagram in FIGURE 9 is designed in order to down-convert the output spectrum of the PA and then to digitize it for the DSPC as monitoring signal for signal conditioning algorithms like DPD.

The transmit path of the small signal chain was designed for the direct-up conversion architecture which converts the digital baseband signal directly to the modulated analogue RF signal centred around the channel frequency without using any intermediate frequency conversion neither in digital domain nor in the analogue domain. This architecture enables an energy saving thanks to the relatively low baseband frequencies to be processed compared to the high IF TX architecture counterpart. For instance, the measurement results show between 100 and 130mA of current reduction for DAC operation with 1.8V supply. However, the direct-up conversion transmitters need some baseband calibrations (differential and quadratic) either in the DSPC side or in the DAC in order to guarantee the required EVM performance defined by standards.

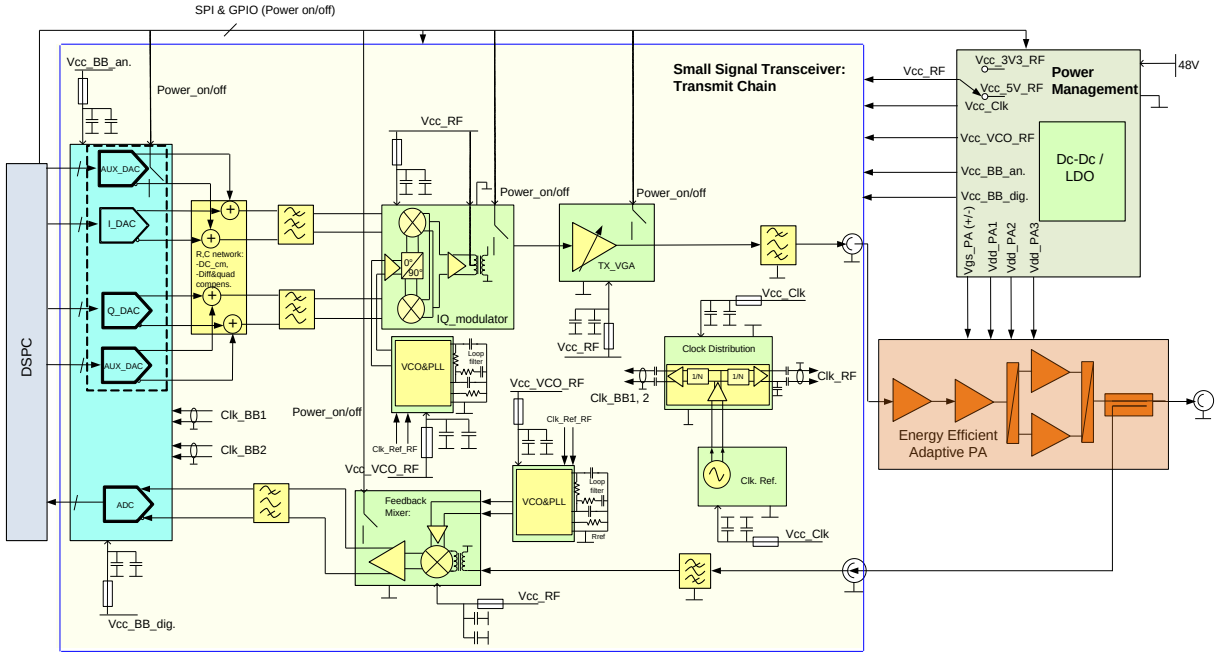

FIGURE 9. Block diagram of the small signal transmitter

Moreover, the small signal transmitter is capable to be configured by the DSPC according to the component control algorithms which enable additional energy saving by deactivating some of the transmitter blocks when there is no symbol to be transmitted. The power consumption breakdown of the dual mode SS transmitter is given in TABLE 1 for macro context.

TABLE 1. Power consumption breakdown for the dual mode small signal transmitter in macro context

	Block Name:	Vcc (V):	Icc_ON (mA):	Pdc (W)_ON	Icc_OFF (mA):
RF	IQ Modulator	5	185	0,925	7
	VGA (single block)	5	115	0,575	15
	VCO&Synth_frwd	3,3	90	0,297	not applicable
	VCO&Synth_fb	3,3	90	0,297	not applicable
	Feedback Mixer	5	200	1	40
Clock	Clock Distributor	3,3	250	0,825	not applicable
Digital Converter	Dual DAC	1,8	640	1,152	not applicable
		3,3	43	0,1419	not applicable
	ADC	1,8	280	0,504	not applicable
Idc and Pdc in ACTIVE mode	Icc_total_5V (mA):	500	Pdc_5V (W):	2,50	**Pdc_total (W):**
	Icc_total_3V3(mA):	473	Pdc_3V3 (W):	1,56	
	Icc_total_1V8 (mA)	920	Pdc_1V8 (W):	1,66	**5,72**
Idc and Pdc in DEACTIVATED mode	Icc_total_5V (mA):	62	Pdc_5V (W):	0,31	**Pdc_total (W):**
	Icc_total_3V3(mA):	473	Pdc_3V3 (W):	1,56	
	Icc_total_1V8 (mA)	920	Pdc_1V8 (W):	1,66	**3,53**

In order to support this feature the small signal blocks intended to be controlled need to be sufficiently fast against the on/off control signals provided by the DSPC as well as having a dedicated on/off control input. FIGURE 10 can be referred in order to see the commutation speed of the parts to be controlled: modulator, TX VGA and the feedback down-conversion mixer.

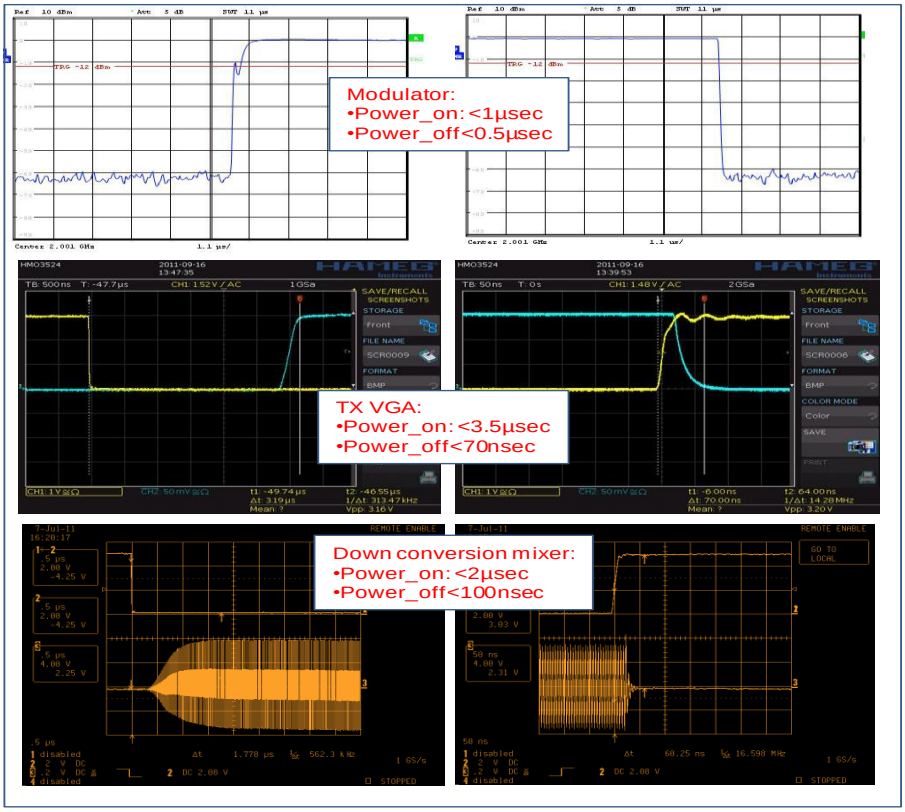

FIGURE 10. Activation and deactivation time of the blocks via ON/OFF control pins.

As presented above (TABLE 1), the Component Deactivation concept applied for the dual power mode small signal transceiver provides around 2.2W of DC power saving compared to SOTA solution, while the reconfiguration can be achieved during time duration shorter than 3.5µs.

2.4. ADAPTIVE ENERGY EFFICIENT POWER AMPLIFIER

An Adaptive Energy Efficient PA has been defined for supporting the key features of the SLA-TRX concept: the Operating Point Adjustment and the Component Deactivation. Both concepts can be applied for the PA to optimize the power consumption depending on traffic load.

In order to evaluate these concepts, an AEEPA has been developed for LTE signals in the frequency band from 2.11 to 2.17 GHz with 40W average output power. The reference case for EARTH project is 2 Tx antennas with 20W output power per antenna. A 3dB loss has been assumed between AEEPA and antennas. The hardware shows different stages:

- The Pre-DRIVER is a module with fixed bias including the CD feature enabling energy saving during empty symbols.
- The DRIVER is a module enabling the OPA and CD features. This stage can be adapted to different RF output power levels depending on the maximum signal load and can be switched off during empty symbols.
- The HPA is a Doherty amplifier including the OPA and CD features as the previous one.

The block diagram of the AEEPA for macro BS is presented in the following figure:

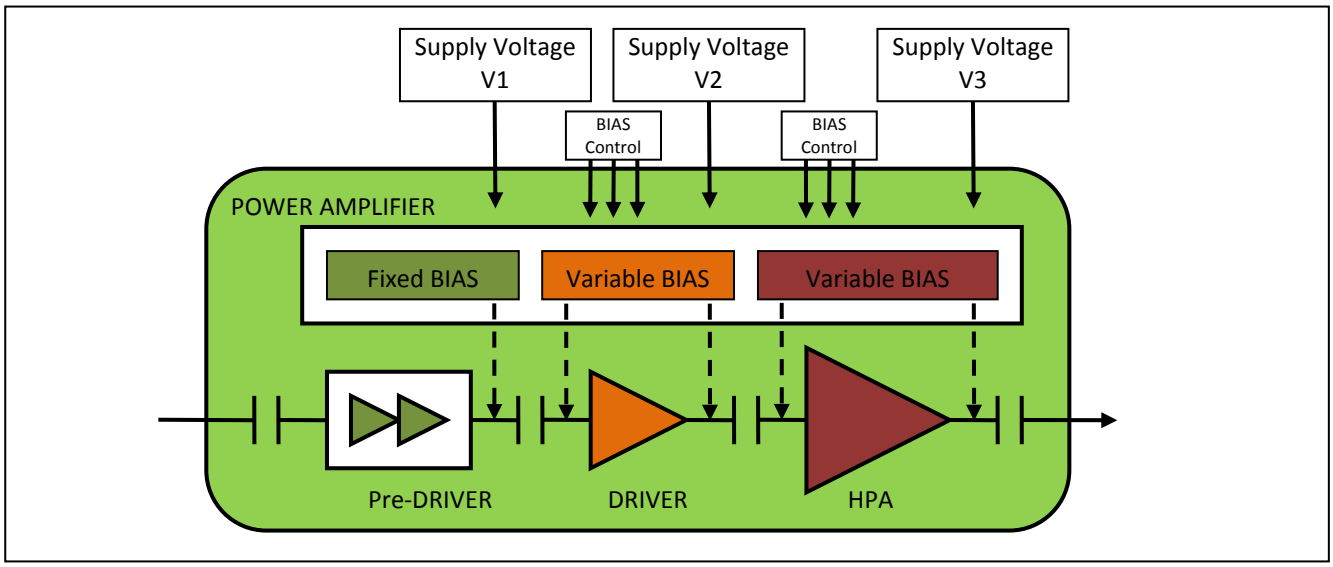

FIGURE 11. Block diagram for Adaptive Energy Efficient PA for macro BS.

The AEEPA hardware for macro BS is composed by three aluminium housings and a heatsink with three fans to control the performance in temperature (see FIGURE 12). There is a housing that integrates the pre-driver and the driver. It contains a RF board and a biasing and control board. The HPA has an individual housing integrating a RF board and two biasing and control boards, one for the carrier amplifier and one for the peak amplifier in a Doherty configuration. The third housing is used for interfacing the PA with DSPC and APSU. All these modules are above a heatsink with three fans to operate the PA at a suitable temperature for maintaining its performance.

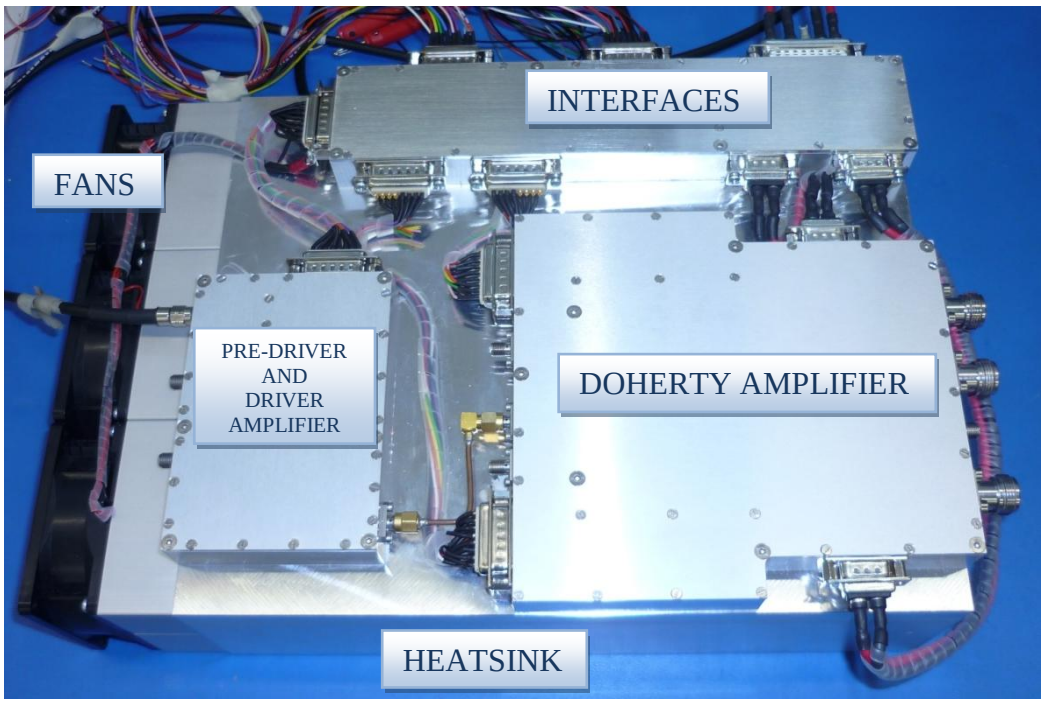

FIGURE 12. Photograph of AEEPA for macro-cell BS.

The hardware prototype has RF and biasing connections with different blocks: DSPC, SS RF-TRX and APSU. A DB15 connector is used to interconnect DSPC and AEEPA. DSPC provides control information aligned to the signal level for adapting the PA output power according to the signal load.

The CD feature is implemented in all PA stages to reduce the energy consumption during empty symbols. This technique allows for suppressing a significant amount of power consumed in the PA. A control signal is to be send from DSPC to the PA for deactivating all three stages when empty symbols occur and a further signal is to be send from DSPC to the PA for reactivating the three stages to normal operation.

The OPA feature in the PA is performed by adjusting the supply voltages in driver and HPA to the maximum required RF output power level, leading to the optimal power efficiency value for the related signal load. This adjustment is controlled by the DSPC, initiating changes in supply voltages of PA and APSU via SPI and GPIO interfaces. This supply voltage adaptation limits the maximum output power level and leads to increased power efficiency for the related signal load.

The AEEPA is connected to the SS RF-TRX using two SMA connectors. The RF output of the SS RF-TRX is connected to the RF input of the PA, while a feedback signal is provided from the PA output via the SS RF-TRX to the DSPC as monitor signal for the signal conditioning algorithms.

Finally, there are two connectors between AEEPA and APSU to provide supply voltages. In the PA, some control signals will be generated and send to the APSU causing the deactivation of the drain voltages for protecting the PA if some deviations are detected in supply voltages and PA temperature range. A sensor is integrated in driver and HPA to control the temperature of the semiconductor components.

The challenge in this development is the transition time when executing the CD and the OP features applied for LTE signals. In the case of AEEPA, an amplifier design requires some capacitors in the supply voltages to avoid oscillations, reduce noise at low frequencies, etc. The value of these capacitors determines directly the transition time to change the biasing point. If the required capacitors are high, the transition time will be high. For achieving a limited transition time duration, these capacitor values must be lowered by maintaining the AEEPA performance.

Furthermore the transition time to adjust the operating point in the AEEPA is connected with the transition time in the APSU for modifying the supply voltages. Therefore a joint optimization of both components is required in order to enable a limited transition time for the OPA feature.

The power performance of the AEEPA has been analyzed by considering the features CD and OPA and presented for 5 operating points in FIGURE 13. The AEEPA allows an unlimited number of operating points, but in the figure below it has been limited to five for a good visibility in the diagram.

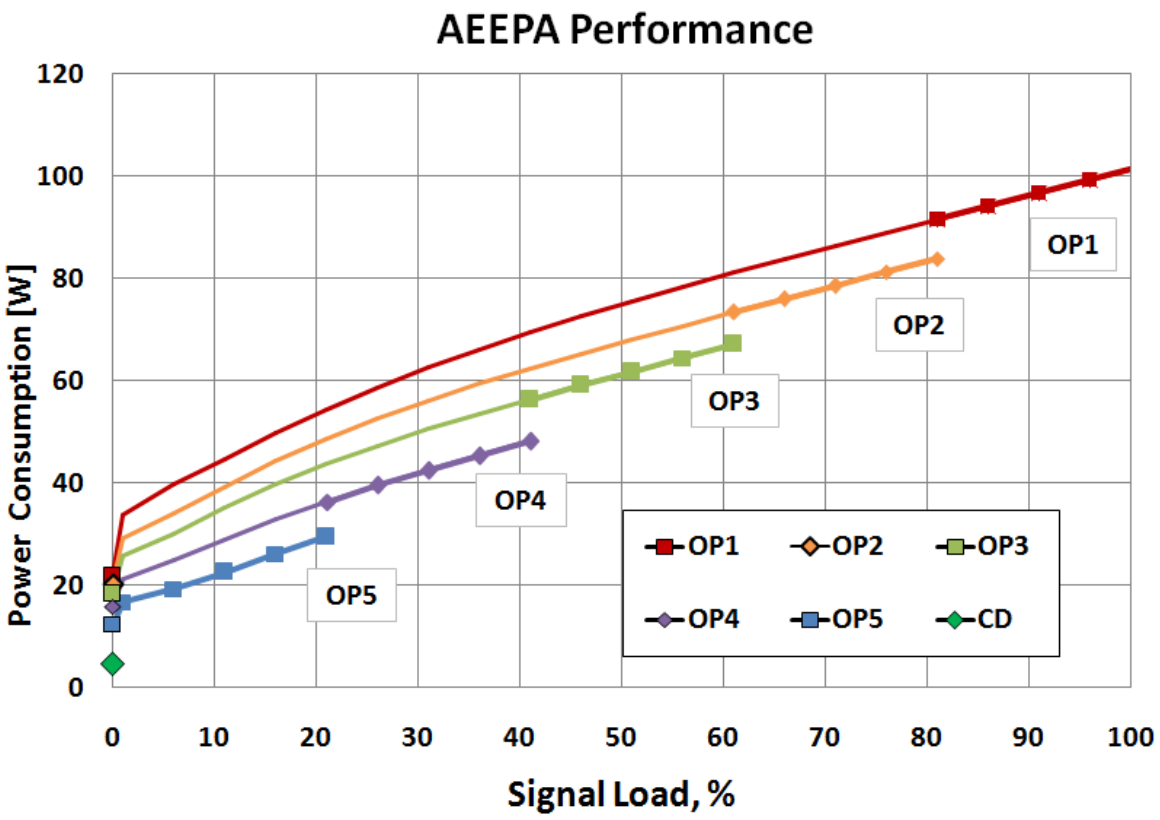

FIGURE 13. Power consumption of a 40W AEEPA.

The energy efficiency performance of the AEEPA is used as input for the energy efficiency performance analysis of the SLA-TRX presented in section 2.6.

2.5. ADAPTIVE POWER SUPPLY UNIT

For the SLA-TRX a specific power supply unit is proposed to adjust the power supply voltage for the PA, supporting the OPA and CD features.

A power supply system has been proposed for the SLA-TRX which includes the specific power supply (APSU) dedicated to the AEEPA together with the power supply units for the SS RF receiver (PSU RX) and for the SS RF transmitter (PSU TX) as presented in FIGURE 14. The APSU block is the block connected to the AEEPA, where power saving solutions are implemented. The APSU contains 4 DC-DC converters to supply several stages of the PA:

- The first block “Stage 1” supplies the pre-driver of the AEEPA, with 5V and 2A max.
- The second and the third blocks “Stage 2” and “Stage 3” supply the driver and the HPA supporting the OPA features. The output supply voltages of the DCDC will be controlled by the DSPC (using fast line switching), and can be adjusted for seven operating points (OP1 to OP7). The corresponding output voltages are defined by the DSPC and communicated to the APSU via SPI. The deactivation of Stage 2 and 3 is possible as well (state OFF). For these stages the highest performance is requested. The transition time between two stages must be very short (between 10 and 100µs), output oscillation must not exceed 10mV, and the circuit have to be very efficient.
- The last stage is the “gate driver” used to supply the AEEPA.

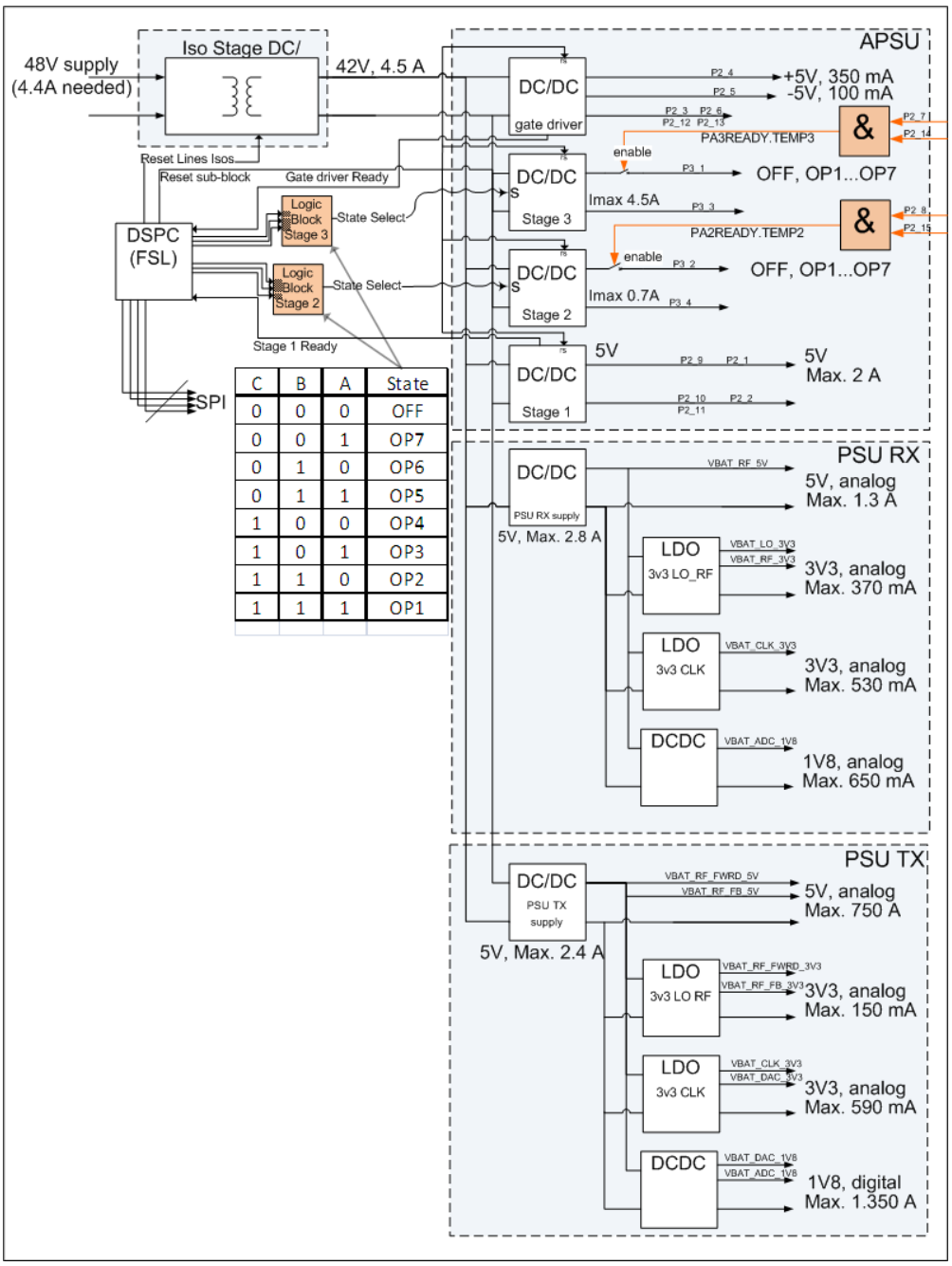

FIGURE 14. Power Supply System of macro base station composed of 4 main blocks: the isolated stage, PSU Tx, PSU Rx and the APSU

The concepts and solutions used for the core of the APSU circuit and especially for the Stages 2 and 3 enable the adaptation of the voltages supplied for the AEEPA.

In the first version of hardware prototypes, the same operating points have been defined for Stage 2 and 3. They are limited to three points for this first hardware realization namely OP1 with 28V/4.5A, OP2 with 20V/3.2A, and OP3 with 12V/2.2A. In the final prototype version, Stage 2 and Stage 3 will be defined and controlled independently following the operating points presented in FIGURE 14.

As high power is to be supplied (max 140 W) by the DC-DC converters, we choose a Buck converter due to its efficiency characteristics. The changes of the states in Stages 2 and 3 make use of a feed-back loop as presented in FIGURE 15. Using only one inductor and one capacitor enhances the rapidity of the system during

reconfiguration. The main challenge is to define values for L and C for a good efficiency and to define the compensation loop especially for achieving a good ripple of the out voltage and a good stability of the circuit.

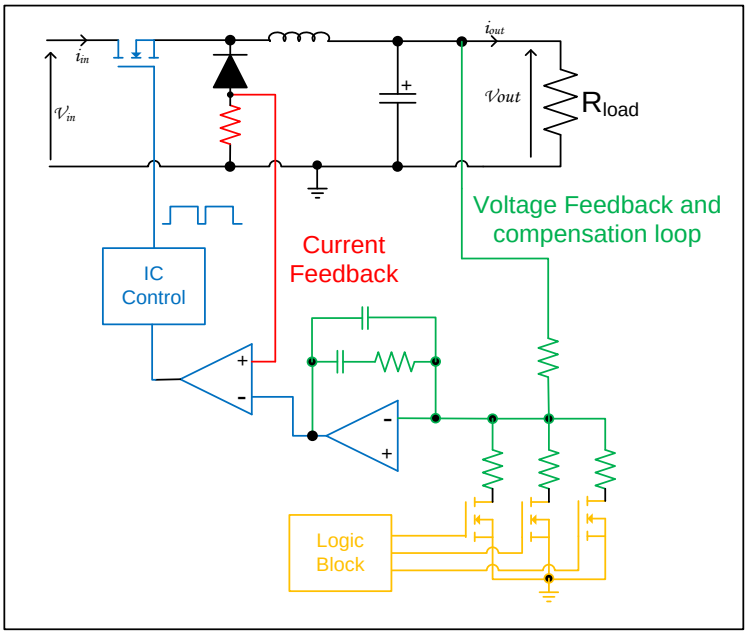

FIGURE 15. Stages 2 and 3 architecture

First evaluations show a quite good switching rapidity as expected. For example, the circuit needs only 50µs to change the voltage from 20V to 28V with a load of 4.5A. The efficiency performance is presented in FIGURE 16 showing for the Stages 2 and 3 a maximum of 94% power efficiency for 28V regulation.

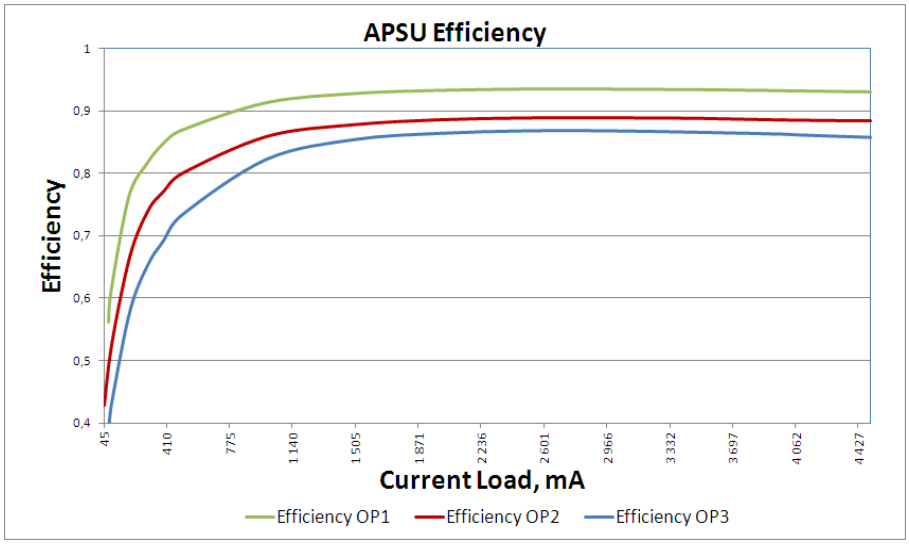

FIGURE 16. Efficiency results of Stages 2 and 3

The performance has been evaluated for operating points defined for three different levels of maximum output power with the related operating points (OP1, OP2, and OP3) defined above.

The power characteristic of the APSU is presented in FIGURE 17 showing the DC input power versus the DC power supplied to the AEEPA.

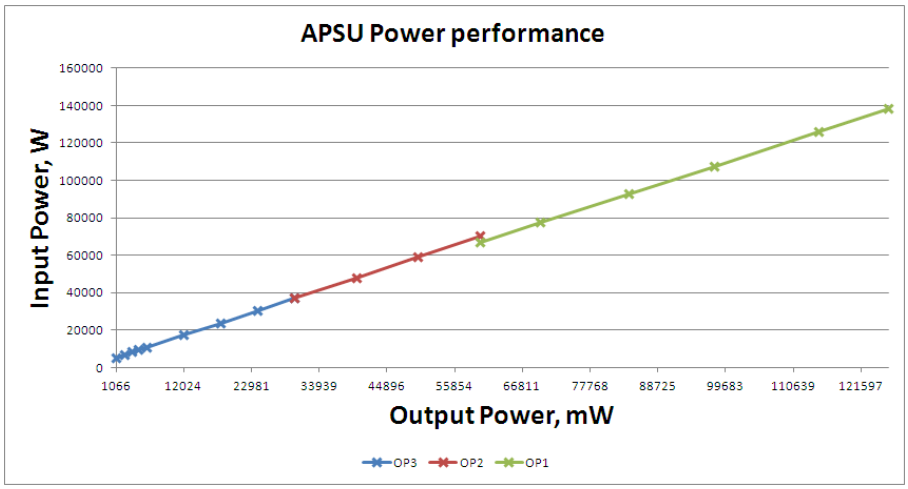

FIGURE 17. APSU power characteristic

FIGURE 18 shows the power dissipated in the APSU for the three evaluated operating points and arbitrary signal load defined for the AEEPA (see section 2.4). This characteristic allows generating the power characteristics of the SLA-TRX presented in section 2.6.

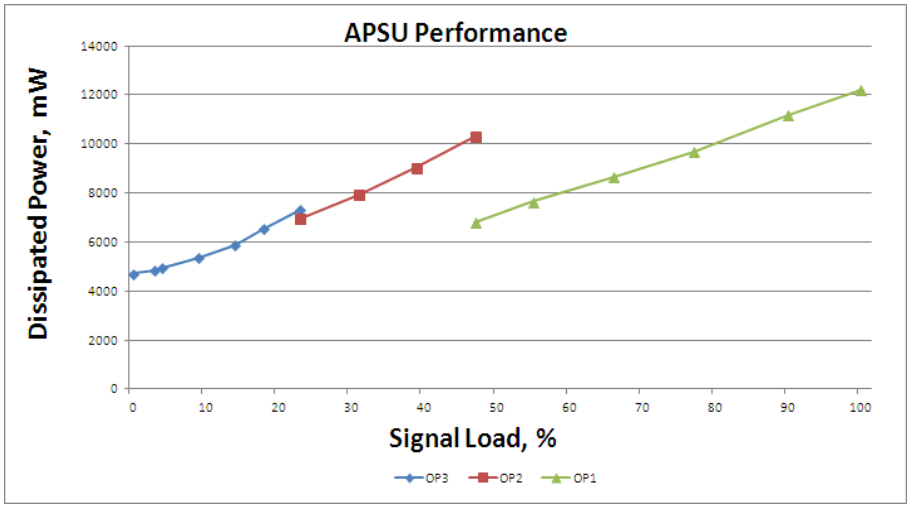

FIGURE 18. APSU power dissipation

The main problem encountered during the evaluation of this first APSU hardware is the ripple, which is higher as expected with more than 1 Volt (around 20mV expected, 10mV targeted), and a stability problem at very low load. The ongoing work focuses on solutions for solving these problems.

As shown above, the experimental evaluation of the first version of the APSU shows promising results but the expected performance is not achieved yet. Current activities are focusing on a second version with enabling a stable operation with improved efficiency supporting seven operating pints and minimized transitions times.

2.6. BENEFITS OF SIGNAL LOAD ADAPTIVE TRANSCEIVERS

The combination of the individual concepts on DSPC, SS RF-TRX, AEEPA, and APSU sets up the SLA-TRX system. Based on the performance evaluated for these SLA-TRX blocks, the performance expected for the whole transceiver system is determined and provides the power consumed for arbitrary signal loads as the basic component characteristic.

The application of the SLA-TRX solutions achieves significant energy saving for medium and low loads according to the optimization of operating points and the deactivation of certain components. The SLA-TRX concept is evaluated in the defined operating points for the complete ranges and presented in FIGURE 19. The power characteristics are based on a SLA-TRX system with a 40W power amplifier for three different operating points (OP1 for maximum signal load, OP2 for 60%, and OP3 for 20%) and the component deactivation (CD). The operating points are directly linked to the three operating points defined by the APSU hardware presented in section 2.5. The power consumption for DSPC and SS RF-TRX are constant independently of the signal load. For zero signal load the SS RF-TRX shows lower power consumption due the deactivation of some of its components. In contrast, the AEEPA and the APSU perform different consumption according to the signal load and the selected operating points.

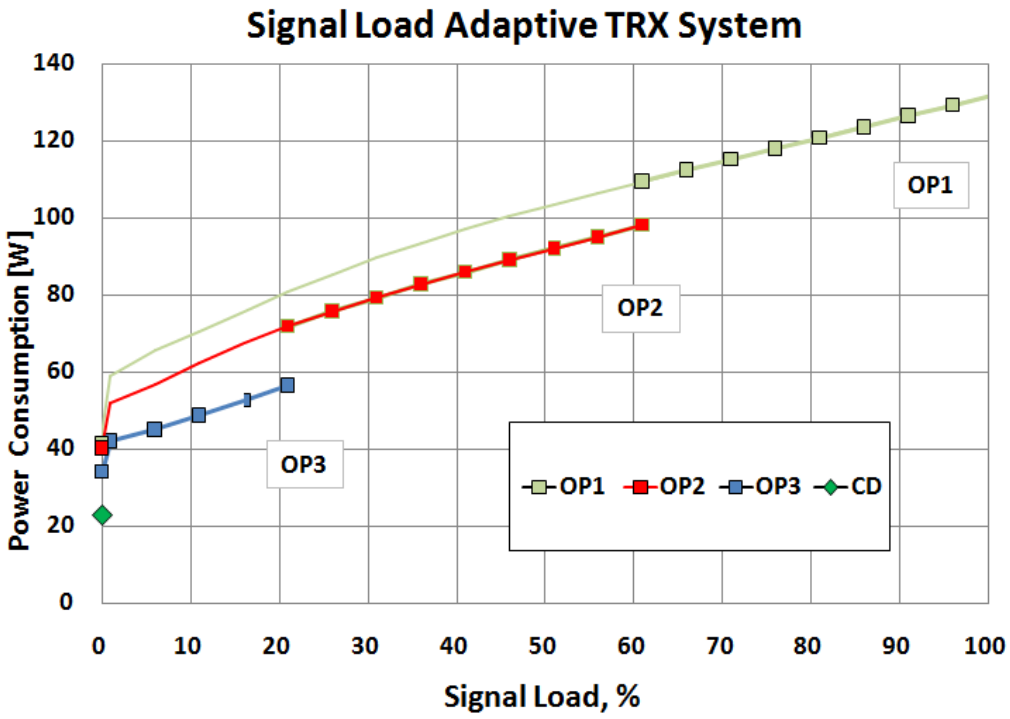

FIGURE 19. SLA-TRX systems performance vs signal load.

The characteristics in FIGURE 19 are partly based on theoretical, partly on experimental evaluations and can be considered as preliminary results. They will be updated with consolidated values before the end of the project.

The green curve defined by the OP1 shows the reference characteristic serving for the assessment of the power saving features. The operating point adjustment applied in this example for two additional operating points shows around 12 % of power reduction in OP2 and 29 % in OP3. The power reduction increases with the decrease of signal level. This behaviour can be exploited for energy efficiency improvement at low and medium traffic load by applying scheduling algorithms which reduce the instantaneous transmitted output power allowing for applying operating point adjustment. Such an application is shown in chapter 7 of this document.

In the case of the component deactivation (CD operating point), the consumption of PA and power supply is drastically decreased. The SS RF-TRX also deactivates certain blocks, allowing for additional power savings. However, the DSPC block keeps constant the consumption even in case of no signal load. The total reduction in CD operating point is near to 54 %. By applying scheduling solutions which provide longer time slots without data transmission and especially with increased number of successive empty symbols, the power saving due to component deactivation can be increased. Such applications are shown in chapter 6. Component deactivation and operating point adjustment can be applied in combination for minimizing the power consumption. Such an application is shown in chapter 7 of this document.

The fragmentation of the signal load range into 3 sections was done due to the availability of experimental values for the APSU limited to three operating points in the first hardware prototype. The AEEPA shows no restrictions concerning the number of operating points. Different fragmentations can be used for concrete applications based on their special requests and on hardware implementation constraints, which could limit the applied step sizes. For the next prototype version seven operating points will be realized.

The elaborated power characteristics are used in the base station power model, which shows a basis for the energy efficiency evaluation on network level. In this way the impact of the SLA-TRX solution will be considered by the evaluation of the integrated solutions which are going to provide the final results of the project.

The SLA-TRX solution proposed for macro base stations can be applied for different cell-sizes from dense urban to wilderness and supports energy efficiency enablers acting on different time scales as presented in FIGURE 20. This positioning as energy efficiency enabler follows the classification defined in [EARTH-D6.2a].

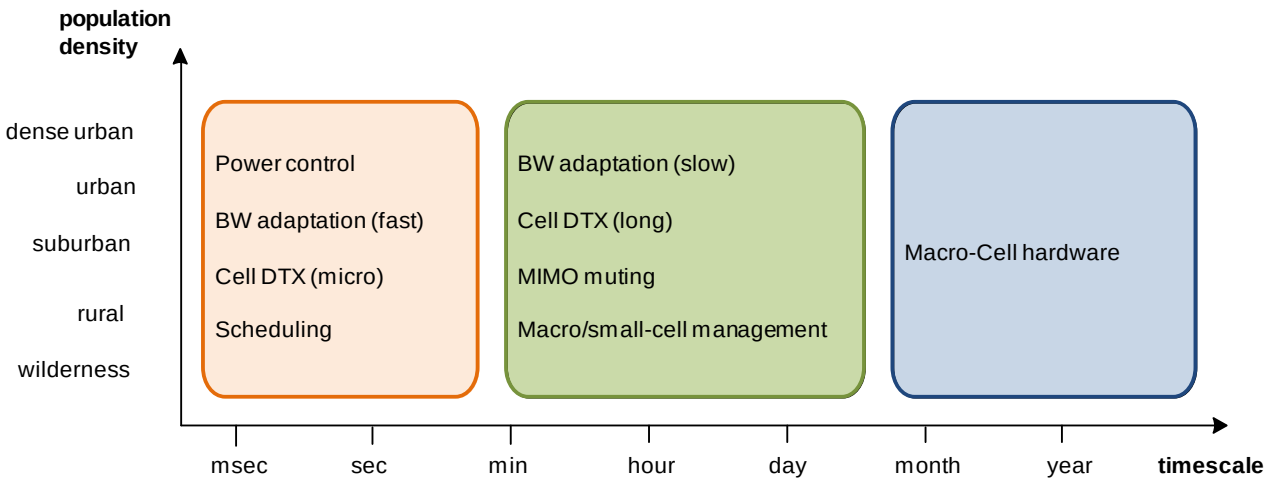

FIGURE 20. Positioning of the relevant energy efficiency enablers supported by the SLA-TRX according to the deployment scenario (y-axis) and the optimization time scale (x-axis).

The relevance of different energy efficiency enablers on time scale shows three categories:

- As it represents a hardware solution it is a matter of deployment by considering equipment implementation and provides impact on long time scale of months and years.
- Supporting solutions acting on medium time scale like slow BW adaptation, long DTX, MIMO muting or macro/small-cell management, the impact is within minutes or hours.
- Supporting solutions acting on short time scale like power control, fast bandwidth adaptation, micro Cell DTX and special scheduling, the impact is within milliseconds and seconds.

The impact of the SLA-TRX solution on the overall energy efficiency improvement will be analyzed with the evaluations based on system level simulations which are defined in the task “Integrated solutions” of the EARTH project.

3. TRANSCEIVERS FOR SMALL-CELL BASE STATIONS

In areas with urban and dense urban population densities, the wireless communication scene is growing rapidly. To support this trend, the traditional approach of adding powerful base-stations might not be the best option because the capacity is mainly consumed in-doors and shows large variation in time, space and frequency. In a densely populated office environment for example, users will move in-doors with their communication devices. Depending on their activities, the users might require low or high capacity. To support this dynamism, adding small-cell base-stations closer to the users is more beneficial to increase the link performance and to reduce the radiation power. Although the power consumption of an individual small-cell base-station is relatively low, a heterogeneous network of some large-cell and multiple small-cell base-stations might lead to an intolerable ecological footprint and electrical cost. From an energy efficiency perspective, it is essential that the small-cell base-stations are not only **energy efficient** but also **energy flexible** to adapt to the capacity dynamics.

Different energy efficiency and adaptive solutions have been proposed for Green Radio Technologies as described in [EARTH-D4.1]. The tracks related to hardware components for small-cell base-stations are grouped in the topic 'transceiver for small-cell base-stations'. This topic is covered in this section by identifying the solutions and representing their energy efficiency potential. The architecture of the small-cell base-station is illustrated in FIGURE 21, supporting multiple transceivers, antennas and antenna interfaces (L). Each transceiver comprises a Power Amplifier (PA), a Radio Frequency (RF) transceiver, a baseband (BB) interface and a DC-DC power supply. Both the RF and BB components offer reception and transmission capabilities for Up-Link (UL) and Down-Link (DL) operation respectively. FIGURE 21 shows on the right the energy distribution over the different base stations components for different cell sizes [EARTH-D2.3]. For macro-cell base-stations, the power consumption is mainly concentrated in the PA. Scaling down the cell size reduces the relative weight of the power consumption from the PA towards the BB and RF components. For small-cell base-stations such as pico- and femto-cell, the power consumption of the RF component is more than 12% and the BB and PA consume about 30% each. For small-cell base-stations, it is opportune to investigate energy enhancement and adaptation techniques for these three components. Note that the power consumption of the antennas and their interface are minor consumers, but as they co-determine the energy efficiency of the PA, they are also considered as potential energy savers.

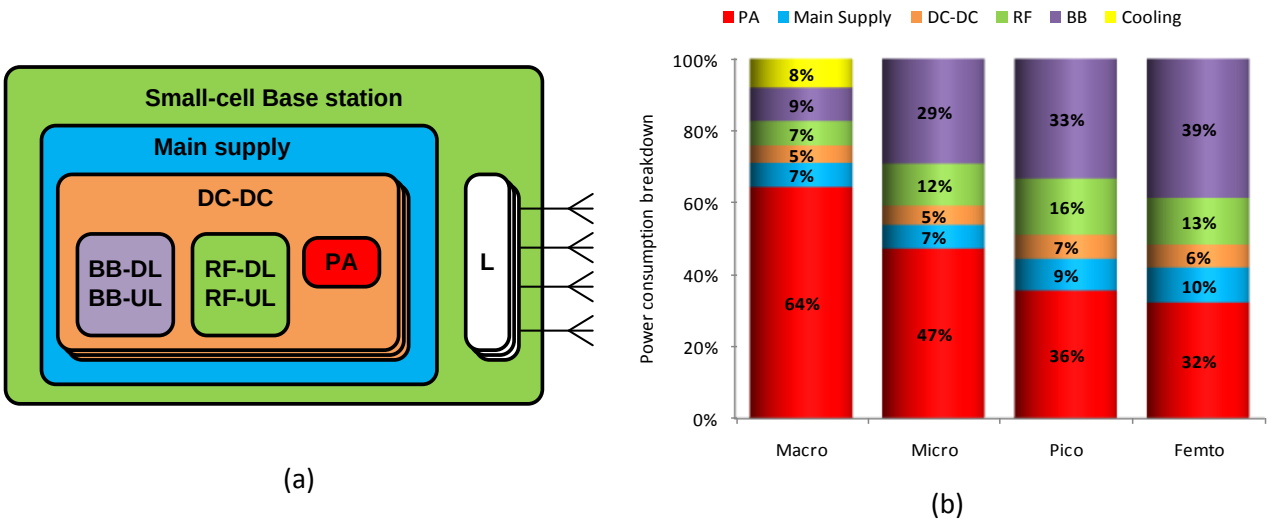

FIGURE 21. Simplified block diagram of a small-cell base station (a) and the BS power consumption breakdown for different cell-sizes (b).

The 'transceiver for small-cell base-stations' topic consists of 5 different tracks, covering the BB processor, the RF transceiver, two approaches on the PA and an antenna interface solution. All tracks target an innovative architecture that combines high performance with energy efficient operation. All tracks, except the antenna interface, are energy flexible depending on the traffic load. The energy flexible knobs implemented in the hardware components are controlled according to the EARTH energy efficiency enablers [EARTH-D4.1]. FIGURE 22 (inspired on [EARTH-D6.2a]) illustrates the EARTH energy efficiency enablers which are relevant in the small-cell topic. The relevant deployment scenarios for small-cell base-stations are limited to areas with urban and dense urban population. The optimization timescale covers the complete spectrum from milliseconds towards years, where in the short timescale the operation point of the components are adapted and in the long timescale new architectures and technologies are implemented. The energy adaptation solutions on the BB engine, the RF transceiver and one PA solution are mainly beneficial at low and medium traffic load. One PA approach is also beneficial at higher traffic load.

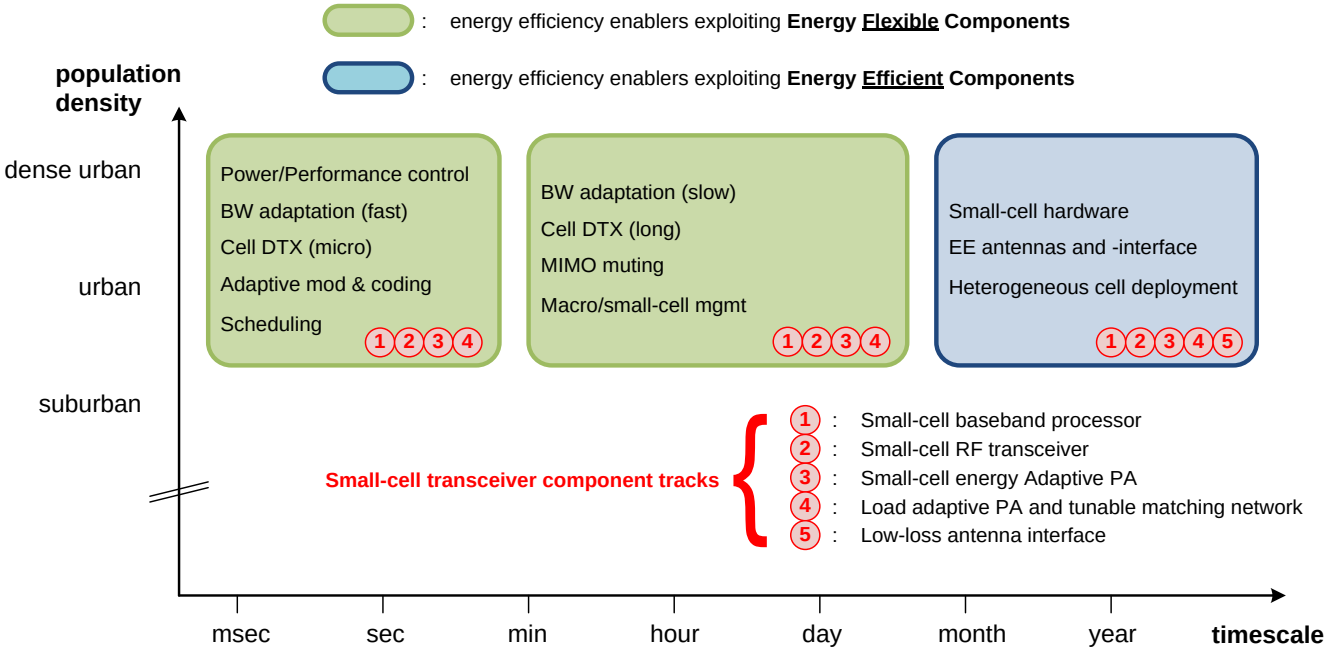

FIGURE 22. Positioning of the relevant energy efficiency enablers [EARTH-D4.1] according to the small-cell component tracks (colour), the deployment scenario (y-axis) and the optimization time scale (x-axis).

In the following subsections, the small-cell transceiver component tracks are discussed and quantified in terms of energy flexibility and energy efficiency.

3.1. ADAPTIVE SMALL-CELL BASEBAND PROCESSOR

Due to the shrinking cell size and the rapidly growing signal processing complexity, the energy consumption of digital baseband implementation is becoming more and more dominant. Hence, optimizing the energy efficiency of digital baseband processing is crucial. Two aspects are considered to reduce the power consumption of the baseband part: the hardware/architecture side and the algorithm/software side. Note that the physical processor design is not considered in this project - the potential gain of energy efficiency is investigated based on literature study and simulations.

On the hardware side, the energy efficiency of baseband processing is increased by using ASIP's (Application Specific Instruction Processors) rather than FPGA's. ASIP based baseband platforms are dedicatedly optimized

for the workload of signal processing tasks. For instance, consider four categories of ASIPs for energy efficient signal processing:

- Digital front end processors and Analogue-Digital Convertors that are optimized for mixed signal filtering, synchronization and data conversion.
- Baseband processors (time and frequency domain) that are optimized for various diversified signal processing tasks in the inner modem, such as MIMO-OFDM processing, channel estimation, equalization etc.
- Channel error correction processors that are optimized for various FEC en-/de-coding tasks.
- Platform control processors such as power regulation and micro-processors.

Due to the high degree of specialization, a much higher intrinsic energy can be achieved. The energy efficiency improvement when porting a small-cell baseband processor from an FPGA platform towards an ASIP platform exceeds 20%. Additionally, technology scaling enhances the dynamic energy efficiency, expressed in Giga Operation per Watt (Gops/W). Each scaling step (every two years) increases the Gops/W with 20%. This increase of energy efficiency is however tempered by the increase of leakage when migrating to dense technologies. This leakage increases the static power consumption and doubles (or even triples) per scaling step. In 2012 technology, about 30% of the consumed power in the baseband processor is dedicated to leakage. It is expected that technological research will tackle this problem and reduce the impact of leakage. From a design perspective, the stand-by leakage (when part of the processor is in sleep) can be reduced by power gating: transistor switches are placed in-between the supply/ground connections and the logic to additionally cut-off leakage currents when the circuit is not operating.

Further, the digital baseband hardware should support the flexibility in the algorithm/software. This flexibility creates instances in time and frequency where parts of the processor operations get no or low priority. Then, the dynamic power consumption is reduced by applying clock gating and voltage- and frequency scaling. These techniques require a specific circuit topology. For clock gating, different clock lines are implemented that can be deactivated to avoid digital logic from switching when they are not addressed. For dynamic voltage scaling, the processor is designed in different regions with dedicated supplies. Depending on the importance or intensity of the operation, the multi-level general supply will distribute the voltages over the different regions. Similar strategy applies for the frequency scaling.

The focus on the algorithm/software side is on flexible energy aware baseband signal processing algorithms for small-cell base-stations that can dynamically adjust their energy consumption at run-time, according to the varying user requirement and communication environment. Flexibility in the signal processing algorithms, cover adaptation of the bandwidth, modulation, coding rate, number of antennas and duty-cycling in time and frequency. These techniques are beneficial for the small-cell EE enablers depicted in FIGURE 22.

The diversity and interaction of hardware and software techniques have been implemented in a power model [DeDG12]. This model calculates the digital processing dynamic power consumption for up-link (UL) and down-link (DL), covering frequency-domain processing (up/down-sampling and filtering, MIMO-OFDM processing with an FFT, equalization and mapping/demapping), channel en/decoding (FEC) and platform control. This model also considers the static power consumption due to leakage. FIGURE 23 shows the power consumption of a 2x2 MIMO pico-cell baseband processor over the signal load. It is observed that the UL consumes almost twice as much power then the DL because MIMO processing of equalization and detection is more complex and because the FEC decoding is significantly more complex than encoding. The Energy Adaptive (EA) results consider the energy flexible processor solutions discussed in this subsection. The potential for EA is mainly concentrated in the UL case because most of its signal processing is proportional to the data throughput. In the DL case, baseband processing is relatively independent of the throughput (time-domain processing of the signal, platform control overhead...). The overall power reduction ranges up to 20% at signal loads <20%. At higher signal loads, the power reduction decreases.

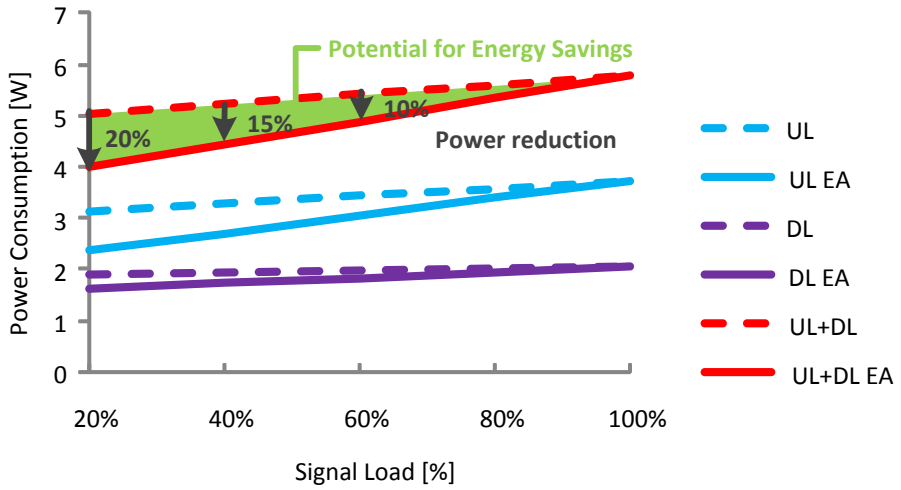

FIGURE 23. Power consumption of a 2x2 MIMO pico-cell baseband processor over the signal load.

It can be concluded that for small-cell baseband processing, part of the energy efficiency is gained from technology: more than 20% from using ASIP's instead of FPGA's and 20% in Gops/W from technology scaling. Contrarily, technology scaling also increases the static power consumption due to leakage. Further, energy efficiency is gained both in hardware as in software. In hardware, innovative techniques to slower or shut-down parts digital switching logic can be implemented. In software, scalable algorithms to ease computations while offering the required instantaneous performance. These techniques have been modelled to quantify the power efficiency improvement depending on the signal load. The proposed baseband processing techniques are complementary with and facilitating some of the small-cell energy efficiency enabling techniques for Green Radios. The energy efficiency enabling technique 'bandwidth adaptation' for example is exploited in the baseband processor by changing the FFT length, the digital filtering characteristics and eventually the sampling rate; thus by changing the amount signal processing operations.

3.2. ADAPTIVE SMALL-CELL RF TRANSCEIVER

Scaling down the cell deployment towards small-cells shifts the relative weight of power consumption in the base-station from the PA towards the baseband and the RF transceiver. This subsection describes how the energy efficiency is optimized in the small-cell RF transceiver on a long and short timescale.

On a long timescale of months and years, the power consumption is reduced by using energy-efficient implementation technologies and transceiver architectures. These two approaches are inspired by recent work in the area of handheld communication devices where energy efficiency is crucial to increase the battery lifetime. With respect to *implementation technology*, the low-cost and power-efficient CMOS technology can be used because the small-cell RF transceiver operates on small signals. This technology also benefits from technology scaling every year or two, which results in an energy efficiency improvement of about 20% per scaling step. With respect to the *transceiver architecture*, dense integration and reduction of the circuit complexity offer high potential to increase the cost- and power-efficiency. Changing the architectural structure is justified because the small-cell base-stations have less stringent linearity and blocking requirements with respect to large-cells because their deployment provides more flexibility to system dynamics and fewer users should be serviced. Using a direct-conversion architecture instead of a heterodyne architecture shows a power reduction of about 20%. The direct-conversion architecture comes, however, with several drawbacks: increased sensitivity to even order non-linearities and to circuit imperfections in the quadrature paths. These drawbacks can be countered at design time by improving the matching and by adding complex circuits, which degrades the power reduction factor. Recent research [DeWV09] however, presents a method that deals with

the architectural drawbacks in the digital domain without impacting the implementation complexity and thus maintaining the power reduction factor.

To support the energy efficiency enabling techniques depending on the traffic load, as indicated in FIGURE 22, the small-cell RF transceiver component is made flexible. This flexibility covers different tuning knobs:

- sub-component muting and deactivation: to enable micro- and deep-sleeps and for complete transceiver deactivation
- bias point adaptation, gain distribution adaptation and linearity scaling: to scale the Signal to Noise and Distortion Ratio (SiNAD) performance and the transmission power
- filter order and bandwidth adaptation: to change the baseband bandwidth and to adapt the interference suppression

Tuning these knobs impact the power consumption of the RF transceiver component and can be exploited to increase the energy efficiency in function of the traffic scenario. The large amount of tuning knobs requires an advanced protocol to reconfigure the RF transceiver. An on-chip serial protocol has been developed as described in [EbG08]. This generic protocol offers different instruction lengths to facilitate normal and fast addressing. The sampling speed depends on the technology and ranges up to 300MHz for 40nm CMOS technology.

To observe the possible cooperation between the energy efficiency enablers and the small-cell RF transceiver, FIGURE 24 indicates the optimization timescale for the transceiver sub-components.

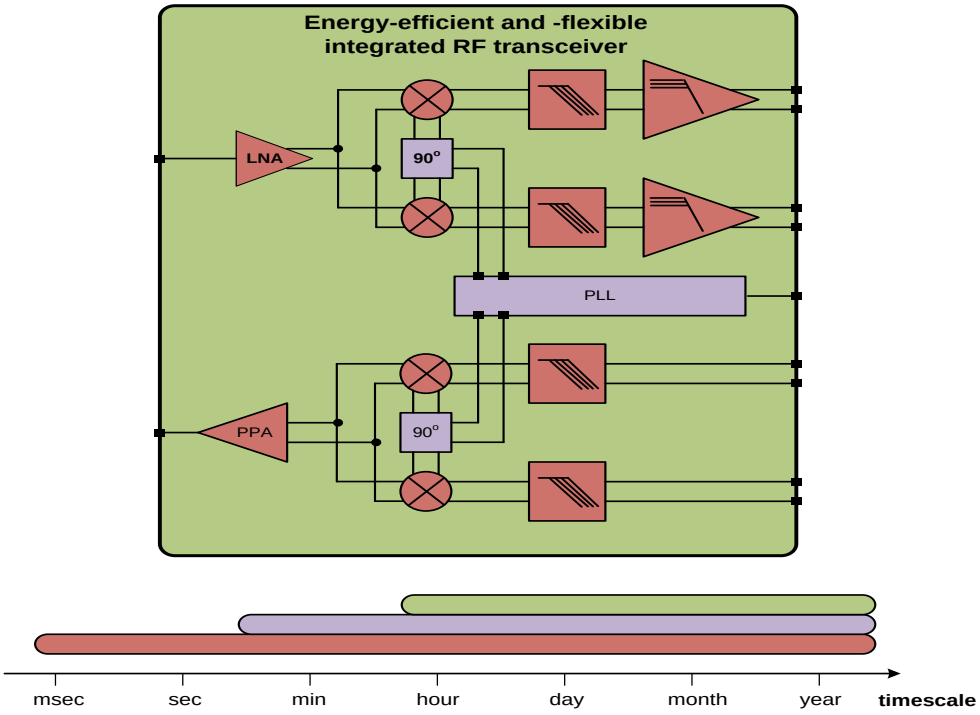

FIGURE 24. Small-cell RF transceiver block diagram based on a direct-conversion architecture. The energy efficiency optimization timescale of the energy flexible sub-components are indicated on an indicative timescale.

Nearly all sub-components allow rapid reconfiguration as their ramp-up and/or settling effects are small and limited in time. The sub-components linked with the Voltage Controlled Oscillator (VCO) however suffer from transition effects at power-up: it takes several milliseconds to lock the Phase Lock Loop (PLL) and during this process, the LO signal does not match the wanted carrier frequency. The VCO should also remain operation for

background processing such as sensing. Complete deactivation of the RF transceiver chip is only appropriate within a long optimization timescale, because of the start-up calibration and configuration procedures for the different transceiver sub-components.

Now, the energy efficiency improvement is quantified when exploiting the RF transceiver tuning knobs. In traditional base-stations (no EARTH optimisation), the RF transceiver always targets the best SiNAD performance independent of the signal load. From an energy consumption perspective (EARTH optimization), it is more advantageous to scale the transceiver to provide a 'just good enough' SiNAD performance and to schedule sleep states and bandwidth adaptation based on the load and the channel conditions. The energy efficiency impact of this approach is illustrated in FIGURE 25, which shows the measured power consumption for a 2x2 MIMO pico-cell base-station RF transceiver over the signal load. This figure, derived with the power model presented in [DeDG12], depicts the power consumption for the UL receiver, the DL transmitter and the complete transceiver (UL+DL). The dotted lines correspond to the traditional approach whereas the solid lines consider energy adaptation of scaling the SiNAD performance. Energy adaptation is mainly beneficial at lower traffic load, where the transceiver power consumption is reduced beyond 30% (signal load <50%) and up to 55% (signal load <5%).

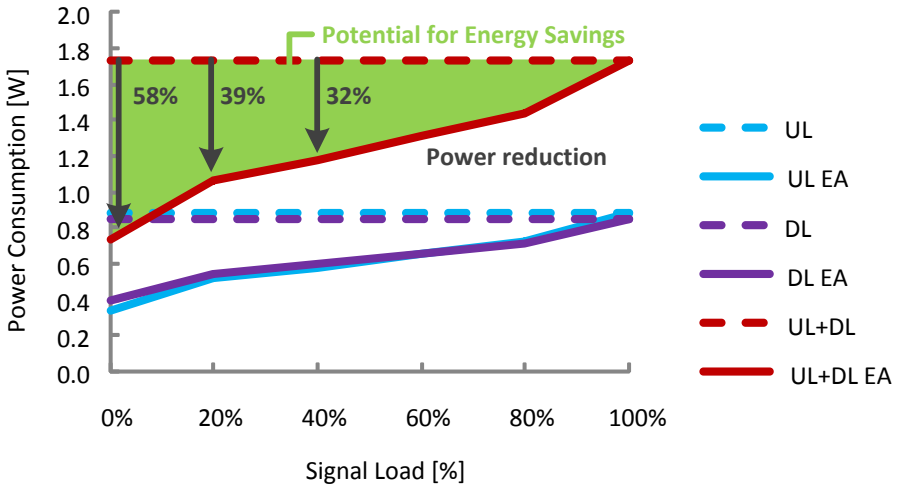

FIGURE 25. Power consumption of a 2x2 MIMO pico-cell base-station RF transceiver over the traffic load.

It can be concluded that the traffic load independent power efficiency improvement of the RF transceiver is about 35% due to technology scaling and architecture, and that the traffic load dependent power efficiency improvement is 30% on average due to SiNAD adaptation and time- and frequency duty-cycling (respectively sleep modes and bandwidth adaptation). The flexible RF transceiver component track is complementary with all small-cell energy efficiency enabling techniques and even facilitates some of them.

3.3. ADAPTIVE ENERGY EFFICIENT POWER AMPLIFIER

Unlike in a macro base-station (BS), the power amplifier in a small-cell BS is not the most power consuming component. Although the relative power consumption decreases with the cell size, the energy efficiency requirement of the PA remains crucial. This requirement is given by the fact that in small-cell base-stations digital pre-distortion is rarely used and thus the PA should support the high peak to-average-power-ratio (PAPR) offered by the LTE signal. To support the high PAPR, the PA is forced to operate with a large back-off and thus with a low energy efficiency. It is therefore crucial to investigate techniques to improve the energy efficiency, as discussed next.

An Adaptive EE PA can reduce the power consumption in a small-cell BS by using techniques as in a macro BS. These techniques can be operating point adjustment (OPA) and component deactivation (CD). They enable to adapt the operating point of PA to different RF output power levels depending on traffic load and to deactivate some PA stages when empty symbols occur. These techniques avoid to waste energy.

The energy adaptation solution on the PA is mainly beneficial at low and medium traffic load. At low traffic, the required output power level is lower and it is possible to adjust the operating point in the PA. Adjusting the operating point reduces the maximum output power and the power consumption. The Adaptive EE PA can work in different operating points according to the traffic load to save energy.

This optimization using the Adaptive EE PA for small-cell BS covers the timescale from milliseconds to years, because in the short timescale the OPA is performed and in the long timescale a suitable architecture is implemented using advanced RF technologies.

In order to evaluate these concepts, an Adaptive EE PA has been developed for LTE signals in the frequency band from 2.11 to 2.17 GHz with 0.25 W average output power. In this case, PAPR is 12 dB because digital pre-distortion will not be implemented.

The hardware development for the Adaptive EE PA is implemented in an aluminium housing which integrates a RF board and a biasing and control board. Besides, a small heatsink is incorporated to maintain the performance in temperature.

The block diagram for the Adaptive EE PA for small-cell BS is presented in the following figure:

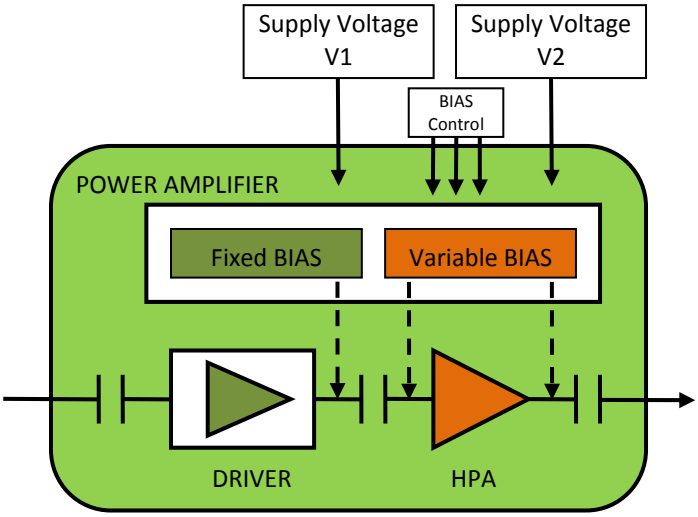

FIGURE 26. Block diagram for Adaptive EE PA for small-cell BS.

The design is based on two stages. The first stage is a driver with fixed bias and the second stage is a HPA with variable bias. This last module includes the CD feature and can be adapted to different RF output power levels depending on traffic load through changes in supply voltages.

The CD feature is implemented in HPA stage to save energy during empty symbols. This technique allows for suppressing a significant amount of power consumed by the PA. A control signal is applied to the PA to switch off the second stage when empty symbols occur or to switch it back to normal operation.

The PA is implemented in a GaN HEMT technology and operates on a supply voltages of +28V. The OPA feature in the PA is performed by changing the gate voltage in the HPA while keeping the drain voltage constant. Through these variations, the PA adjusts the required RF output power level to the most efficient one

depending on the traffic load. Modifying the output power depending in function of the traffic load thus increases the efficiency of the small-cell BS. This adjustment is controlled via a SPI interface.

The next figure depicts the Adaptive EE PA for small-cell BS. The hardware development differs between two boards: a RF board with two SMA connectors providing RF input and RF output, and a biasing and control board with a DB15 connector. This DB15 connector provides the supply voltages, +28V and +5V, and the control signals to implement the CD feature and the OPA feature.

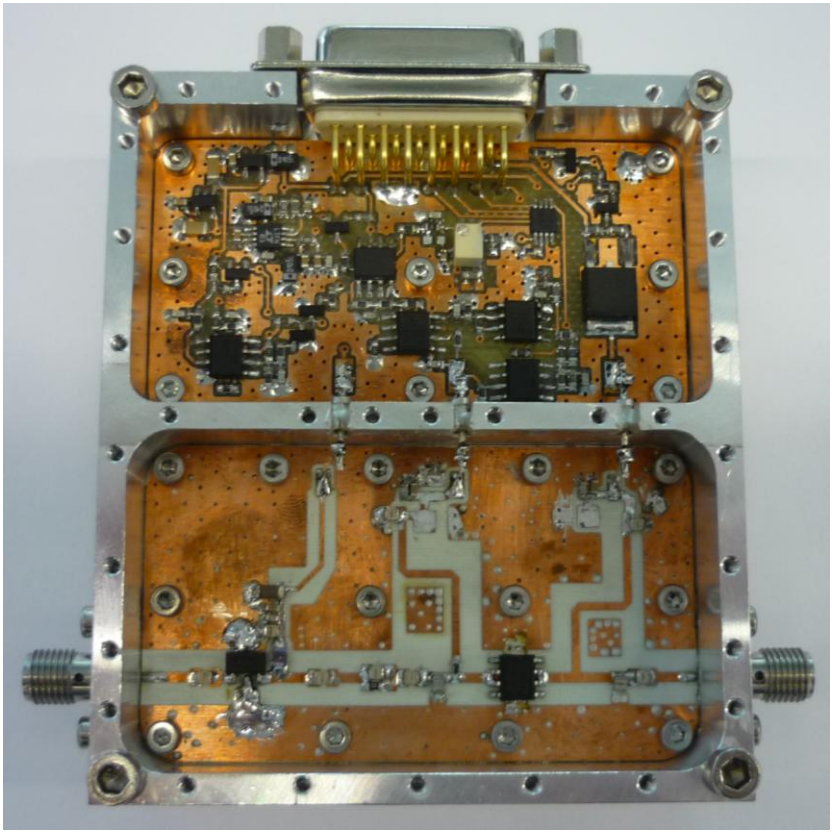

FIGURE 27. Photograph of Adaptive Energy Efficient PA for small-cell BS.

There is a dedicated control signal to make available the deactivation/reactivation feature.

The OPA feature is implemented through a SPI interface because different supply voltages are required to provide different output power levels in AEEPA.

Preliminary tests have been done to measure the transition time to implement both features to follow LTE signals as fast as possible to implement different radio interface techniques. According to the preliminary results, it is possible to deactivate and reactive the PA in less than 20 µs. Furthermore, the OPA feature is performed in less than 20 µs. The performance of the Adaptive EE PA for small-cell BS is presented in Figure 25. The improvement due to component deactivation is shown on the left for 0% signal load. The deactivation achieves a great reduction, around 80% from the OP1. Some components maintain operative during this procedure to optimize energy efficiency.

The OPA feature is defined in five signal load ranges: 100-80% for OP1, 80-60% for OP2, 60-40% for OP3, 40-20% for OP4 and 0-20% for OP5, providing significant enhancements. The power reductions are around 14% for OP2, 26% for OP3, 40% for OP4 and 55% for OP5.

The combination of both features provides a significant energy saving and improves energy efficiency in small cell base stations, which typically are deployed in urban and dense urban scenarios.

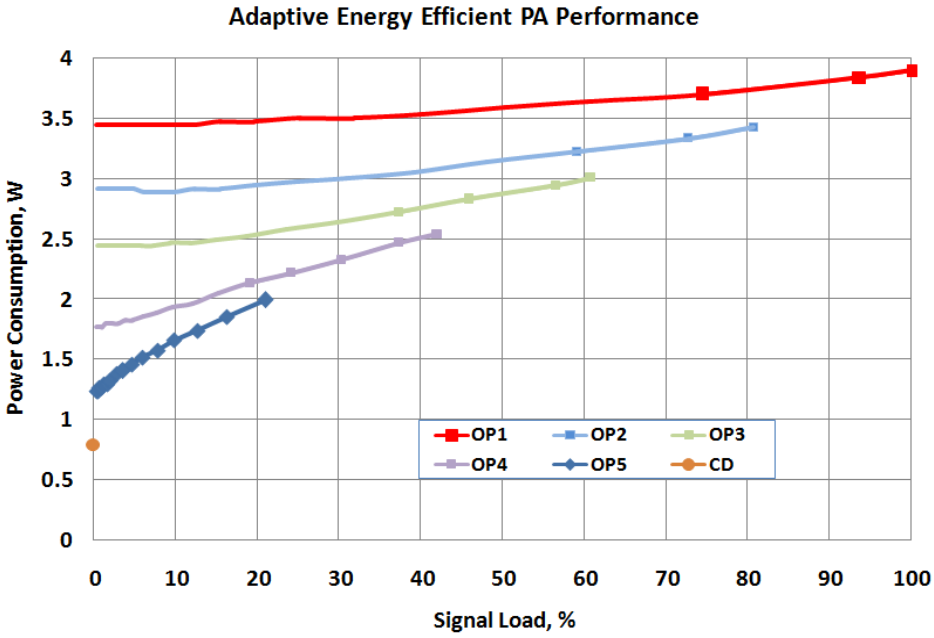

FIGURE 28. Performance of Adaptive EE PA for small-cell BS.

3.4. TUNEABLE MATCHING NETWORK FOR LOAD ADAPTIVE PA

Various efficiency enhancement techniques, such as dynamic supply modulation (DSM) [JeKK09], Doherty [PeNG08], out phasing [QuPM09], etc. have been proposed in literature to enhance the PA efficiency for modern wireless signals having high PAPR. Load impedance modulation of the PA is one of the techniques that can be used to boost PA efficiency [EARTH-D4.1] when a variable envelope modulated RF signal is used. In this technique, a tuneable load matching network is used to reduce the PA power consumption in back-off. A general block diagram of the proposed architecture is shown in FIGURE 29, where the tuneable matching network (TMN) provides optimum load impedance to the PA according to the modulated signal amplitude to get reduced power consumption in back-off.

In the literature, some varactor-based configurations have been proposed for the tuneable matching network to achieve such efficiency improvement, but with limited peak power levels and frequency of operations [FuMo08], [NeLL06]. In addition, varactors typically suffer from linearity problems, although improvements have recently been demonstrated by exploiting proper topology configurations [HuBM09]. In the proposed work, high voltage SOI CMOS switched capacitors have been designed and implemented to dynamically control the load impedance of a LDMOS PA. SOI CMOS provides an attractive trade-off among performance, cost and integration capability. Compared to standard bulk CMOS process, SOI CMOS features higher speed and reduced power consumption since the drain/source capacitances are substantially reduced. Moreover, the use of a high resistivity substrate enables high-Q integrated inductors [GiFM10], as well as excellent crosstalk isolation. Besides, by exploiting transistor stacking, SOI RF switch can be designed to handle arbitrarily high off-state voltages, which is a crucial feature for the implementation of a high power tuneable matching network. Despite a higher wafer cost compared to standard bulk CMOS, the net impact of substrate cost on a fully packaged integrated circuit is quite small, and it is believed to further decrease in the near future, eventually reaching parity with standard bulk CMOS [Soi09].

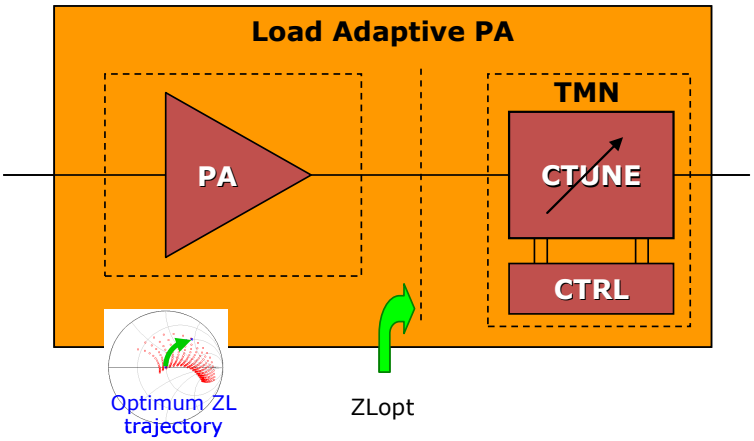

FIGURE 29. Load adaptive PA architecture with Tuneable Matching Network

The TMN can be co-designed with the PA (integrated design approach) or designed separately (modular design approach). The modular design approach, based on a 50Ohm interface between PA and TMN, allows some flexibility but suffers from bandwidth limitations since extra circuitry (PA output matching network and transmission lines optimized for a 50Ohm termination) is needed. In the proposed track, the TMN has been co-designed with the PA to avoid 50Ohm interface and provide optimized bandwidth. Different load-pull simulations of a SOI LDMOS device have been performed to determine the optimal PA load impedance for different output power levels. Efficiency curves for these different power levels, obtained after load-pull simulations of a 2.14GHz SOI LDMOS device under 4V supply, are shown in FIGURE 30.

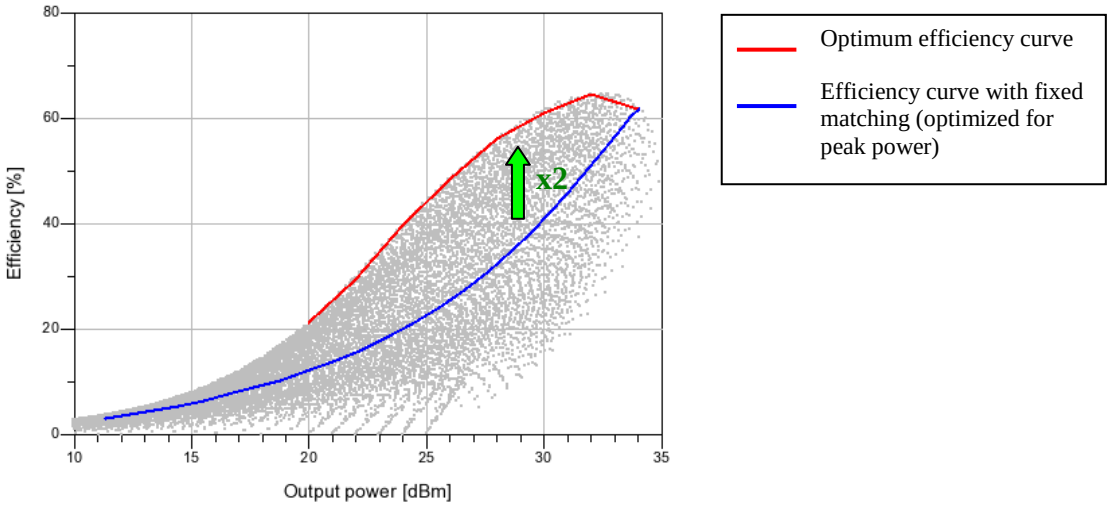

FIGURE 30. PA efficiency for different load impedance and drive level

When load impedance (Z_L) and input drive level (P_{in}) are properly selected (red curve), large efficiency improvements can be obtained in back-off. At 9dB back-off, efficiency increases from 21% up to 42%, which corresponds to an improvement by a factor of two. Actually efficiency improvement is less important because of TMN loss and tuning range limitations which depend on the TMN configuration and technology.

The TMN configuration and capacitance range has been selected through electrical circuit simulations with the goal of achieving maximum PA efficiency at different back-off levels. The resulting tuning capability of the

tuneable matching network is shown in FIGURE 31, which displays the simulated load impedance through all the capacitor settings (green dots) and the optimal load impedance trajectory (blue curve) when decreasing output power level. The green arrow indicates the load impedance trajectory orientation when moving from maximum output power (Pmax~34 dBm) to 10 dB back-off (BO) power.

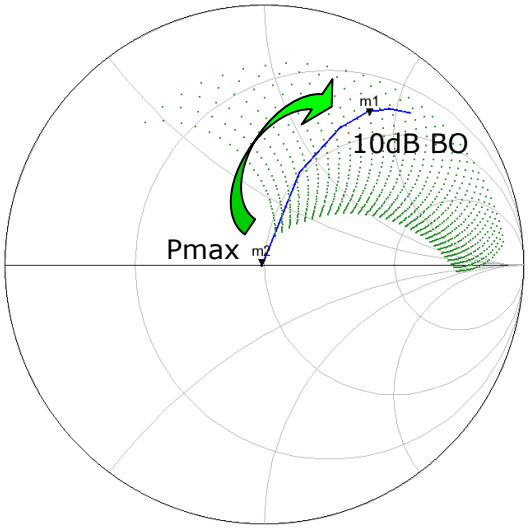

FIGURE 31. TMN impedance coverage (green dots) and optimal load impedance trajectory (blue curve)

The achievable dynamic range is directly related to the available tuning range of the tuneable capacitors. Variable capacitors have been implemented through banks of binary weighted SOI CMOS switched capacitors, with several floating body NMOS transistors stacked in series to achieve high voltage handling (>20V). The simulated Q factor of the designed tuneable capacitors is greater than 50 at 2.1GHz and insertion loss of the TMN (IL TMN) built with these tuneable capacitors stays lower than 1dB on a large power range as shown on FIGURE 32.

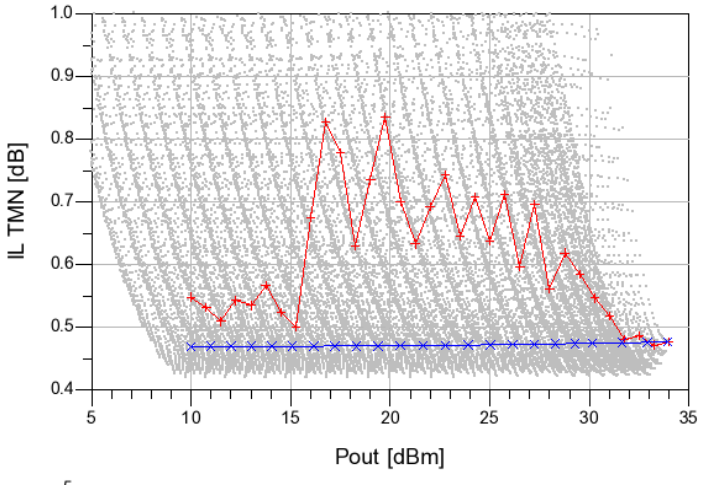

FIGURE 32. Simulated insertion loss (IL) of the TMN (red curve) compared to a fixed matching network (blue curve)

The resulting energy efficiency improvement when combining the TMN with the LDMOS PA to get the load adaptive PA is shown on FIGURE 33. Despite TMN insertion loss, around 50% efficiency improvement is obtained from 7dB to 12dB power back-off (PBO), and more than 30% improvement is obtained from 3dB to 14dB PBO.

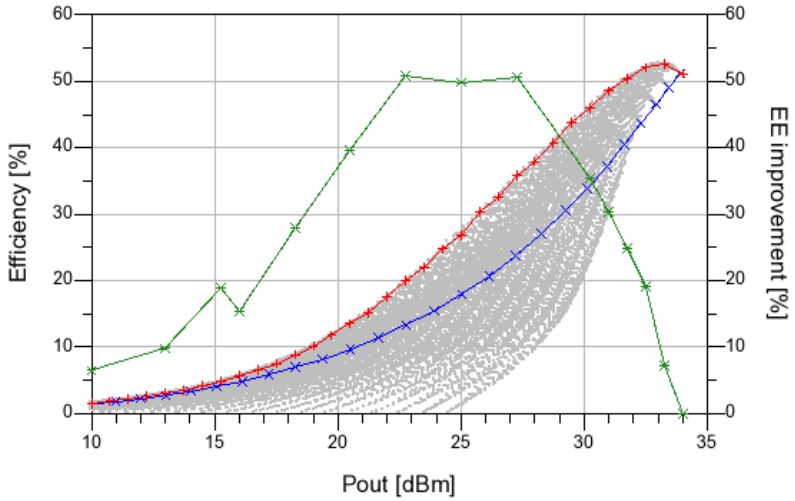

FIGURE 33. PA efficiency vs output power (Pout) for fixed matching (blue curve) and tuneable matching (red curve). Resulting energy efficiency improvement obtained with load adaptive PA (green curve)

The improvements in terms of power reduction are shown on FIGURE 34. The proposed load adaptive PA leads to important energy savings, with more than 30% power consumption reduction from 3dB down to 14dB PBO.

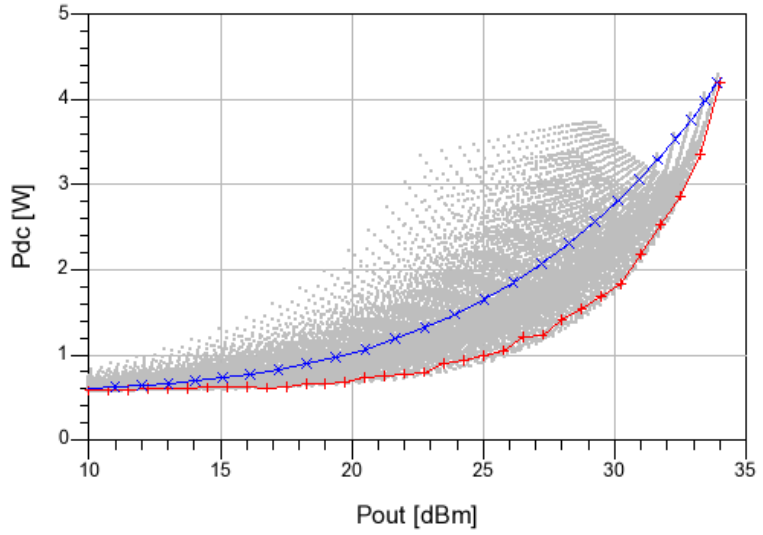

FIGURE 34. PA power consumption (Pdc) vs Output power (Pout) for fixed matching (blue curve) and tuneable matching (red curve)

Current simulated results are obtained considering static tuning of the TMN and will have to be checked by measurement. In addition, low distortion operation of the proposed concept will have to be checked with LTE

signal through further investigations on dynamic tuning of the TMN and time alignment between the RF signal and the TMN control signal.

In conclusion, the proposed concept of load adaptive PA shows significant potential for energy savings in the context of small-cell BS, with an average power reduction of 30%. This concept is complementary with the other energy efficiency enabling techniques for small-cell BS, except with the adaptive energy efficient PA presented in the previous section.

3.5. LOW-LOSS ANTENNA INTERFACE

The efficiency of commercial base station antennas is rarely specified, but can be estimated in the range of 80-90% which leaves low margin for improvement. The *Low-loss Antenna Interface* task aims at a global optimization of the Tx front-end with a focus on the opportunities offered at the antenna level to reduce the constraint on other components. More specifically, it deals with the improvement of the energy efficiency of the front-end in classical FDD architectures for LTE small-cell applications [BoDG11]. The key idea consists in eliminating the duplexer by using a dual polarization antenna which ensures at least 30dB isolation between Tx and Rx accesses [EARTH-D4.1], FIGURE 35. Compared to the end-user terminal, the concept of *duplexing antenna* is more relevant in this context because no close vicinity of the user hand can degrade the isolation between the Tx and Rx antennas.

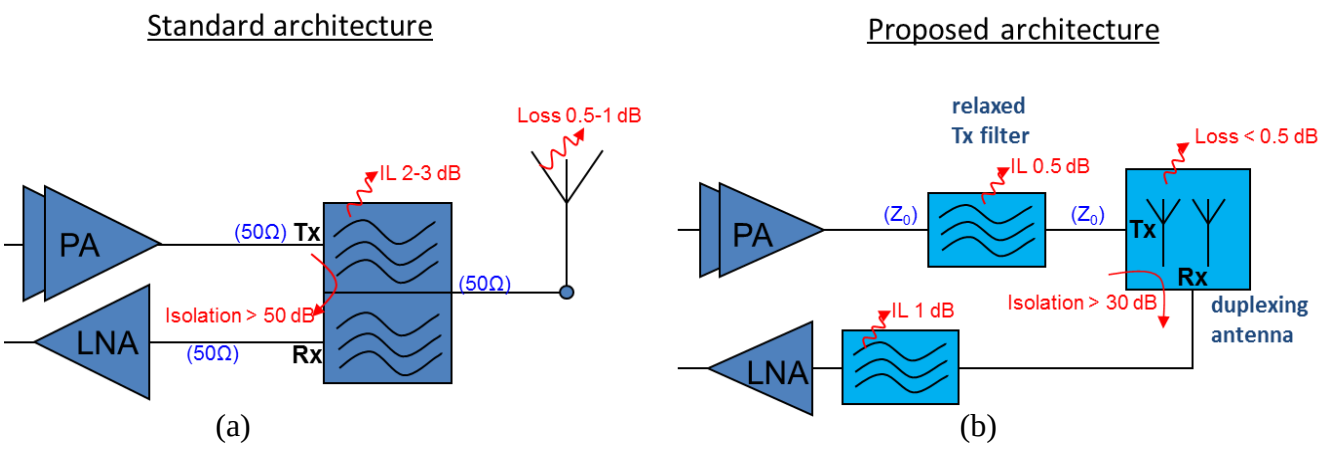

FIGURE 35. Comparison between standard (a) and proposed (b) RF front-end architectures with different places of the duplexing function

Typical state-of-the-art duplexers for small cell BSs, which are based on SAW or BAW technology, exhibit isolation levels between Tx and Rx ports in excess of 50 dB. Insertion losses depend on the Tx and Rx frequency-bands separation and are typically in the range 1.5-3 dB. A SAW duplexer from Anatech® [duplex] with 2.2 dB losses has been selected to be incorporated on the standard RF front-end which will be used as a reference for the energy efficiency validation of the task. To reach the classical required 50 dB Tx/Rx isolation level for the proposed architecture, an additional Tx filter with relaxed constraints has been designed. This allows reaching excellent insertion loss lower than 0.5dB measured over the whole DL frequency band.

The concept presented above is investigated through electromagnetic (ANSYS HFSS®) and circuit (ANSYS Designer®) simulations for the antenna and circuit components respectively. Two different antennas have been designed: the *Full Band1* antenna and the *Dedicated UP/DL* antenna. Both have two accesses, one for the Tx chain and the second for the Rx chain.

Both accesses of the *Full Band1* antenna cover the whole LTE band 1 frequency range (1920 – 2170 MHz); whereas the Tx access of the *Dedicated UP/DL* antenna covers only the DL frequency band (2110 – 2170 MHz) and the Rx access covers only the UL frequency band (1920 – 1980 MHz). The FIGURE 36 illustrates the return loss and isolation between the Tx and Rx accesses for both simulated antennas. Compared to the *Full Band1* antenna, the Dedicated UP/DL antenna presents a better impedance matching ($|S_{11}|$<-15 dB) and a simulated isolation better than 45 dB on the more critical Rx frequency band.

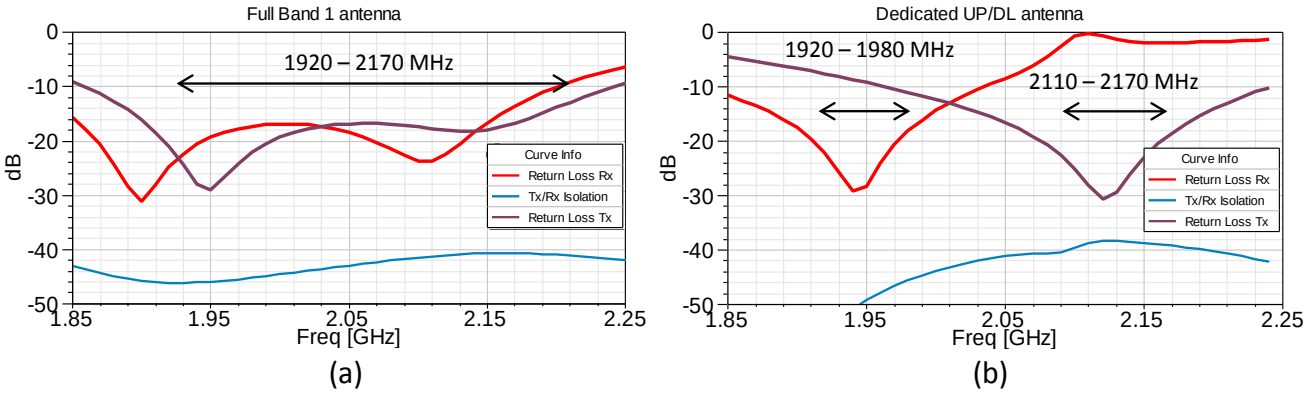

FIGURE 36. Return Loss and Tx/Rx isolation for the Full Band1 (a) and Dedicated UP/DL antennas (b)

The FIGURE 37 illustrates the dual-port slot-coupled patch antenna which is the main structure of both presented antennas. A back cavity has been added both to ensure better front to back radiation ratio and also to improve the Tx/Rx isolation. A thin (0.8 mm) dielectric substrate is used for the patch; which minimizes dielectric losses and so ensures a radiation efficiency better than 90 % for the patch antenna. Its radiation pattern presents a 90° lobe aperture with a maximum gain of 8 dBi over the whole frequency band. The plastic radome is positioned 2 cm above the patch to check whether its impact on Tx/Rx isolation level is kept non-significant.

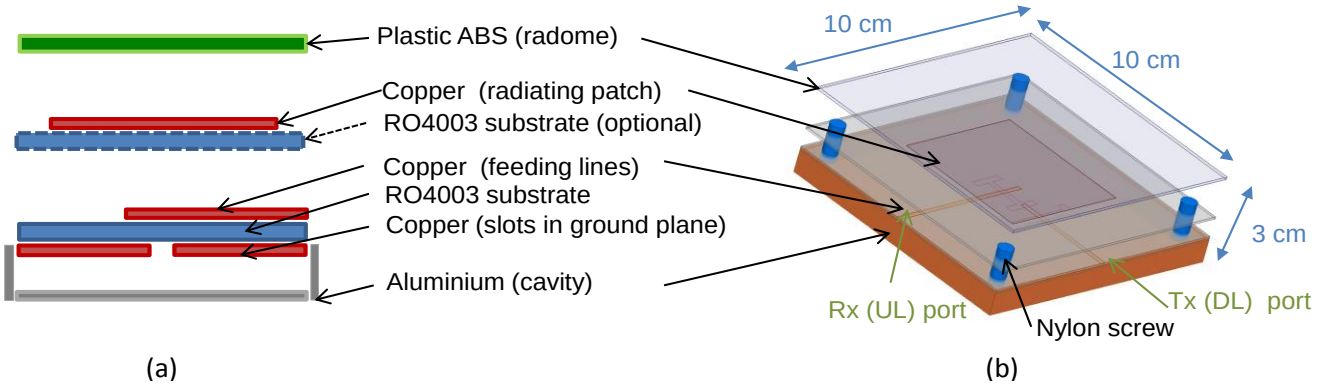

FIGURE 37. Antenna structure: layers description with material (a), 3D view of the simulated structure (b)

Concerning the energy efficiency improvement, a detailed comparison between standard and proposed front-ends provides a significant loss reduction of 2 to 3 dB on the Tx chain, TABLE 2. Next step concerns the antenna prototype measurements. Antenna Tx/Rx isolation could be delicate to retrieve in measurements due to prototype realization dispersion.

TABLE 2. Loss for the different components and energy efficiency of the proposed concept

	Standard Arch. (EARTH OFF)	**Proposed Arch. (EARTH ON)**
Anatech Saw Duplexer/Relaxed Filter Loss	2 – 3 dB	0.5 dB
Antenna Loss	0.5 – 1 dB	0.5 dB
Total Loss	**2.5 – 4 dB**	**1 dB**
Antenna Interface energy efficiency (%)	56 % – 40 %	80 %

This part of the RF front-end is a passive hardware solution, thus this task and its results are fully scenario-independent. This energy efficiency improvement can be applied for each small-cell base station, whatever traffic load and scenario deployment. Nevertheless a stronger Tx/Rx isolation specification may be one of the major limitations of the proposed solution by applying it to macro-cell BS.

Condition 1: Polarization channel distribution
The proposed approach assumes that the propagation channel in the small-cell, re-distributes the energy from the base-station on both polarizations on the handset antenna(s). Thus a +45° orientation polarised signal radiated by the BS will be received with the both +45° and -45° orientations on the user terminal antenna. This assumption is usually used in dense multipath radio channel propagation.

Condition 2: Linear polarisation
The *duplexing antenna* radiates and receives two orthogonal (here linear) polarizations with the same co-located radiating element. This antenna concept cannot be used to implement polarisation diversity.

To conclude, the *Low-loss Antenna Interface* solution improves from 40 % to 80 % the global energy efficiency of the antenna interface. This passive solution is fully scenario-independent and is complementary with all energy efficiency enabling techniques for small-cell BS. To reach this improvement, both the Tx/Rx isolation and Tx filtering functions are partially moved from a lossy duplexer component to an efficient *duplexing antenna*. The out of band TX rejection have still to be characterized on the whole RF front-end prototype.
This work is actually coordinated with the investigations on the PA and its tuneable matching networks. The proposed architecture is a first step aiming to characterize the role of the relaxed Tx filter. A further step concerns how this filter can be removed to process an efficient co-design between the PA matching network and the *duplexing antenna*.

4. LOW LOSS ANTENNAS

The antenna is a very special component of the transmission and reception chains. In fact, as the last (first) block of the transmission (reception) chain, its energy efficiency has a direct impact on the overall energy efficiency of the telecommunication system. This chapter deals with energy efficiency improvement of arrays of printed antennas used in BSs.

The analysis is focused in using a cheap foam substrate to improve the antenna energy efficiency. Foam provides a good compromise between electromagnetic and mechanical requirements. From the electromagnetic point of view it is (macroscopically) almost air (low losses and a typical relative dielectric constant of 1.06) but it is mechanically enough stiff. Moreover, a bandwidth enhancement can also be obtained [IsKBCY08].

4.1. VALIDATION OF SOFTWARE TOOLS

Software tools are essential in the design and optimization procedure of modern antenna systems. However, even nowadays powerful software tools need experimental validation. The patch configurations shown in FIGURE 38 have been used to validate several software packages. For sake of compactness only the results obtained for the square patch with ENSEMBLE [ENS98] and CST Microwave Studio [CST11] are considered here. Simulation input reflection coefficient and radiation pattern results are compared with experimental results in FIGURE 39.

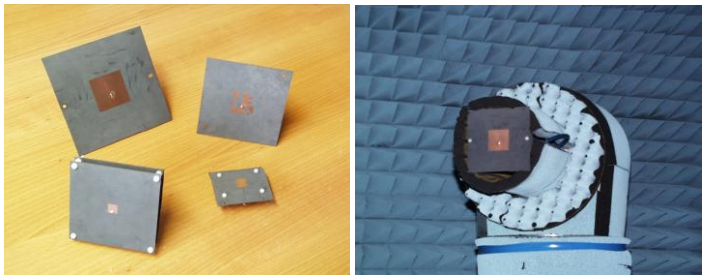

FIGURE 38. Antenna prototypes used to validate software tools.

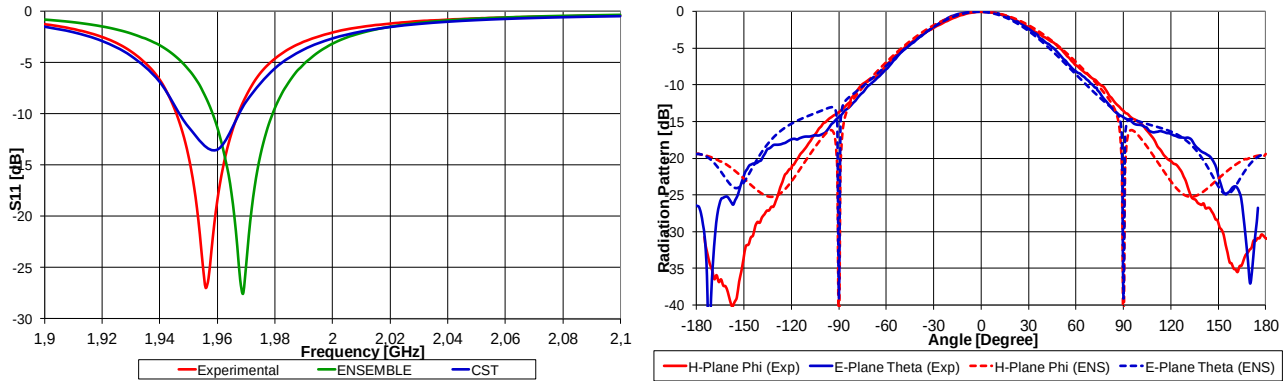

(a) (b)

FIGURE 39. Comparison of square patch simulation and experimental results; (a) Input reflection coefficient, (b) Radiation pattern (at 1.96 GHz).

The input reflection coefficient has been measured with a Vector Network Analyzer and the radiation pattern has been measured in a far-field anechoic chamber. The test case is a square patch (L=W=50 mm) printed on a 1.575 mm thick Rogers Duroid 5880™ substrate (ε_r=2.20, tanδ=0.001) over a square ground plane (L_{gp}=W_{gp}=3L). The patch is fed with a 50 Ohm coaxial probe 17.4 mm from the border.

Both software tools predict very well the patch behaviour. The resonance frequency deviation is smaller than 0.7% and there is a perfect bandwidth agreement. The radiation pattern results show also a very good agreement, except at the back of the antenna ($|\theta|>100°$) due to the shadow effect of the azimuth positioner. Therefore, for the square patch, both software tools provide reliable simulation results.

4.2. MEASUREMENT OF FOAM CHARACTERISTICS

There is no information available concerning the macroscopic characteristics of the foam under consideration. Therefore both relative dielectric constant (ε_r) and loss tangent (tanδ) need to be measure. Due to its simplicity the free space method [Mont47] has been chosen. As shown in FIGURE 40a, a set of standard horn antennas covering the frequency range 1.5-12 GHz has been used. The measurement setup configuration is shown in FIGURE 40b.

(a) (b)

FIGURE 40. Measurement of foam characteristics; (a) Standard horns; (b) Measurement setup.

The results obtained are shown in FIGURE 41. The relative dielectric constant is 1.06±0.02. The loss tangent results are not accurate but can be estimated as 0.001±0.0005.

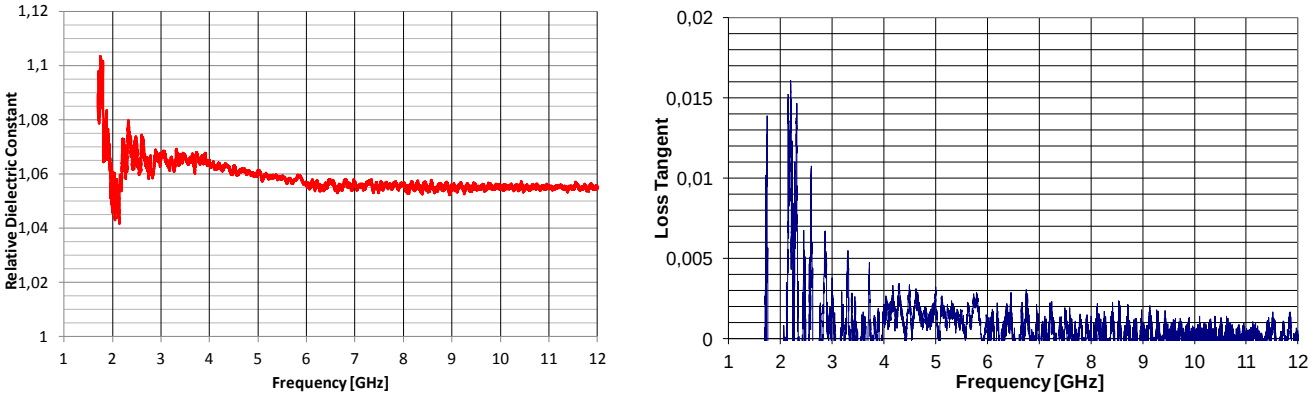

(a) (b)

FIGURE 41. Experimental macroscopic foam characteristics; (a) ε_r; (b) tan δ.

A 29.7 mm thick large panel has been used. As it can be observed in FIGURE 41, the method is more accurate for the higher frequencies. This is because the electrical thickness (thickness in wavelengths) increases with frequency (from 0.1485 at 1.5 GHz to 1.188 at 12 GHz) providing a more pronounced effect of the dielectric material in the transmitted signal phase (calculation of ε_r) and amplitude (calculation of tanδ). If more accurate results are needed a different setup (with the panel inclined to increase the electrical thickness) must be used in a complete anechoic environment [Mont47].

4.3. PRINTED ARRAY EE IMPROVEMENT

The horizontal plane radiation pattern of a single patch (shown in FIGURE 39b) is usually adequate for coverage of a 120 ° BS sector cell. The -10 dB beamwidth in that plane is about 130 °. However, a more directive radiation pattern is required in the vertical plane. Therefore base stations usually use vertical arrays of several elements (typically 4 to 8) to cover each 120 degrees sector with down tilt.

A 2 GHz vertical uniform array of 4 patches with vertical polarisation and parallel microstrip transmission line feeding is considered as a case study. The array inter-element spacing is 90 mm (0.6 λ). The analysis is carried out for the array (elements and feeding line) printed on the selected foam substrate and on three other common substrates (Rogers Duroid 5880™, Rogers RO 3003™ and FR4) 3.175 mm thick. Rogers Duroid 5880™ is a high quality and expensive microwave substrate, and Rogers RO 3003™ is a RF and microwave low cost substrate. FR4 is a very cheap substrate used in low frequency printed circuit board applications. The macroscopic characteristics of these substrates, at 2 GHz, are indicated in TABLE 3.

For low loss substrate arrays most of the losses come from the narrow feeding line metal. That is not the case of the FR4 where most of the losses are dielectric losses. The mutual coupling between antenna elements can also contribute to decrease the energy efficiency. However, in this case, the mutual coupling is below –15 dB meaning that its contribution to losses is below 3%.

The array total energy efficiency is indicated in TABLE 3. The foam substrate provides an energy efficiency improvement of about 15% over RO 3003™ and about 58% over FR4. The improvement over the Rogers Duroid 5880™ is only 1% in this case study. However, substrates with the same thickness have been considered and, to fulfil the bandwidth specifications (for instance, as stated in section 3.1, LTE band 1 requires a frequency range 1920-2170 MHz, which is about a 12.2% bandwidth), the Duroid 5880™ must be substantially thicker, leading to more losses. Moreover, if an 8 elements array is needed, the foam improvement will be even higher.

TABLE 3. Energy efficiency of a 4x1 array of patches printed on different substrates.

Substrate	ε_r	tan δ	energy efficiency [%]
Foam	1.06	0.001	96.4
Rogers Duroid 5880™	2.2	0.001	95.4
Rogers RO 3003™	3.0	0.005	81.8
FR4	4.0	0.03	38.2

To illustrate the above mentioned dependence of bandwidth on substrate dielectric constant and thickness, the input reflection coefficient of a square patch printed on 3.175 mm thick foam and Duroid 5880 substrates is presented in FIGURE 42. For a reference level of -10 dB (which corresponds to 10% reflected power) the (input impedance) relative bandwidth of the Duroid 5880 printed element is 2.3% while the one printed on foam provides 2.7%.

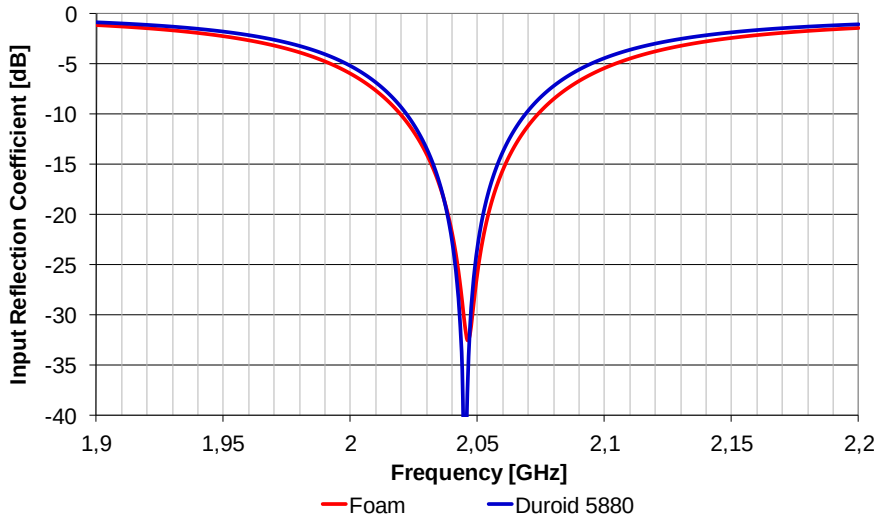

FIGURE 42. Input reflection coefficient of foam and Duroid 5880 printed patches.

In an LTE BS array (for instance with 8 elements) printed on a Duroid 5880 substrate the energy efficiency is lower than the foam substrate solution not only because the dielectric losses are higher (thicker substrate) but also, and mainly, because surface wave losses are also higher (thicker substrate with higher dielectric constant). The drop in energy efficiency can be estimated to be about 2-4%.

The radiation pattern of the 4x1 elements array printed on the foam substrate is shown in FIGURE 43. The vertical plane –10 dB beamwidth is about 36 ° (the horizontal plane -10 dB beamwidth remains about 130 °).

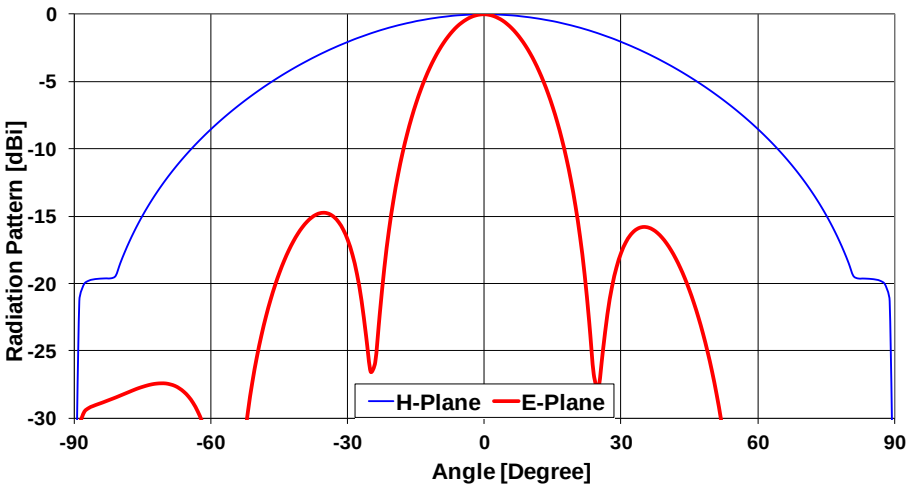

FIGURE 43. 4x1 foam array radiation pattern (at 2 GHz).

4.4. CONCLUSIONS

Being the first device of the BS uplink (last device of the downlink) the antenna energy efficiency has a net effect on the system energy efficiency. Therefore the proposed antenna solutions can be combined on top of any integrated solution for the reception and transmission chains.

It has been shown that the proposed foam substrate can provide an average improvement of about 15% over a common printed array solution (printed on RO 3003 substrate). Even comparing with an expensive LTE array configuration with 8 elements, printed on Duroid 5880 substrate, the energy efficiency improvement has been estimated as about 2-4%. These energy efficiency improvement figures provided by the foam substrate are based on numerical simulations obtained with validated software tools. Antenna array prototypes will be fabricated and tested to confirm the simulation results. The overall energy efficiency improvement provided by the proposed antenna solutions depends on the percentage of printed antennas used on the BS networks. Just as an indication, a Portuguese operator estimates that 30% of its 3G network BSs are equipped with printed antenna arrays.

5. ADAPTABILITY TO SYSTEM DYNAMICS

As described in [EARTH-D4.1], there is a large difference in energy consumption per bit when transmitting with the highest modulation and coding rate compared to the lowest one. To meet BER performance constraints, the appropriate modulation and coding rate is selected by means of a channel quality indicator (CQI) index that is an indication of the channel quality. Adaptive modulation and coding rate adapts the transmission scheme to the channel conditions, i.e., when the channel conditions are good, a high CQI index will be used since a high throughput communication is possible. In bad channel conditions, energy-inefficient modulation and coding schemes need to be selected to ensure that BER requirements can be met.

However, by not transmitting under bad channel conditions in certain time slots in the hope of having better conditions in the next slots, we can trade off packet delay with energy consumption. This can be reflected in a scheduling algorithm that sends packets as long as good channel conditions are present, therefore using medium to high rate transmission schemes. When the conditions are not good enough, these packets could be buffered expecting to be sent when the conditions improve or, if too long, when a delay timer expires. This can be explained through FIGURE 44.

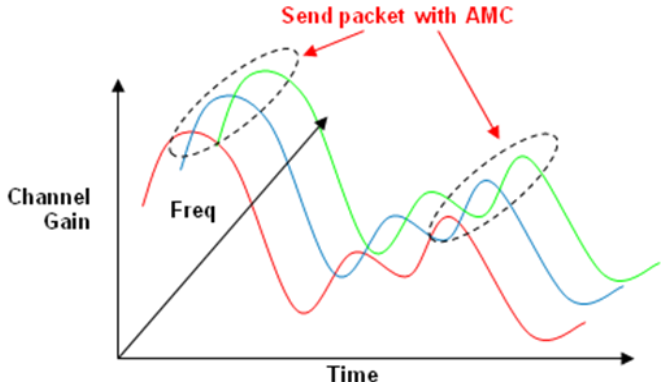

FIGURE 44. Time-dependent scheduling: send more bits when energy-efficient modulation and coding rates can be used.

The energy saving comes from the scaling down of the baseband power by processing only the resources to be transmitted at a certain moment. The energy efficiency per transmitted bit is higher with higher modulation and coding rates since we process more useful bits with the same amount of power. In other words, for the same throughput less power will be consumed if the channel characteristics in time and frequency are exploited to allow higher modulation and coding rates. Evidently, the drawback of not transmitting during periods with bad channel conditions is that packets will get delayed, but in a small cell scenario, with limited number of users, and different user applications, the packet delay should have a minor impact. Additionally, with less users, the system can find more opportunities to scale down and even to go completely to sleep mode.

In a multi-user environment, it is unlikely that all the users will be in a channel dip. However, for the users facing a bad channel, we could avoid the processing of their resources during those dips. Although in a macro-cell the contribution of the baseband power to the total power breakdown is small, in smaller cells this contribution is larger as can be seen in FIGURE 45. This contribution is even higher with UL traffic where the PA of the base station is not active and the baseband consumes hence a larger portion of the power breakdown.

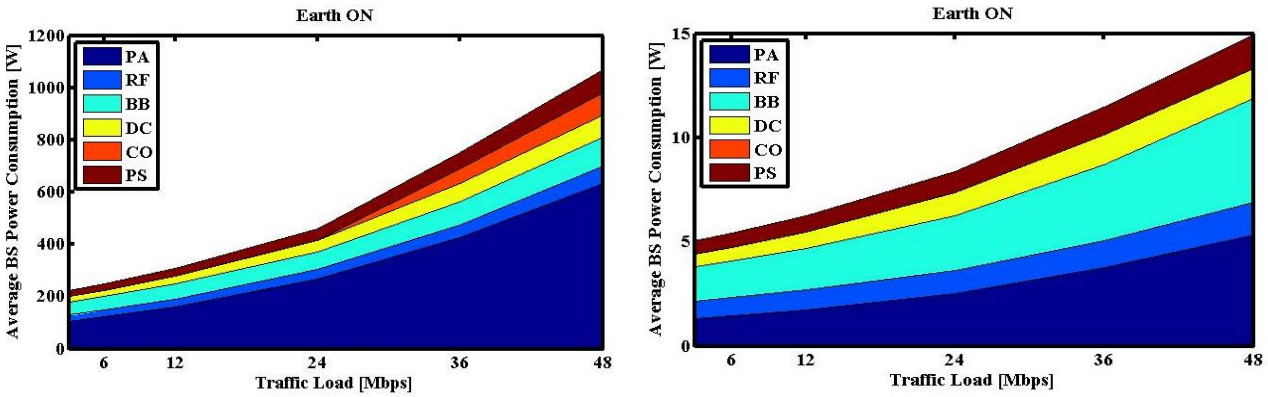

FIGURE 45. Power consumption of a macro base station on the left plot (a) and a pico base station on the right plot (b).

To validate our approach we propose the following scenario. We simulate the system/network level scheduling behaviour of a pico base station with 10 MHz of frequency bandwidth, 2 antennas, and 3 users randomly located in a radius of 60m. In our benchmarking scheduling approach we will assign resources to the terminals on those resource blocks with the highest reported CQI at every certain time slot, but we will keep some fairness by assigning the same amount of resources to each user. The CQI reported by the UE represents the highest modulation and coding rate that an UE can use to achieve a transport block error rate of less than 10%. In our energy efficient scheduling approach, we will assign resources only if the CQI reported on those resource blocks is higher than a threshold; otherwise we will buffer the packet until the reported CQI exceeds that threshold. For each user we assume a constant application throughput that sends packets in a random way every 2.5 ms in average.

In FIGURE 46, we observe an example of the variation of the mean CQI reported for the resource blocks allocated to each UE. We can observe that dips in the reported CQI are frequent but not long lasting. Therefore, during these dips we could benefit of downscaling the aggregate system/network power to serve only the UE with best channel conditions at that moment.

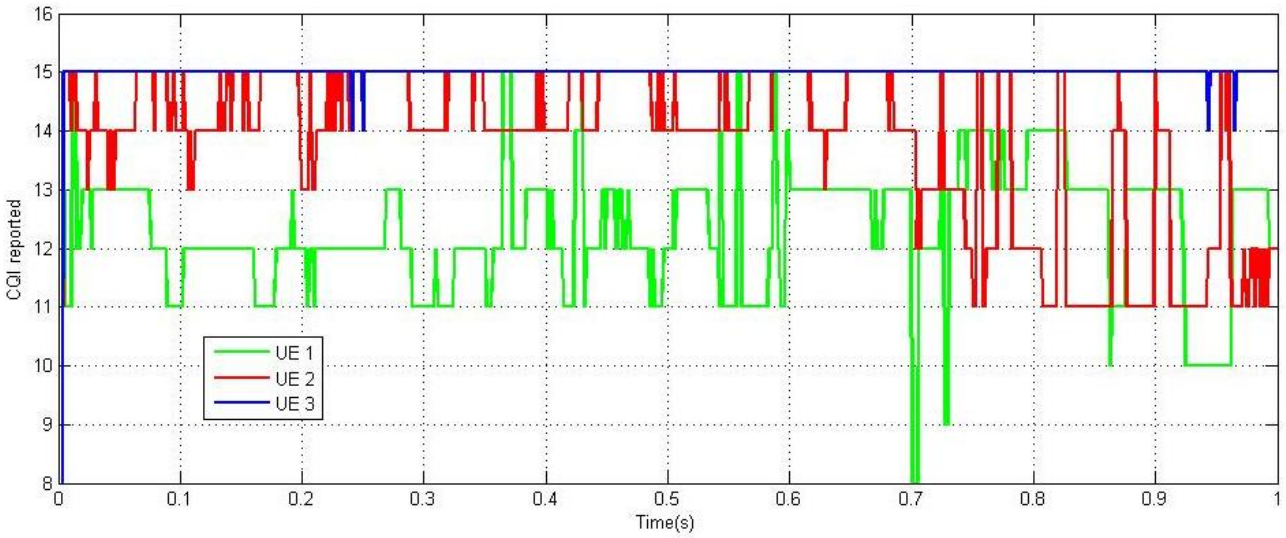

FIGURE 46. CQI reporting for three UEs.

The main parameter in the proposed scheduler is a threshold that determines when we should buffer a packet. This threshold is given by the CQI reported by the UE in a certain resource block. If the CQI is larger

than this threshold for a particular user, we postpone its transmission to the next time slot with a CQI higher than the threshold. With this measure, the base station will not process the blocks corresponding to the users with bad channels.

FIGURE 47 shows the instantaneous and the average energy consumption with different CQI thresholds compared to the case with no threshold at all. As can be seen, the average energy per bit can be reduced by 1%, 5%, 14% or 33% as we increase this threshold from CQI 9, 11, 12, and 13. Evidently, the price to pay is the packet delay, which was computed in average per user every time a packet need to be delayed for 1 ms. The average delays were computed as 0.05 ms, 0.15 ms, 1.4ms and 6 ms, which in the worst case represents a marginal degradation. For users with constantly bad channels a delay timer was implemented to avoid starvation of resources.

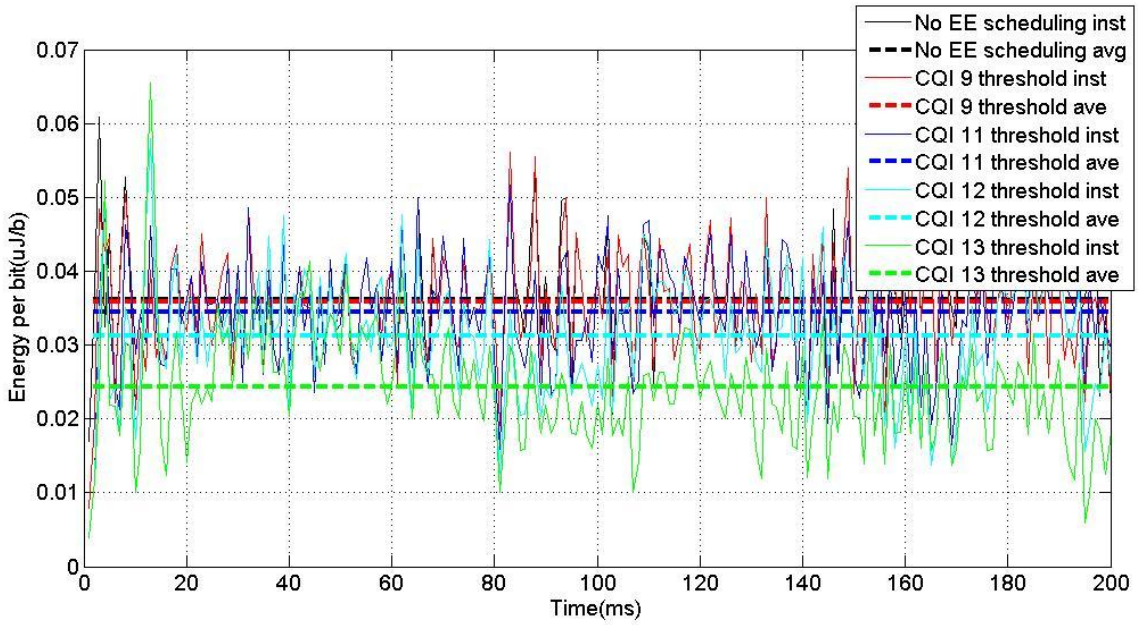

FIGURE 47. Instantaneous energy consumption.

Obviously we are dealing with a small-cell scenario where the channel statistics are normally good. In a scenario with more variable channel statistics, the system could profit more from the channel dips of the users. Furthermore, we could exploit information from application layers to buffer packets.

The main area of application of this solution is the scenario where the network load can be considered low or medium and there are hence margins in the application layer requirements to buffer or delay packets. More specifically this solution finds the largest potential when user applications are less delay or throughput sensitive and can allow some buffering of the packets until good channel conditions arrive. In a small cell environment, dips in the channel frequency response can be common but usually not long lasting. This allows the base station to scale down the system and to serve only those users that have good channel conditions reported at a certain time slot. As such, the optimization time scale of this approach is in the range of milliseconds.

This approach can fit perfectly in the rest of the solutions at network, system, and node level. The complete picture of the application areas for each solution can be seen in [EARTH-D6.2a]. Our solution is based on buffering packets at millisecond level based on the channel conditions reported by the users, therefore all the techniques considering MIMO techniques, beamforming, and energy efficiency transceivers and antennas are independent from our approach so they can be perfectly coupled because their area of application is different from our approach. Particular attention is needed with solutions such as bandwidth adaptation (fast) and Cell DTX (micro) since they have the same area of application. Since the buffering of packets might slightly increase

the network load in future time slots, these might impact the sleeping periods or the adaptation of the bandwidth in such periods. However, we expect this impact to be marginal in the case of bandwidth adaptation and beneficial in the case of sleeping periods.

6. CELL DTX

The main motivation behind this chapter is to further elaborate the discontinues transmission (cell DTX) concept, i.e. when de-activating the radio parts of a transmitter at the network side, which was introduced in [EARTH-D4.1]. Cell DTX is an enabler for energy efficiency improvements.
There are four modes of DTX, ranging from duration from one or a few OFDM symbols to several hours. For LTE it makes sense to relate the DTX mode to the sub-frame (1 ms) and radio frame duration (10 ms) as follows:

1. Micro DTX: Radio unit is turned off in time intervals less than 1 ms. No changes occur in the control signals. This type of DTX is supported in LTE Rel-8 and is depicted in FIGURE 48.
2. MBSFN-based DTX: Radio unit is turned off in time intervals less than 10 ms. Radio frame consists of a combination of micro DTX transmission configuration and MBSFN sub-frames. It is visualized in FIGURE 49.
3. Short DTX: Radio unit is turned off in time intervals less than 10 ms (but at least equal to 1 ms). As can be seen in FIGURE 50, CSRSs are removed; therefore, UEs perform mobility measurements on primary and secondary synchronization signals (PSS, SSS). Only SSS, PSS and PBCH transmissions are mandatory.
4. Long DTX: Radio unit is off in 10 ms or longer durations. The long DTX duration shall however not be so long that the UEs are not able to perform initial cell search and mobility measurements.

During this chapter, focus will be on the first three ones, and details on how they can be realized and operational will be given. Moreover, system simulations are performed and presented in the following section in order to evaluate the network energy consumption reduction by the proposed cell DTX modes.

6.1. MICRO DTX

An example of a downlink radio-frame in LTE is presented FIGURE 48. It consists of 10 sub-frames of 1 ms duration each, numbered from 0 to 9. In FIGURE 48, one radio resource block element is visualized. It consists of 14 OFDM symbols in time domain and 12 sub-carriers in frequency domain.

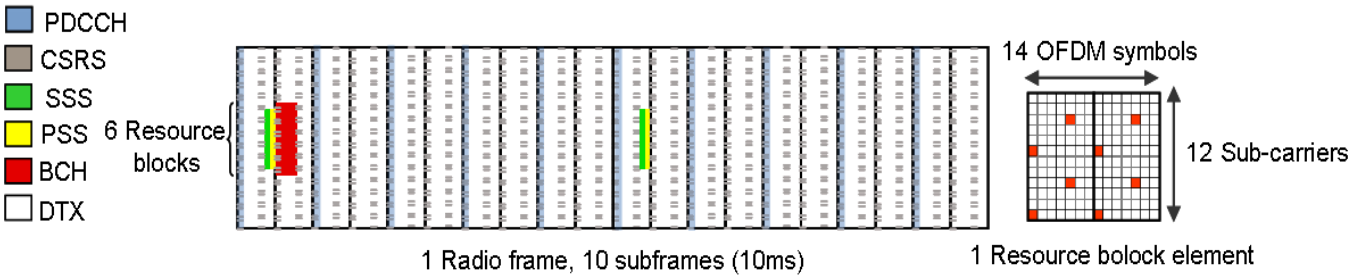

FIGURE 48. LTE downlink radio frame with 10 sub-frames showing cell specific reference symbols (CSRS) for one antenna port, downlink control region (PDCCH) with a size of one OFDM symbol, primary and secondary synchronization signals (PSS and SSS), and broadcast channel (BCH). Only micro DTX is possible.

The duration of the entire radio frame is 10 ms. At the beginning of each sub-frame there is a downlink control region (not shown in the figure) spanning one to three OFDM symbols. The primary and secondary synchronization signals (PSS and SSS, respectively) are transmitted in the last two OFDM symbols of the first slot in sub-frames 0 and 5 and the physical broadcast channel (PBCH) is transmitted over three OFDM symbols in the second slot of sub-frame 0. CSRS are used as demodulation reference, for channel quality estimates, and

for mobility measurements as discussed in [EARTH-D4.1]. The white resource elements are intended for user specific data.
By switching off the radio during the OFDM symbols in between the CSRS transmission, **micro DTX** can be realized in LTE.

6.2. MBSFN-BASED DTX

Beside the normal (unicast) data sub-frames, LTE Rel-8 also provides a special type of sub-frames, i.e. the multi-cast and broadcast single frequency network (MBSFN) sub-frame (which is standardized for broadcasting data from a single BS or couple of BSs to the UEs), as illustrated FIGURE 49. This type of sub-frame consists of a short control region at the beginning of the sub-frame, similar to the normal sub-frames, while the rest of the sub-frame may be empty. Six (1, 2, 3, 6, 7, and 8) out of the ten sub-frames in a radio frame can be configured as such MBSFN sub-frames (LTE standard does not support configuration of 8 MBSFN sub-frames currently).

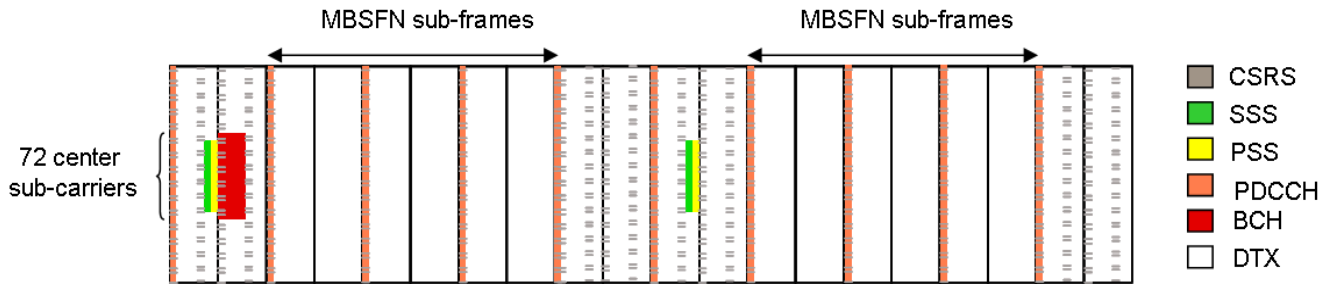

FIGURE 49. Example of a downlink radio frame in LTE with 6 MBSFN sub-frames showing downlink control region (PDCCH) with a size of one OFDM symbol, primary and secondary synchronization signals (PSS and SSS), and broadcast channel (BCH).

One Rel-8 compatible method to improve the cell micro DTX scheme is to introduce one or several MBSFN sub-frames. This can reduce the average cell power use at low load since fewer cell-specific reference symbols need to be transmitted. Thus when the traffic load is low we can, in order to reduce energy consumption, configure a cell with up to 6 MBSFN sub-frames that are not used. Hence, in FIGURE 49 we see the minimum amount of signals that need to be transmitted in a cell with no traffic at all (in addition higher layer system information is required on a less frequent time scale than a radio frame, not shown in FIGURE 49). There is a significant possibility to reduce energy consumption with cell DTX in LTE Rel-8. When counting the actually transmitted OFDM symbols in a radio frame with 6 MBSFN sub-frames and assuming a PA wake up time of 30 µs it becomes apparent that the PA can be in low power DTX mode in 74% of the time when there is no traffic in the cell. This simple calculation alone gives some indication that cell DTX is an effective method for reducing energy consumption in LTE when there is no or very little traffic.

It should be clear that introducing MBSFN sub-frames can lower the power use by allowing for a more efficient DTX scheme. There are, however, also negative consequences, both in terms of reduced cell capacity and degraded user throughput. Hence, it is of importance, if not inevitable, that fast switching between MBSFN configurations can be performed in an adaptive manner. The adaptive mechanism would switch from many MBSFN sub-frames at low activity and react to changes in the traffic situation by removing the MBSFN sub-frames when traffic increases. The current mechanism for switching between MBSFN configuration is via system information and hence not a particularly fast method; in LTE Rel-8 we may only change the information on the system broadcast channel once every 40 ms according to specifications, in practice even longer. Therefore, in future LTE releases it is important to allow for unicast data transmission also in sub-frames that are configured for MBSFN use.

6.3. SHORT DTX

By examining FIGURE 48 precisely, one realizes that the CSRS are the most abundant signals which need to be transmitted up to four times per sub-frame. CSRSs are used as demodulation reference, for channel quality estimates, and for mobility measurements. To put the radio in DTX mode, one logical idea is not to transmit the CSRSs all the time. CSRSs are used by the idle and active UEs to identify the cell during mobility measurements. If it is possible for the UE to perform the mobility measurements on the secondary synchronization signal (SSS) instead of CSRS, Although not included in the LTE standard today, this would enable turning off the radio units in more than four sub-frames (between the transmissions in sub-frame 0 and 5). This mechanism is called **short DTX** and is depicted in FIGURE 50.

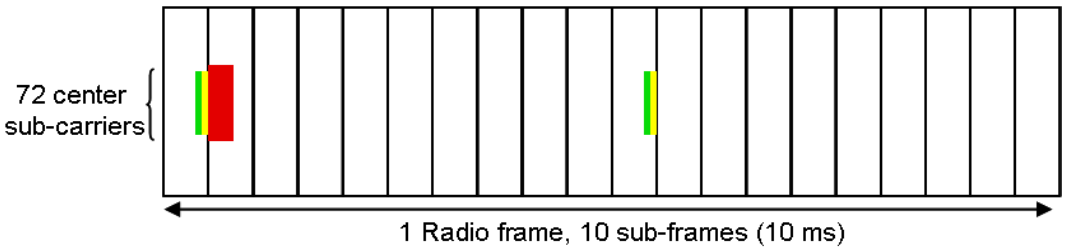

FIGURE 50. Proposed LTE downlink radio frame without CSRS. Short DTX can be applied.

6.4. EVALUATIONS

In order to determine in more detail how the network energy consumption depends on the traffic, we have performed system simulations that are presented in this section. The system simulations/evaluations are fully compliant with the EARTH scenarios and the Earth Energy Efficiency Evaluation Framework (E^3F) in [EARTH-D2.2] and [EARTH-D2.3].

Short-term, small-scale evaluations were conducted for a macro-cellular network with regular hexagonal cell layout. 19 sites, each with 3 sectors, 10 MHz bandwidth operating at 2.1 GHz carrier frequency are assumed. Moreover, for 2x2 MIMO transmission cross-polarized antennas are employed at both base station and user terminal. The transmitter utilizes adaptive precoder selection with rank adaptation; whereas the two receive antennas perform MMSE combining for interference suppression. The inter-site distance (ISD) for urban environments is set to 500 m, whereas the ISD for suburban and rural areas is 1732 m. In all deployments users are uniformly distributed and move with a velocity of 3 km/h. Users arrive in the network according to a Poisson process and each user downloads a single file of 0.5 MB, according to the FTP file download model. To model different levels of (average) traffic load, system level simulations are conducted for different user arrival rates. Results are recorded for stable operational points only, i.e., for operational conditions in which packets, on average, enter and leave the system at the same rate. Four cases are simulated: 1) Transmission without DTX, 2) micro DTX mode, 3) short DTX mode, and 4) MBSFN-based DTX. When neither data nor control signals (broadcast channels, scheduling information, synchronization and reference signals, etc.) are to be transmitted, so that $P_{\text{out}} = 0$, a base station may go into micro sleep with reduced power consumption $P_{\text{sleep}} < P_0$.

FIGURE 51 shows the power per area unit P/A, as a function of the traffic demand per unit area. The difference between the results visualized in the two figures is that it is assumed that the power consumption during short DTX is identical to the power consumption in micro DTX in FIGURE 51 a). This is the case for the

current hardware being developed in the chapter 2. However, since short DTX facilitates longer sleep intervals, there should be potential for a deeper sleep mode in which more components are turned off in this case. In this scenario, technology potential for energy consumption reduction becomes higher and to illustrate this we have here assumed that the power consumption in short DTX mode (deeper sleep mode) is one fourth of the power consumption in micro DTX mode ($P_{Short-DTX} = P_{Micro-DTX}/4$) which is presented in FIGURE 51 b).

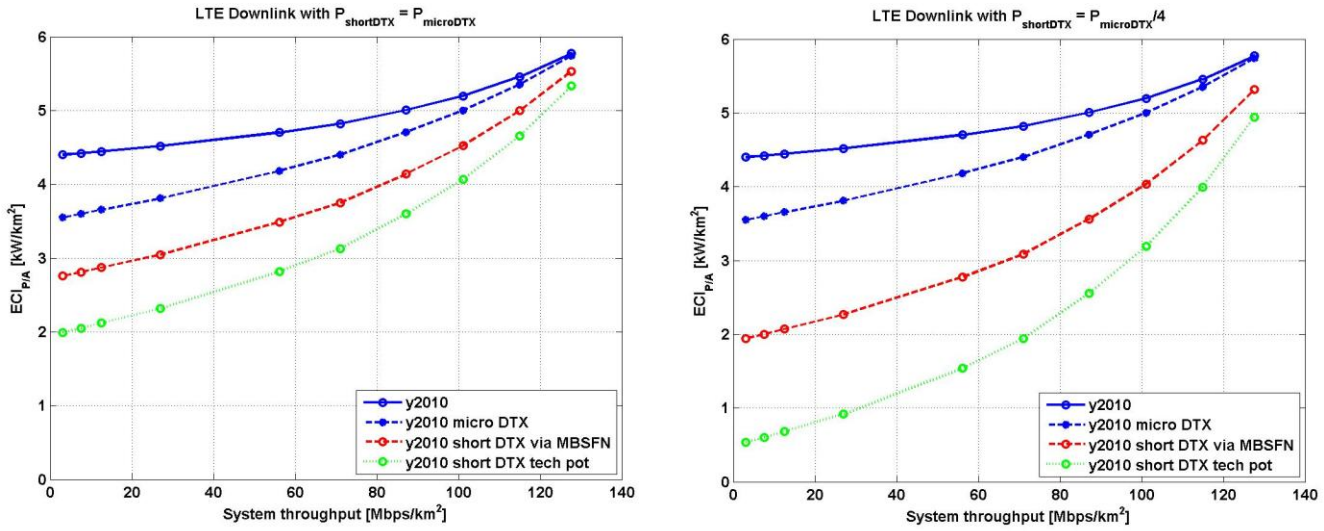

(a) (b)

FIGURE 51. Power per area unit as a function of system load and $P_{Short-DTX} = P_{Micro-DTX}$ (a), Power per area unit as a function of system load, system has deeper sleep mode and $P_{Short-DTX} = P_{Micro-DTX}/4$ (b).

As it is presented in FIGURE 51 a), the power consumption decreases from 4.4 kW/km^2 at low loads to 2 kW/km^2 when going from normal transmission to short DTX mode and when the empty sub-frames are totally shut down, the power consumption decreases to 0.5 kW/km^2 in short DTX mode shown in FIGURE 51 b). In an urban scenario, with an ISD of 500 m corresponding to a coverage area of 0.22 km^2 per site, the power per area unit is around 4.4 kW/km^2 at low loads, whereas it approaches 5.7 kW/km^2 at high loads. For the network with micro sleep capable base stations, the area power reduces to 3.55 kW/km^2 at low loads, whereas energy savings are diminishing at high loads. However; the energy consumption reduction is even more at short DTX via MBSFN. In MBSFN-based mode, six of ten sub-frames contain only the one slot PDDCH region which reduces the energy consumption to 2.8 kW/km^2 at low loads and 5.5 kW/km^2 at high loads (FIGURE 51 a). Assuming complete shut-off of the empty frames of the system in the MBSFN-based DTX, the energy consumption reaches 2 kW/km^2 at low loads and 5.3 kW/km^2 at high loads (FIGURE 51 a)). It should be mentioned that in short DTX via MBSFN case, a faster reconfiguration than what the standard allows is assumed.

The power consumption per area unit for suburban and rural areas (not shown here) is substantially lower, which is due to the increased ISD of 1732 m, corresponding to a coverage area of 2.6 km^2. However, the system throughput per area unit decreases accordingly, due to the increased site coverage area.

6.5. EVALUATION RESULTS AGGREGATED TO GLOBAL SCALE USING THE E^{3}F

To assess the gains of MBSFN and short DTX at a larger scale, aggregation to global scale according to the long term traffic model and large scale deployment model in [EARTH-D2.3] is done. The global average power consumption per area unit and energy per bit is given for two cases; $P_{Short-DTX} = P_{Micro-DTX}$ and $P_{Short-DTX} = P_{Micro-DTX}/4$.

FIGURE 52 presents the simulation results for power consumption per area unit and power consumption per bit in the high traffic density scenario. As is shown in the simulation results, MBSFN based DTX gives a power consumption reduction of one third compared to the reference system, while for the technology potential short DTX scheme, the energy consumption drops to less than half of the legacy system.

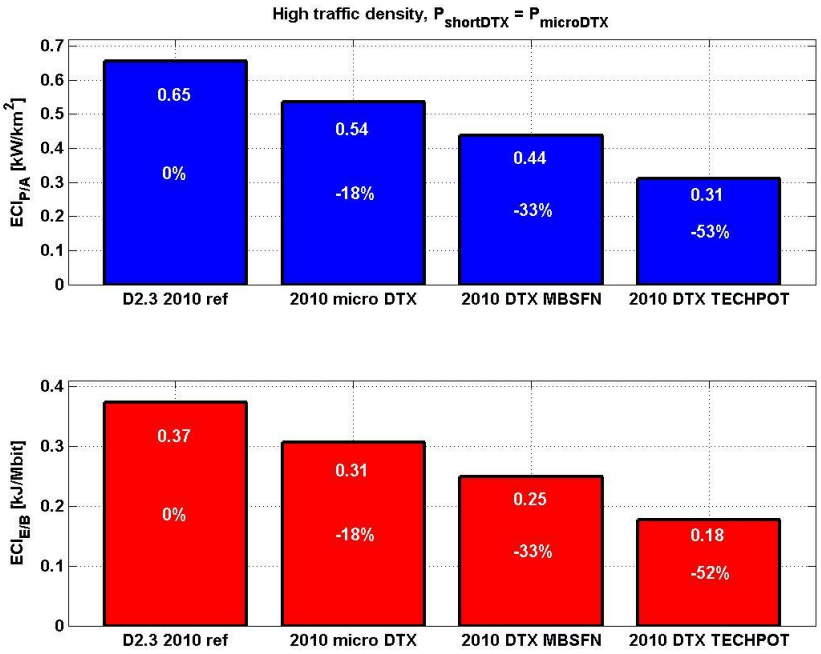

FIGURE 52. Global energy consumption per area-time unit and per bit in high traffic density network, using $P_{Short-DTX} = P_{Micro-DTX}$.

FIGURE 53 shows that the gains from reducing the short DTX idle power level below the micro DTX level ($P_{Short-DTX} = P_{Micro-DTX}/4$) also carries over to the global scale. This is due to quite low overall resource utilization in the aggregated scenarios.

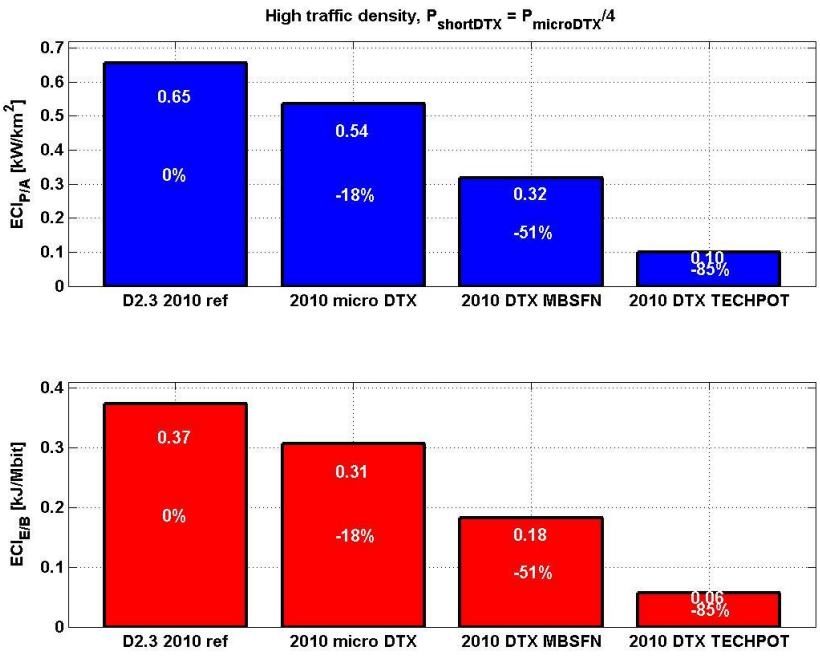

FIGURE 53. Global energy consumption per area-time unit and per bit in high traffic density network, using $P_{Short-DTX} = P_{Micro-DTX}/4$.

The overall energy reduction is 85 per cent for the technology potential short DTX case compared to the legacy LTE without DTX.

7. BANDWIDTH ADAPTATION

In macro base stations (BS) the power amplifier (PA) is the component with the highest energy consumption. Even when no data is transmitted the PA requires a DC voltage holding its fixed operation point. At present, the supply voltage is fixed independently of the traffic load. Power reduction can be achieved by:

- Adapting the operating point of the PA when the required signal load is below the maximum level.
- Deactivating the PA whenever no data or signalling is transmitted.

Very promising energy savings are possible in low load situations by making the scheduler aware of power saving modes of the PA. Therefore, different approaches have been investigated:

- **Bandwidth Adaptation (BW)**, which is based on the adjustment of the bandwidth to the required traffic load. Depending on traffic load the bandwidth can be stepwise downscaled that lower numbers of physical resource blocks (PRBs) are allocated. Then the PA can adapt to lower supply voltage and less reference signals have to be sent. This can be performed either by the usage of a fast carrier aggregation (CA) procedure or by an approach based on the reconfiguration of BS system parameters. The required CA procedure is currently not standardised by 3GPP and needs specification of a fast stepwise switching, e.g. between the lowest BW usage at 1.4 MHz and up to the highest BW usage at 10 MHz, which may be applied during night or in busy hours, respectively. The other solution using a reconfiguration of cell parameters is very slow and may impact the performance of cell-edge users.
- **Capacity Adaptation (CAP)** is a method, which does not change the maximum used bandwidth and the number of reference signals. An adaptation to lower load is performed by scheduling only a part of the subcarriers, i.e. limiting the number of scheduled PRBs. This approach allows lowering the PA supply voltage, but it is transparent to the mobile terminals and maintains frequency diversity.
- **Micro Discontinuous Transmission (DTX)** keeps the maximum used bandwidth and is based on a scheduling strategy, which creates as much as possible empty data transmission intervals at low traffic load. During an empty OFDM symbol, i.e. when no data and signalling are transmitted, some components like the PA could be deactivated. The required transmission for the reference signals limits the duration of micro DTX sleep intervals to only two or three OFDM symbols. More details on micro DTX are given in section 6.1.
- **Combination of BW Adaptation and Micro DTX**, and
- **Combination of CAP Adaptation and Micro DTX**.

The energy saving potential of above approaches and their combination with new PA solutions, which are described in section 2, has been evaluated by using a detailed power model for 2012, which is a function of signal load. The model is described in [EARTH-D2.3].

The characteristic of a Doherty PA with energy savings features (see FIGURE 54) has been used for these investigations. The state-of-the-art (SOTA) characteristic describes the energy consumption with over 100 W DC input power at full load, where a 10 MHz macro cell typical radiates up to 40 W output power. The lower curves show an improved PA with adaptability of the operation point by changes in the DC voltage. The use of a lower voltage limits the maximum output power due to saturation of the PA. The deactivation of the PA enables a micro sleep mode that allows very low power consumption of only 4.4 W during OFDM symbols with no transmission.

Other components, which make a significant contribution to the power consumption of a cell, are baseband processing, RF part, cooling, the limited efficiency of DCDC conversion, and ACDC power supply. A load dependent power consumption that is much lower as for SOTA has been considered for these other components [EARTH-D2.3]. For more efficient BSs, especially with the PA mounted close to the antenna (“remote radio head”, RRH), even passive cooling by air convection can be sufficient, which requires no power

consumption compared to an indoor BS system with constant high power consumption. Therefore, improvements by these other components including the PA have been additionally considered.

Beside the power characteristic of the components the traffic load is a significant aspect in assessment of the power consumption of a BS. The EARTH traffic model [EARTH-D2.3] is used for a cell in dense urban areas with 3000 subscriber/km² as well as a rural coverage cell with 100 subscriber/km².

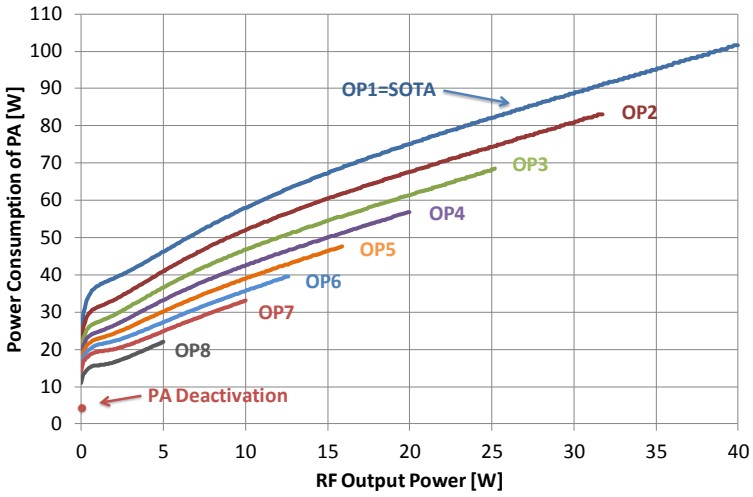

FIGURE 54. PA characteristics over RF output, depending on Operation Point settings (OPi with i=1,…,8)

The scheduler sets the principal physical parameters for the transmission at each subframe and, in consequence, decides about the radiated power. For the BW and CAP adaptation modes the scheduler adapts resources to bandwidths by equal utilisation of PRBs over a given time period. Depending on this load an optimised PA characteristic with limited output RF power can be used. On the other hand, a scheduler can reserve some of the time intervals (micro DTX) and set an energy saving deactivation mode of the PA during these times. The difference between the resource utilisation strategies is shown in FIGURE 55 for a BS at 40% of the maximum user data load. The scheduled user data is shown under consideration of the same fixed modulation and coding scheme for a standard LTE radio frame as illustrated in FIGURE 48. For the used example a bandwidth of 5 MHz meets already the load requirements for the BW adaptation approach compared to 10 MHz for the micro DTX approach. Therefore, less reference signals are transmitted for the BW adaptation approach.

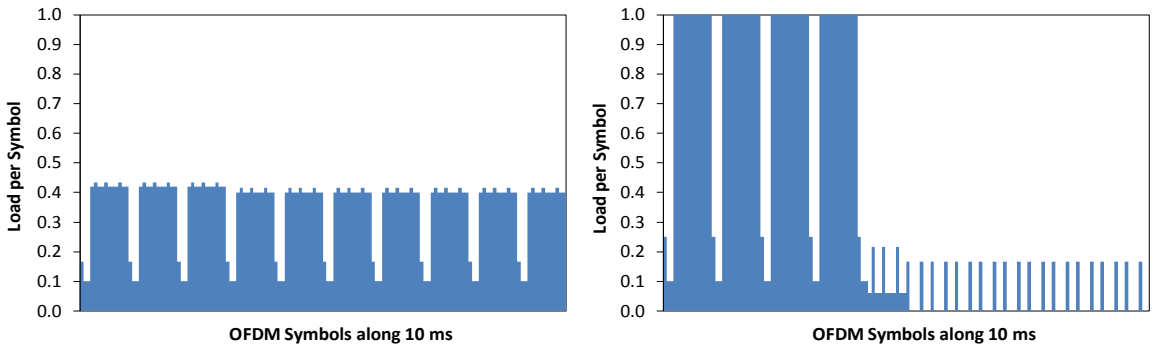

(a) (b)

FIGURE 55. Resource utilisation per symbol at 40% user load: (a) BW adaptation, (b) micro DTX

It is assumed that 1 user per subframe is scheduled, which requires on average 10% load during the first 3 symbols of a subframe for the control signalling information. The modelling of Physical Broadcast Channel and synchronisation is slightly simplified by reserving 6 PRBs in every 10th subframe. This leaves resources of 494 PRBs per 10 ms for scheduling of user data.

For a specific time t of a day the resource utilisation is calculated as a function of traffic load R(t) and of RRM strategy. Assuming a mean spectral efficiency of 1.76 bps/Hz the maximum user data capacity of a cell is C = 14.3 Mbps, excluding resources used for control channels and reference signals. The user resource utilisation r(t) is then given by r(t) = R(t)/C, which corresponds to a minimum number of required PRBs. These are scheduled over 10 ms according to the applied scheduler strategy. FIGURE 55 depicts the resource utilisation u(t) including additional reference signals and control channels for a user resource utilisation of r(t) = 40%, both for BW adaptation and micro DTX. With the help of these utilisation patterns, the instantaneous power during each individual symbol is determined according to the power model and then averaged over 10 ms.

To obtain a daily power consumption profile, for every hour a resource utilisation pattern and power consumption is generated from the corresponding mean traffic and finally the average daily power consumption is evaluated.

For DTX intervals, a more realistic switching speed is considered when the PA switches from empty active state to deactivated state and vice versa, i.e., a linear slope of 20 µs duration and a guard interval of 5 µs are assumed.

The evaluated daily total power consumption of a cell is illustrated for all scheduler strategies in FIGURE 56 both for a typically dense urban (a) and rural traffic scenario (b). FIGURE 57 shows the energy savings per cell for these green scheduling strategies for improvements by the PA only (a) and improvements by all other components including the PA (b).

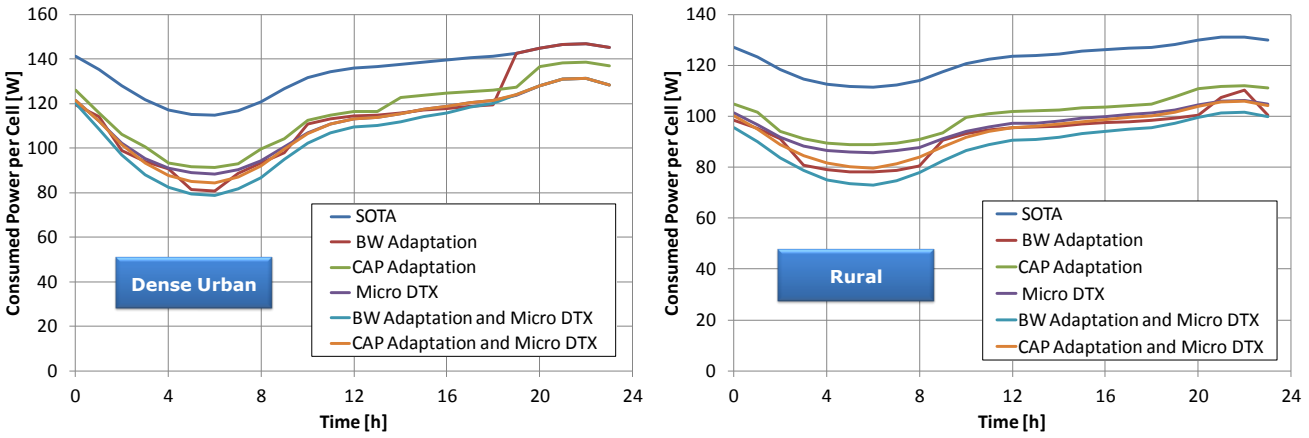

(a) (b)

FIGURE 56. Daily power consumption of a cell for SOTA and improvements by the PA only based on different scheduling strategies in dense urban scenario (a) and rural scenario (b)

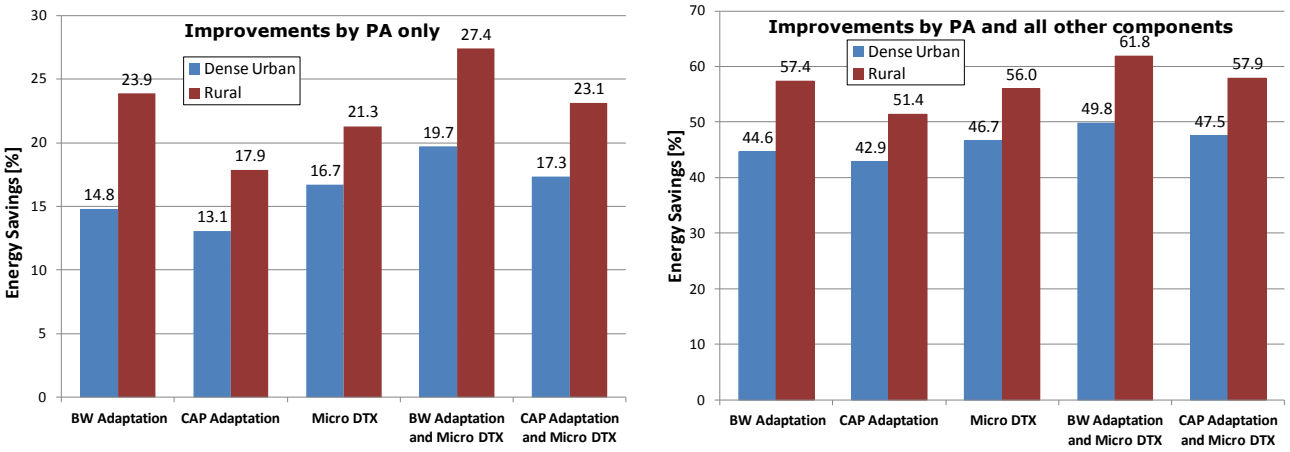

(a) (b)

FIGURE 57. Daily energy savings for different scheduling strategies by PA only (a), by PA and all other components (b)

A comparison of not combined solutions as BW adaptation, CAP adaptation and micro DTX shows that during night at lowest traffic load highest energy savings can be achieved by using the BW adaptation approach. Micro DTX is more beneficial at busy hours in dense urban scenarios, because due to the traffic load BW adaptation here cannot use one of the adaptation modes. The CAP adaptation approach yields the lowest energy savings along a day.

Highest energy savings up to 19.7% and 27.4% can be achieved by using BW adaptation combined with micro DTX in a dense urban scenario and rural scenario, respectively, if only the improvements of the new hardware features of the PA are considered. Much higher energy savings up to 49.8% and 61.8% can be achieved in dense urban and rural scenarios, respectively, when considering not only the improvements by the PA but also the improvements of all other components of a cell, especially by using passive cooling. The second best result is based on a combination of CAP adaptation and micro DTX. In this case slightly lower energy savings can be achieved.

The EARTH power model and traffic profile have been applied to compute energy consumptions of LTE deployments. Different integrated energy saving approaches have been compared by applying either a scheduling policy with adapted BW or CAP using a PA with adaptive operation point or a micro DTX scheduler using a PA with a deactivation mode or combinations of both approaches.

At rather high resource utilisation micro DTX can more flexibly utilise the void resources, where the fixed steps of BW or CAP adaptation limits the saving potential. For low utilisation BW adaptation has the highest saving because rather low efficiency for sending reference signals limits the saving for micro DTX and CAP adaptation. Applying a combination of BW adaptation and micro DTX is the best solution according to energy savings, because this approach takes always benefits from low and high load conditions. For all strategies higher savings can be achieved in rural cells compared to dense urban cells, because the lower resource utilisation leaves more scheduling potential for energy savings.

The recommendation for an integrated solution is a combination of BW adaptation and micro DTX, which results in highest energy savings for macro BSs deployed in dense urban or rural scenarios.

8. BEAMFORMING IN ACTIVE ANTENNAS

Beamforming is a general technique to control the radiation pattern of a radio signal transmitted from an antenna. Typically this is done by means of using several elements and applying a proper weight, amplitude and/or phase, to each of the signal components feeding each antenna element. Beamforming can be implemented for different purposes and on different time scales. A first aspect is covered in chapter 8.1, "Reconfigurable Antenna Systems", where radiation patterns are configured, on a "long" time scale according to the spatial traffic distribution in order to improve performance. In this case all users in a cell are served via the same antenna(s), i.e., with the same radiation patterns, and thus is sometimes denoted as cell-specific beamforming. Another aspect is covered in chapter 8.2, "Adaptive Beamforming on Active Antennas", where users-specific radiation patterns are created, on a "short" time scale, to improve link budget by means of narrow beams giving increased antenna gain and improved spatial filtering. Further chapter 8.2 also addresses impact of base station architecture highlighting the benefits of reduced losses and reduced data transportation needs when using active antennas.

Both aspects of beamforming covered in this chapter are enablers for energy efficiency improvements. The first aspect is an enabler for network management, whereas the second aspect is an enabler for radio resource management.

8.1. RECONFIGURABLE ANTENNA SYSTEMS

The role of the antenna system in cellular mobile communications is, in general terms, to act as a pipe making communication resources available, wherever needed, in space. Crucial aspects are to have high antenna gain, for improved signal strength, towards users in the area to be served and to have low antenna gain, for reduced interference, towards users in other areas. As of today most antenna systems deployed have properties that are fixed over very long time, months or longer, whereas changes in traffic load and spatial traffic distribution may occur on a much shorter time scale. Spatial traffic distribution herein refers to a requested traffic and not to the actually served traffic. The idea behind reconfigurable antenna systems (RAS) is to, in such a scenario, adaptively change antenna properties according to changes in average spatial traffic distribution and load, on a "long" time scale, such that communication resources become available where needed and thus efficiently utilized. An immediate effect from adapting antenna parameters is that signal-to-interference-plus-noise-ratio (SINR) is increased for the links carrying the bulk of the traffic. This allows for a more efficient transmission of data, hence, for the same throughput, energy consumption can be reduced, e.g., by applying discontinuous transmission in the time domain. Another effect is that cells can be more equally loaded despite the non-uniform spatial traffic distribution, so called load sharing, making user perception of system performance less dependent of users' location in the system. The concept is typically suited for, and most efficient, in high traffic load and non-uniform spatial traffic distribution but can be applied also in other scenarios. One such example is when the number of cells at a site is reconfigured to according to changes in load. For example reconfiguring an existing three sector site to a two sector site requires antenna parameters to be adjusted to maintain coverage.

The antenna parameters considered in this study are, in addition to electrical tilt which today is commonly deployed but not so often adapted, beampointing direction and beamwidth in azimuth. Other antenna parameters which also can be considered for adaption include beamshape in both elevation and azimuth. The degrees of freedom available for adaption depend on implementation. Both passive and active antennas are possible of which active antennas, especially with distributed radios over antenna elements in both azimuth and elevation dimensions, offering the highest flexibility. Here implementation aspects are not the primary focus and the antenna models used are theoretical ones, as given in [EARTH-D2.2], but with the possibility to change the aforementioned parameters.

The concept of reconfigurable antenna systems is exemplified in FIGURE 58 and FIGURE 59. FIGURE 58 (a) shows spatial SINR distribution, for a reference antenna system (REF). The REF system is deployed for uniform spatial traffic distribution giving that all antennas in the system have the same parameters. For a non-uniform spatial distribution, for example when traffic is clustered in hotspot areas as is indicated by the black circles in FIGURE 58 (a), these antenna parameters will no longer be the most appropriate as is indicated by some hotspots being located in areas with low SINR. An example of non-uniform spatial traffic distribution, is shown in FIGURE 58 (b). Here the traffic in the area served by the central nine cells of the REF system is clustered into six hotspots such that each hotspot represent the same amount of traffic and that the average traffic load for these nine cells are the same as for all other cells in the system. The amount of traffic within the six hotspots in relation the total traffic in the nine cells is given by a parameter, the hotspot probability.

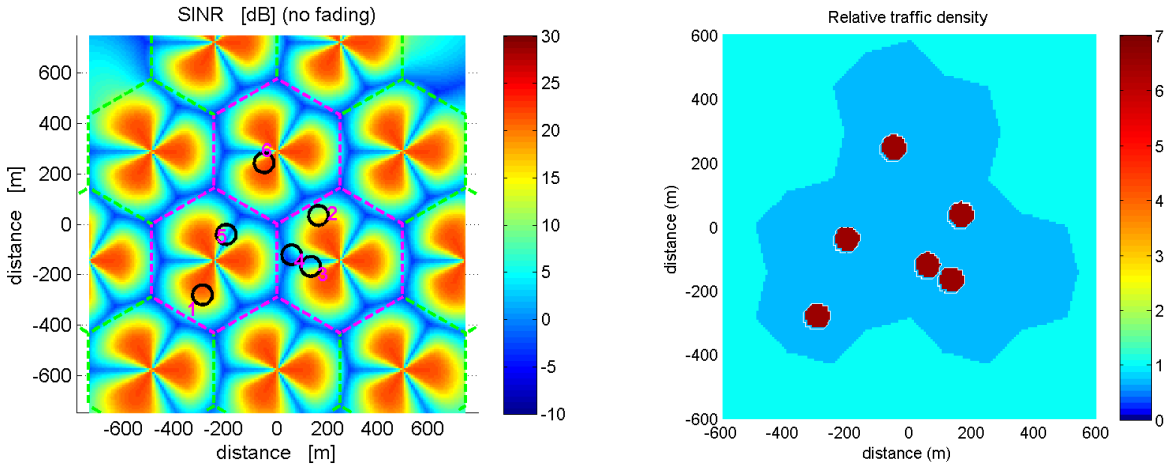

FIGURE 58. Signal-to-interference-plus-noise ratio for a reference antenna system optimized for spatially white traffic (a) and example of non-uniform traffic load (b).

In FIGURE 59 (a) is shown the spatial SINR distribution for the spatial traffic distribution shown in FIGURE 58 (b) but now for a system where the central nine cells are equipped with reconfigurable antennas (RAS) and where antenna parameters are adapted to the current non-uniform spatial traffic distribution. One can clearly see that the use of reconfigurable antennas have improved link performance (SINR) for traffic originating from clusters. FIGURE 59 (b) is shown another example of spatial SINR distribution for another spatial traffic distribution (hotspot location) where, again, the central nine cells have antenna parameters adapted to the new traffic situation.

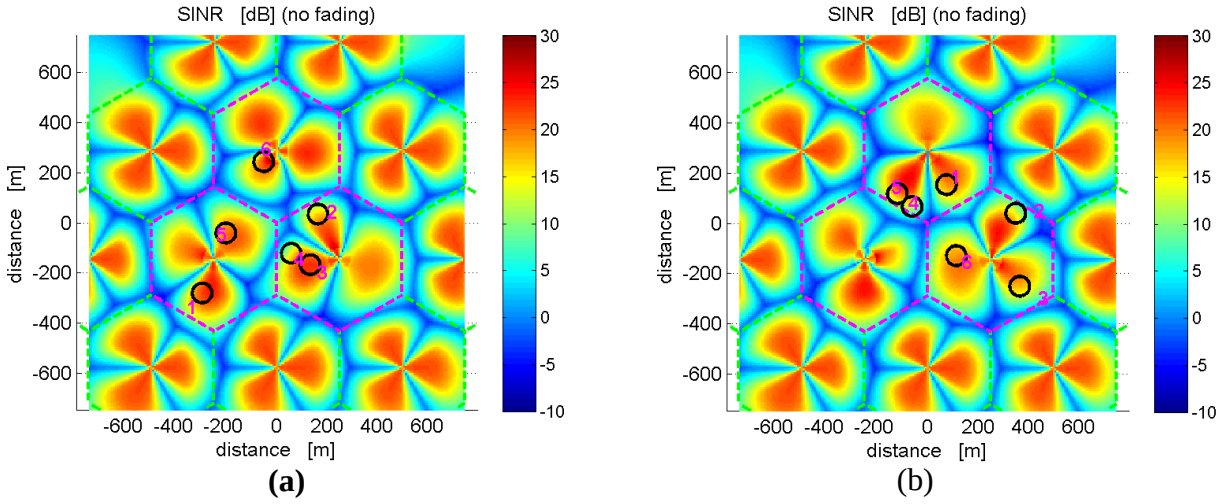

FIGURE 59. (a) Signal-to-interference-plus-noise ratio for a reconfigurable antenna system adapted to the traffic situation according to FIGURE 58(b), (b) The same type of results but for another traffic situation.

From the examples above it becomes evident that the concept of adapting antenna parameters to spatial traffic distribution has a potential of improving link performance and, as a consequence, saving energy for a given system throughput. The concept of reconfigurable antenna systems comprises two major components. A first component is the antenna system itself, for which antenna parameters can be changed, and the other component is a function handling evaluation of the situation in the system and deciding how to change antenna parameters. The second one includes observing the system by means of different measurements which is a challenging task. However the second component is not dealt with in this study. Instead suitable antenna parameters are found by means of an optimization algorithm.

In order to estimate the energy saving potential from using reconfigurable antennas six clusters have been randomly dropped 20 times within the area covered by the nine central cells of the REF system. The total system throughput, over all drops, has been calculated, where for each drop proper antenna parameters are found for each of the nine cells with the goal of maximizing system throughput by means of the genetic algorithm and assuming a Round Robin scheduler. Antenna parameters for other than the nine cells with RAS antennas remain unchanged. Similarly total system throughput is, for the same drops, calculated also for the REF system.

As both the non-uniform spatial traffic distribution as well as the cells equipped with RAS antennas is applied only to the nine centre cells and not to the entire system the evaluation will suffer from “edge-effects” compared to as if this was applied to all cells in the system. Because of this energy savings are estimated for two subsets of cells. The first subset comprises only the nine centre cells which not necessarily cover exactly the same area for the REF and the RAS system due to different antenna parameters. For this reason a second subset is defined including also the surrounding 15 cells which results in the total area covered being the same for the RAS and the REF system. However the potential gain for this second subset is limited since only nine out of 24 cells have RAS antennas. To compensate for this system throughput figures are normalized to mimic a scenario with a large system without edge effects. Given the system throughput figures, which are estimated for continuous operation, and the assumption that both the RAS and the REF system shall offer the same throughput DTX is applied in the time domain for the RAS system, since that system offers the largest throughput in continuous operation, such that both systems offers the same throughput. The relative times in active mode, at full output power, and in non-active mode, at no output power, are applied to the EARTH power model, with sleep mode on, and corresponding average power consumptions are calculated for both

subsets for both the RAS and the REF system. Finally the relative power consumption for the RAS versus the REF system is calculated showing the relative energy saving.

An estimation of the energy saving potential based on 20 random locations of six hotspots with hotspot probabilities ranging from 0.30 to 0.70, based on an antenna setup where antenna parameters are found for a scenario with hotspot probability of 0.66, is shown in FIGURE 60. The solid line shows the estimated energy saving based on the central nine cells (first subset) while the dashed line shows the savings based on 9+15 cells (second subset). As can be seen the energy saving potential is in the order of 10% and is relatively insensitive to the degree of clustering as given by the probability of hotspot traffic.

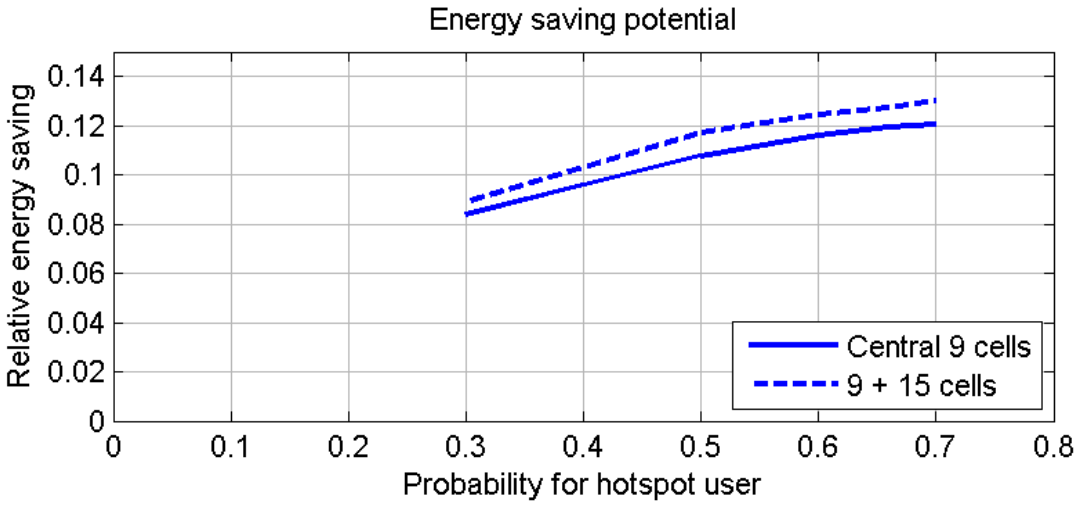

FIGURE 60. Energy saving potential including EARTH power model.

As mentioned the estimation of energy savings is based on both systems delivering the same throughput by means of applying duty-cycling in time. As the duty cycling, in the analysis, is applied to all cells in the system simultaneously there is a potential to increase the energy saving further by applying the duty-cycling in a non-synchronized manner between cells. By this the interference situation for the RAS system will improve, and thus also the energy saving, slightly.

8.2. ADAPTIVE BEAMFORMING ON ACTIVE ANTENNAS

In this paragraph a beamforming study applied to active antennas is considered, working on an adaptive manner. The beamforming methods are generally classified based on the time resolution of the radiation diagram shaping procedure; in case of long term (minutes or more) traffic variations it is commonly used the term of reconfigurable beamforming, in case of short term traffic variations beamforming is called adaptive, directly following users behaviours.

Active antennas (AAS) are deemed to be a valuable means to achieve beamforming goals, both for reconfigurable and adaptive versions, allowing implementing the algorithms also remotely, directly at the antenna level.

The concept of adaptive beamforming and the layout of the active antenna have been fully described in EARTH [EARTH-D4.1].

8.2.1. Results of adaptive beamforming applied to AAS

In the first phase of the project the performance of beamforming with active antennas was compared to a baseline scenario for the full load case. This implied some simpler approach both for the system simulation and for the power model of the active antennas.

In order to better understand the real behaviour with different traffic levels and in tighter compliance with the E^3F model developed by EARTH, new simulations of the envisaged scenario have been performed. A system simulator compliant with requirements defined in [EARTH-D2.2] has been used, and the power model for different load levels in active antenna systems has been employed.

The urban macro scenario has been considered, with an inter-site distance of 500 m; ten users per cell have been evaluated, offering a traffic ranging from 1 to 8 Mbps in the whole cell. Assuming the same rate for each user and imposing the download of 5 files of 0.2 Mb each some snapshots have been simulated, the length of each of them being related to the file size and the offered throughput. A scenario with the baseline assumptions and a scenario with beamforming with DoA estimations have been simulated.

In order to obtain the KPI (Key Performance Indicator), expressed as consumed power over throughput, the power model for AAS has been applied to the load levels simulated in the system. For the AAS power model typical parameters assumption has been performed.

Two sets of results are presented in the following. The first set makes reference to the case where only beamforming is taken into consideration with a comparison to the baseline case (see [EARTH-D2.2] for a complete description of the baseline case, that is a MIMO 2x2 scenario). This first set of results is valuable to highlight the achievable performances that could be obtained by only applying adaptive beamforming to a traditional macro-cellular base station, without any reference to AASs.

The KPI considered is the ECI ("Energy Consumption Indicator") defined in [EARTH-D2.3], namely the ratio of the consumed power in the base station versus the served traffic in the scenario. The power model applied in this case is the same for both the baseline and the beamforming scenario, and in particular it is a linear approximation of the consumed power versus the RF power in the base station. The scenario encompasses 21 cells with no wrap-around at the scenario borders and the throughput is an average of the served throughput in the 21 cells of the scenario.

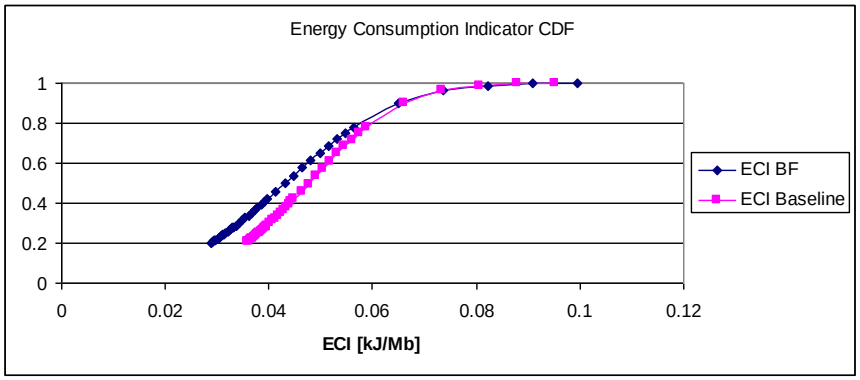

FIGURE 61. Cumulative distribution function of the ECI for Beamforming and Baseline scenarios.

In FIGURE 61 the cumulative distribution function of the ECI for the beamforming scenario compared to the baseline scenario is reported. A gain is achieved, as it can be noticed, by the adoption of adaptive beamforming, leading to less power consumption (computed applying the power model as mentioned above) to serve the same level of traffic. In particular an average gain is estimated about 9% between the two scenarios.

If a daily traffic profile is applied to the results achieved for these two scenarios, as indicated in [EARTH-D2.3], the daily ECI can be obtained, as reported in FIGURE 62. It can be observed that a BS with beamforming presents a daily ECI generally lower than a BS in baseline configuration, especially for peak hour conditions. Averaging on the whole day a saving is estimated about 9%.

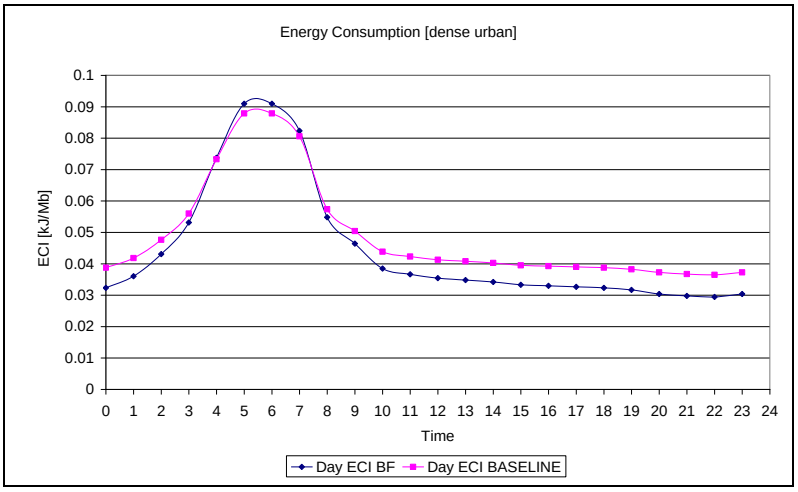

FIGURE 62. Daily ECI for Beamforming and Baseline scenarios.

The same evaluation shown above has been repeated including the effects of the usage of an AAS instead of a traditional BS. This second set of results represents the superimposition of the effects of beamforming in the access network and the effect of the usage of an AAS instead of a traditional macro-cellular BS. The system simulation set-up and the scenario definition are the same as in the previous set.

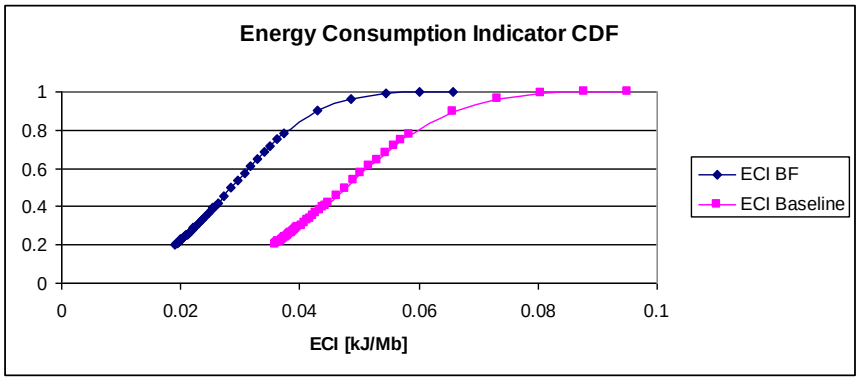

FIGURE 63. Cumulative distribution function of the ECI for Beamforming plus AAS and Baseline scenarios

FIGURE 63 shows the cumulative distribution function of the scenario with beamforming applied on an AAS with 4 active transceivers and of the baseline scenario, the same as in the previous set of results. A much greater gain is clearly noticeable, due to the AAS reduced power consumption with respect to a macro-cellular traditional case. In particular here a simple linear power model has been applied to the AAS case, with an overall consumed power reduction of about 34%, following the results reported in [EARTH-D4.1] for full load EARTH power model and considering that a comparable gain is to be expected also at the other traffic levels. Averaging the results shown above a gain is estimated at about 40% (to be compared to the roughly 9% of the case with beamforming only, under the assumptions made in this case). The daily ECI has been estimated as well, FIGURE 64.

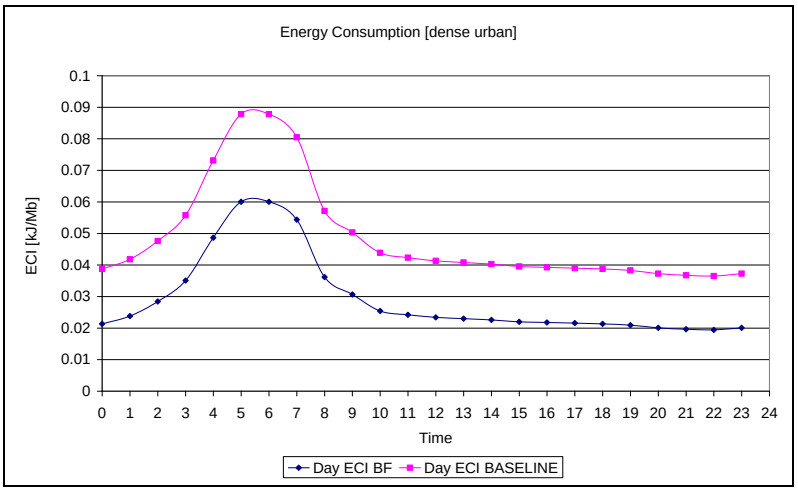

FIGURE 64. Daily ECI for Beamforming plus AAS and Baseline scenarios.

From the observation of FIGURE 64 it's clear the gain derived from the adoption of Beamforming on top of AAS, estimated on average at about 40% daily (as said above). From a more general standpoint the results shown are quite promising in terms of energy efficiency improvements from beamforming and especially from beamforming applied on top of AAS.

9. MIMO

Multiple antennas techniques known as multiple-input and multiple-output (MIMO) systems are crucial to achieve the high data rates and good spectral efficiency in the most recent and future wireless communication systems, e.g., LTE and LTE-advanced. The scope of this chapter is to consider MIMO methods from the energy efficiency point of view. The most spectral efficient MIMO mode does not necessary lead to maximum energy efficiency. The most suitable MIMO mode depends on the network load, the offered service type (VoIP, video streaming, ftp), required data rates, users location, etc.

Antenna muting in which the used antennas from available ones are selected according to traffic load is a promising method to enable energy efficient multiple antenna transmission in small cells as well as in cellular base stations. Antenna muting can be applied based on the instantaneous cell load or long term network load. The use of MIMO increases the spectral efficiency which means that less PRBs are needed to provide a certain throughput to users. Resource utilization based duty cycling in time and frequency enables power reduction in any kind of base stations. In order to reduce power consumption, the optimal MIMO mode needs to be jointly selected with possible duty cycling. The MIMO mode selection and duty-cycling can trace short term traffic variation and draft adaptation may also follow variable network load in long term (minutes or hours). The advanced MIMO precoding and multi-user MIMO (MU-MIMO) can provide, in addition to increased throughput, further energy saving in short time scale in densely populated high load cells especially when channel state information (CSI) is available at the transmitter. This chapter investigates the discussed energy efficiency enablers as follows:

- The optimal number of antennas for picocell BS is considered in Section 9.1. Also, the down-scaling of picocell BS power through duty cycling in time and frequency is discussed.
- The energy efficient precoding design for MU-MIMO is discussed in section 9.2. Precoding design is a key to achieve high capacity and low inter-user interference. Also, the precoding affects the transmit power of signal from each antenna depending on coefficients of the precoder. A novel precoding design considering the characteristics of PA, e.g., PAPR or average power, is proposed.
- The energy efficiency of different MIMO schemes and resource allocation strategies in downlink dense urban macro scenario is studied in Section 9.3. The most suitable number of transmit antennas for different network loads are discussed in a particular example case. Capacity adaptation or micro DTX based resource allocation methods are studied in system level simulations. Furthermore, the potential energy savings provided by the full channel state information (CSI) in TDD system is considered.
- Antenna muting is investigated in Section 9.4. The concept is to activate an antenna only when motivated by traffic load and/or data rate while the number of antennas in the cell is kept fixed, i.e., the number of cells at a site is not reconfigured. Three antenna muting techniques are presented and the implementation of the antenna muting in LTE is discussed. Furthermore, system level results are also shown for two adaptive systems with 2 and 4 antenna ports, which activate the optimal number of transmit antennas based on the instantaneous cell load.

9.1. MIMO MODELLING AND POWER-PERFORMANCE OPTIMIZATION IN PICOCELLS

MIMO schemes are now used in most wireless systems, including LTE and LTE-advanced. Selecting the best SISO or MIMO mode as function of the channel and network conditions is crucial for maximum energy efficiency. Evidently, the selection of the MIMO mode, together with link parameters such as the modulation and coding rate, can also affect the peak throughput and change the system frequency and time duty-cycling based on the required data rate. MIMO mode selection could bring energy savings by scaling down the MIMO processing and the number of active antenna chains.

In this section, we analyse the impact on the energy consumption of selecting the best SISO or MIMO mode that satisfies the required throughput in a picocell. Even though the use of MIMO is necessary for high throughput scenarios, important energy gains can be achieved through the use of a single antenna whenever the network load requirements are low. SIMO versus MIMO could also be an interesting point of comparison for high throughput, but with a higher cost of energy consumption at the terminal side.

To prove it, we carried out simulations based on channel, performance, and power models. The focus of the channel and performance modelling is the derivation of the link SNR-PER (Signal to Noise Ratio – Packet Error Rate) characteristics that will help us to select the best mode and link parameters. Such modelling builds on a standard-compliant chain with all realistic effects including non-idealities. By combining PER values with the throughput derived from the selected link parameters, we can determine the goodput (useful data rate from correct packets) of the system, which is proportional to the net spectral efficiency.

Next to specific performance and link analysis, the work on power modelling that is reported in [EARTH-D2.3] is used in order to provide consistent results. The flexibility features of the model are exploited in order to allow energy savings by duty-cycling the system.

Combining the previous models, we obtain the corresponding average power consumption as a function of SNR and required throughput, after optimizing the selection of MIMO mode, modulation and coding rate.

In order to allow energy saving through duty-cycling, two ways are considered to down-scale the system power when the total available goodput is higher than the required application data rate. The first one is based on duty-cycling in frequency (P_Df), which means not loading all the subcarriers (PRBs) of the system bandwidth when not needed. The second one uses duty-cycling in time (P_Dt), i.e., allowing the base station to transmit data at maximum speed and after that to sleep, as long as the required throughput can be achieved on the average.

The targeted throughput was selected corresponding to what the system would provide working at 100% duty-cycling when using a spectral efficiency (Eff) of 1 bit/s/Hz. Hence, for example, using MIMO 2x2 with QPSK and coding rate 1/2 leads a spectral efficiency of 2, meaning that a duty-cycling of 50% is sufficient for the targeted throughput, and enables some savings by reducing the system activation.

From TABLE 4 we observe that time-domain duty-cycling is much better for energy savings than frequency-domain duty-cycling. The reason is that frequency-domain duty-cycling does not enable to have many components sleeping. In fact, the full analogue front-end, PA, and time-domain digital signal processing are continuously active, only the frequency-domain processing of symbols benefits from this duty-cycling. On the other hand, time-domain duty-cycling allows all components to sleep during the symbols without transmission. This is independent of the SISO/MIMO choice, but selecting the best mode can maximize the amount of sleeping time.

Furthermore, we observe that MIMO, compared to SISO, does not lead to energy savings. This can be seen in FIGURE 65. The primary goal of MIMO is indeed to increase the spectral efficiency, which is the main reason why it is deployed in cellular base stations. The energy saving mode actually comes from down-scaling to SISO when the full system capacity is not required, letting one or more chains completely in sleep. In our simulations we found a factor 12 variation between the worst-case power consumption and the optimally selected MIMO mode. This is assuming the constraint of a fixed output power spectral density as present in LTE. Relaxing this constraint and focusing only on the output power could open the door to additional savings. Furthermore, a better precoding scheme and advanced MIMO detection could potentially improve the energy efficiency of MIMO schemes by improving the system performance and goodput.

TABLE 4. Results of SISO and MIMO 2x2 and4x4 modes for minimal power consumption as function of SNR and duty-cycling for a given throughput.

	SISO				MIMO 2x2				MIMO 4x4			
SNR	**Mode**	**Eff.**	**P_Df (W)**	**P_Dt (W)**	**Mode**	**Eff.**	**P_Df (W)**	**P_Dt (W)**	**Mode**	**Eff.**	**P_Df (W)**	**P_Dt (W)**
5 dB	/	0			/	0			/	0		
10 dB	QPSK, 1/3	0.7	3.9	3.9	QPSK, 1/2	2.0	7.0	4.1	/	0		
15 dB	16-QAM, 1/3	1.3	2.8	2.1	QPSK, 2/3	2.7	6.1	3.1	/	0		
20 dB	16-QAM, 1/2	2.0	2.4	1.4	64-QAM, 1/3	4.0	6.0	2.1	/	0		
25 dB	16-QAM, 7/8	3.5	2.2	0.9	64-QAM, 1/2	6.0	5. 6	1.4	/	0		
30 dB	64-QAM, 2/3	4.0	2.1	0.8	16-QAM, 5/6	6.7	5. 6	1.2	QPSK, 1/3	2.7	11.0	5.9
35 dB	64-QAM, 3/4	4.5	2.0	0.7	64-QAM, 2/3	8.0	5.5	1.0	16-QAM, 1/3	5.3	10.2	3.0
40 dB	64-QAM, 3/4	4.5	2.0	0.7	64-QAM, 2/3	8.0	5.5	1.0	64-QAM, 1/3	8.0	10.1	2.0
45 dB	64-QAM, 3/4	4.5	2.0	0.7	64-QAM, 3/4	9.0	5.5	0.9	64-QAM, 1/3	8.0	10.1	2.0

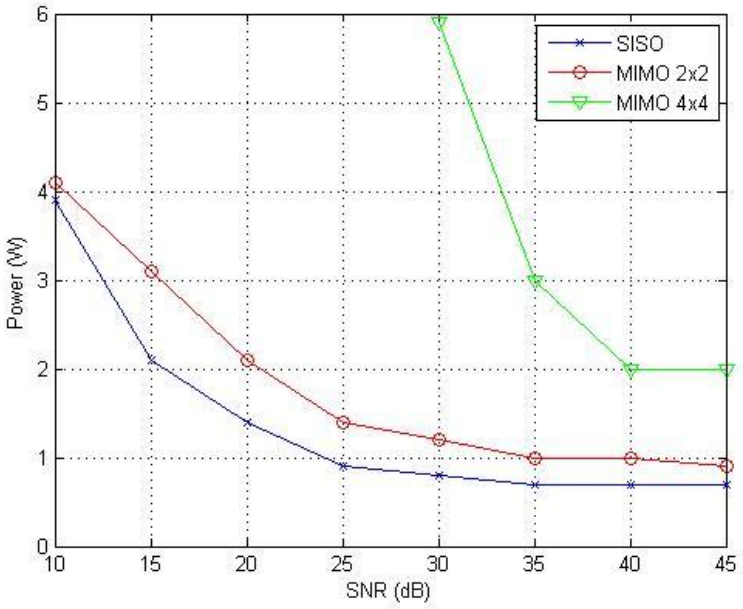

FIGURE 65. Power consumption as a function of SNR by using the most energy-efficient link adaptation.

The main area of application of this solution is the low or medium network load. In fact, this low load scenario allows to down-scale the MIMO to SISO for energy efficiency when the full capacity is not required. On the other hand, the optimization timescale of this approach is in the range of hours since the base station can typically vary the MIMO transmission based on relatively long-term scale. This approach is based on cell reconfiguration. However, a faster timescale could be achieved by using antenna (see Section 9.4). Only when the total traffic within the cell increases, the base station will switch to a more spectrally efficient mode at the cost of some energy efficiency.

This approach can fit perfectly in the rest of the solutions at network, system, and node level. The complete picture of the application areas for each solution can be seen in [EARTH D6.2a]. However, some issues might arise when considering techniques that use multiple antennas to achieve energy efficiency. Despite this fact, solutions such as beamforming and MIMO precoding that use multiple antennas have an application area of densely populated scenarios with high load conditions. Therefore, even in this case, this approach fits in the overall picture as long as the application area with multiple antenna solutions is not overlapping.

9.2. ZERO-FORCING LIKE MULTIUSER MIMO PRECODING SUPPORTING THE CONSTANT MODULUS PROPERTY

In the downlink of MU-MIMO communications systems, precoding design and scheduling of users are the key to achieve high capacity and low inter-user interference. Also, precoding design affects transmit power from each antenna depending on precoder coefficients. A zero forcing (ZF) precoder will be mainly used for MU-MIMO communications in 3GPP Rel.10 Long Term Evolution (LTE) [KDAT10]. It is known that it can fully cancel inter-user interference if perfect channel state information is available at the transceiver. However, the ZF precoder does not possess a constant modulus property [SeTB09]. Here, the constant modulus property means pure phase corrections with no amplitude changes. The precoder without the constant modulus property causes some disadvantages in terms of PAs connected to antennas. Specifically, the ZF precoder loads each antenna with a different transmit power because the coefficients of the precoder have different amplitudes and weigh the input signals differently. Consequently, each PA needs to be designed for a higher transmit output power than that of a precoder fulfilling the constant modulus property in order to amplify this

unbalanced transmit power. For example, in the worst case of two transmit antennas, if the precoder loads the transmit power only on one antenna, then the PA needs to double the transmit power compared to loading both the PAs with the same transmit power. That makes the power consumption of each PA higher, and that goes against the aim of saving energy.

Addressing the problems described above, this chapter shows a new MU-MIMO precoding method for wireless communications systems aiming at the reduction of power consumption caused by PAs. The feature of the presented work is to allow a precoder to fulfil the constant modulus property, while trying to mitigate inter-user interference as much as possible. In order to do this, each element of the proposed precoder consists of a phase shifter. The optimum phase set for the precoder is found so that the inter-user interference can be suppressed best possible.

In multiuser MIMO systems, a precoded signal $\boldsymbol{x} \in \mathbb{C}^M$ is transmitted over M antennas at a base station (evolved node B, eNB) and received by N antennas at a terminal. With the kth users' channel matrix $\boldsymbol{H}_k \in \mathbb{C}^{N \times M}$ and the complex white Gaussian noise term $\boldsymbol{n}_k \in \mathbb{C}^N$, the received signal can be written as

$$\boldsymbol{y}_k = \boldsymbol{H}_k \boldsymbol{x} + \boldsymbol{n}_k . \tag{9-1}$$

Each terminal provides a channel direction indicator (CDI) together with a channel quality indicator (CQI) via the feedback channel. In general, the CDI is an entry in a codebook and usually represented by a codebook index. It is obtained via channel vector quantization (CVQ) of the effective channel vector $\boldsymbol{h}_{\mathrm{eff},k}^{\mathrm{T}} = \boldsymbol{w}_k^{\mathrm{T}} \boldsymbol{H}_k \in \mathbb{C}^{1 \times M}$, i.e., the combination of the channel $\boldsymbol{H}_k$ and the receive filter $\boldsymbol{w}_k$ at user k. Then, each terminal feeds back its quantized version $\hat{\boldsymbol{h}}_{\mathrm{eff},k}$ as the CDI, which is selected from the codebook such that the quantized channel vector has the minimum Euclidean distance to the effective channel [DiBa07] [TrBT07]. The CQI values are used at the eNB to schedule the users in a greedy way as described in [TrBT07] and to choose the proper modulation and coding scheme. The CDIs are used to generate the effective channel matrix $\hat{\boldsymbol{H}}_{\mathrm{eff}} \in \mathbb{C}^{D \times M}$ with rows according to the quantized effective channel vectors $\hat{\boldsymbol{h}}_{\mathrm{eff},k}^{\mathrm{T}}$ of the D scheduled users. For simplicity, we assume at maximum one data stream (symbol) per user, thus, D is also the number of simultaneously transmitted data streams. Assuming a ZF transmission scheme, the precoder is computed as

$$\boldsymbol{P}_{\mathrm{ZF}} = \hat{\boldsymbol{H}}_{\mathrm{eff}}^{\mathrm{H}} (\hat{\boldsymbol{H}}_{\mathrm{eff}} \hat{\boldsymbol{H}}_{\mathrm{eff}}^{\mathrm{H}})^{-1} \in \mathbb{C}^{M \times D}. \tag{9-2}$$

The precoded signal computes as

$$\boldsymbol{x} = \boldsymbol{P}_{\mathrm{ZF}} \boldsymbol{G} \boldsymbol{s}, \tag{9-3}$$

where $\boldsymbol{s}$ and $\boldsymbol{G}$ are the D-dimensional vector of scheduled symbols and a diagonal matrix with elements chosen for equal power loading, respectively. However, as mentioned above, the ZF method does not fulfill the constant modulus property, thus, being very inefficient with respect to the power consumption.

In this section, we propose a new precoding method to fulfill this property while trying to mitigate inter-user interference as much as possible. In 3GPP LTE and LTE-A, codebooks have been chosen to fulfill the constant modulus property in order not to increase the peak-to-average-power ratio due to precoding [SeTB09]. Mathematically speaking, the precoder with the constant modulus property is defined as follows:

$$\boldsymbol{P}=[\boldsymbol{p}_1,\ldots,\boldsymbol{p}_D],\boldsymbol{p}_k=\left[e^{j\theta_{1,k}},\ldots,e^{j\theta_{M,k}}\right]^{\mathrm{T}},k\in\{1,\ldots,D\} \tag{9-4}$$

We describe an optimization method, and we show how to select the best set of $\theta_{i,k}, i\in\{1,\ldots,M\}, k\in\{1,\ldots,D\}$ to minimize inter-user interference. If the following equation is satisfied, inter-user interference is suppressed:

$$\hat{\boldsymbol{H}}_{\mathrm{eff}}\boldsymbol{P}=\boldsymbol{I}, \tag{9-5}$$

where $\boldsymbol{I}$ is the $D\times D$ identity matrix. However, due to the fact that $\boldsymbol{P}$ only performs phase corrections, it is impossible to satisfy (9-5) in most of the cases. Therefore, at least, $\hat{\boldsymbol{H}}_{\mathrm{eff}}\boldsymbol{P}$ need to be as close as possible to the identity matrix by adjusting the phases of elements in $\boldsymbol{P}$. Please note that a precoder is calculated using an effective channel matrix $\hat{\boldsymbol{H}}_{\mathrm{eff}}$ which includes a quantization error compared to the real channel. This is because the effective channel is selected from the limited number of codebooks. Thus, some amount of inter-user interference is also remained if ZF precoding is applied according to (9-2) and (9-3). Therefore, the deterioration caused by the proposed method is expected to be the one of ZF. We can describe the optimization as follows:

$$\boldsymbol{P}_{\mathrm{CM}}=\arg\min_{\boldsymbol{P}\in\Pi}\left\|\hat{\boldsymbol{H}}_{\mathrm{eff}}\boldsymbol{P}-\boldsymbol{I}\right\|_F^2,$$

$$\Pi=\left\{\boldsymbol{P}\in\mathbb{C}^{M\times D}\;\middle|\;\boldsymbol{P}_{i,k}=e^{j\theta_{i,k}};\theta_{i,k}\in[0,2\pi)\right\} \tag{9-6}$$

It is difficult to solve (9-6) analytically and we therefore compute the solution based on exhaustive search. We explain an example of an algorithm for (9-6). First, we define the finite set:

$$\Theta\in\left\{m\frac{2\pi}{N_{\mathrm{res}}}\middle|m\in\{0,1,\ldots,N_{\mathrm{res}}-1\}\right\} \tag{9-7}$$

where N_{res} is an arbitrary integer and decides the resolution of the phase which affects the performance of our method. The algorithm is based on the idea to find the optimum phase tuple $\boldsymbol{\theta}_{\mathrm{opt}}\in\Theta^M$ to minimize $\left\|\hat{\boldsymbol{H}}_{\mathrm{eff}}\boldsymbol{P}-\boldsymbol{I}\right\|_F^2$ calculating all possible combinations. Finally, the optimum precoder $\boldsymbol{P}_{\mathrm{CM}}$ can be obtained from $\boldsymbol{\theta}_{\mathrm{opt}}$.

TABLE 5. Simulation Parameters.

Number of Tx antennas	4
Number of Rx antennas	1
Number of users	20
Number of feedback bits	4 bit
Channel model	Kronecker model
Channel correlation	Uncorrelated, highly correlated

We conducted sum rate simulations for different signal-to-noise ratios (SNRs) according to the parameters as shown in TABLE 5. FIGURE 66 summarizes the performance comparison between the conventional CVQ based ZF method and the proposed method. In the simulation, sufficient number of trails was done with randomly generating the channel characteristics. The performance of the proposed method is close to the CVQ based ZF method. However, the proposed method could not attain (9-5) and therefore some amount of inter-user

interference could not be removed completely. On the other hand, in case of ZF precoding, the effective channel matrix estimate $\hat{\boldsymbol{H}}_{\text{eff}}$ includes the quantization error compared to the real channel. Thus, some amount of inter-user interference would remain due to this error as well. Therefore, the difference between proposed method and the conventional ZF becomes small. Next, we estimated the transmit power of our proposed method and the CVQ based ZF method using the coefficients of the precoding matrix. If the average transmit power of all scheduled symbols is assumed to be the same and unit, the transmit power from each antenna is written as the norm of the row vector of the precoding matrix as follows:

$$P_{TX,i} = \sum_{j=1}^{D} \left| \mathbf{P}_{i,j} \right|^2, i = 1, \ldots, M \qquad (9\text{-}8)$$

The simulation result showed the proposed method was able to reduce the transmit power of a PA by around 0.94 dB and 1.22 dB in the uncorrelated case and highly correlated case, respectively. However, please note that some performance degradation was observed at high SNR region as shown in FIGURE 66. This may require a higher transmit power for the proposed method and the benefit over the conventional ZF method may be reduced.

In conclusion, we proposed a new multiuser MIMO precoding method for wireless communications systems aiming at the reduction of power consumption of PAs. The proposed method is energy efficient due to the constant modulus property while trying to mitigate inter-user interference as much as possible. Despite all these benefits, we showed that the proposed method offers similar performance as the conventional CVQ based ZF multiuser MIMO technique in terms of sum rate.

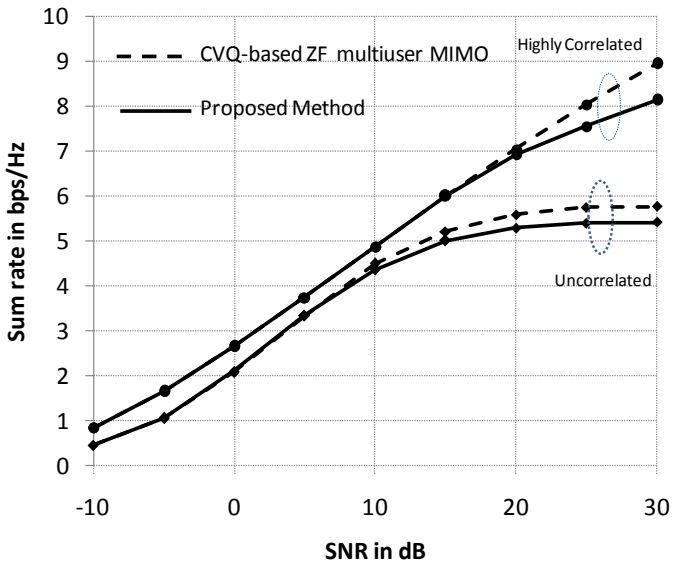

FIGURE 66. Performance comparison between the conventional method and the proposed one.

9.3. ENERGY EFFICIENCY OF MIMO SCHEMES AND RESOURCE ALLOCATION

Usually MIMO methods are used to improve the spectral efficiency of the communication links. However, transmission mode with many antenna and high spectral efficiency is not always the optimal from the energy consumption point of view. The most energy efficient transmitter mode depends on the required data rates, traffic type, users' locations, BS power characteristics and the availability of the channel knowledge. The

number of used transmit antennas and the number of used PRBs play important role in the energy consumption of the macro base station. For example, if the number of users is low and the BS needs only few PRBs, single antenna transmission with appropriate scheduling may provide the required QoS and low energy consumption although it is not very spectral efficient. The scope of this section is to discuss power consumption of different number of transmit antennas, MIMO schemes and resource allocation methods in a particular downlink macro cell example scenario. In order to see the overall network energy consumption, system level simulations are considered. The number of needed transmit antennas is studied in the simulations. Furthermore, the energy efficiency savings via full channel state information (CSI) is considered in the numerical examples. The availability of CSI at the base station enables good beamforming and RB-wise channel frequency response whereas fixed codebook based precoding and sub-block based channel quality indicator (CQI) are usually utilized at the LTE systems. Due to the improved energy and spectral efficiency, less PRBs are needed to serve users when CSI is utilized. The spectral and energy efficiency can be also improved by using multi-user MIMO (MU-MIMO) techniques which is illustrated in the results. In order to obtain system level results, the MIMO methods need to be combined with an appropriate scheduling to decrease the number used of PRBs. The proportional fair (PF) scheduling strategies are based on capacity (CAP) adaptation or micro DTX, see Chapters 7 and 6. In DTX scheduling, time domain duty-cycling is applied whereas frequency domain duty-cycling is used in CAP resource allocation strategy. LTE specific reference signals have been assumed to be transmitted in every sub frame.

It is assumed that the base station is equipped with four transmit antennas and the receiver uses two transmit antennas to detect the received signal. BS may use one, two or all the four antennas for transmission. The air interface and system model is LTE specific and the system simulation assumptions can be found in [EARTH-D2.2]. 10MHz transmission bandwidth with TDD is considered in the network consisting of 19 three sector sites. The inter site distance is set to 500 meters. TDD enables also the assumption of the full CSI at the BS due to the channel reciprocity in uplink (UL) and downlink (DL). The CSI estimate is periodic and delayed due to the assumption of periodic uplink sounding reference signal. The network load of particular interest ranges from low load of 10 Mbps/km^2 to high load case of 120 Mbps/km^2. This study focuses on the traffic model, where input data for each user comes continuously with rate 1 Mbps. This traffic model is valid for video streaming. Also operators may offer mobile data services with a limited rate. Users are uniformly distributed over the network area. For example, the number of the users is 124 with 30 Mbps/km^2 load.

The mean BS power needed per square kilometre [kW/km^2] is shown in TABLE 6 for different network loads and single user MIMO (SU-MIMO) modes as well as for multi-user MIMO (MU-MIMO) mode. The power model presented in [EARTH-D2.3] for 2012 macro BS is used in the power consumption evaluation. EARTH component improvements are considered to enable efficient operation with variable PA output power. The maximum total output power for any number of used transmit antennas is 40 W. Also the cell edge user throughput is shown to illustrate the capability of the schemes to provide QoS for all the users. Cell edge performance measure is the 5 percent value of the UE throughput CDF. In the case of low network load, the single antenna transmission is the most energy efficient. Furthermore, LTE standard compliant CQI and precoding matrix indicator (PMI) is enough for scheduling and link adaptation to serve users satisfactorily up to medium network load. Notable energy savings can be obtained via DTX resource allocation, e.g., it saves power about 23 % or 37 % compared to CAP scheduling when SIMO or 2x2 MU-MIMO is applied at 30 Mbps/km^2 load. For 60 Mbps/km^2 network load, 2x2 MIMO provides the acceptable coverage and the good energy efficiency. Let us consider 2x2 MIMO with LTE specific CQI and PMI based system applying CAP resource allocation as a reference system for 60 Mbps/km^2 load. The energy efficiency of this reference system can be improved by 22 % applying DTX scheduling. Further energy savings can be obtained by utilizing full CSI when the total power saving is 43 %. The better CSI improves the spectral efficiency yielding energy savings due to the deceased number of used PRBs. In the case of high 120 Mbps/km^2 network load, four transmit antenna is needed to guarantee desired 1 Mbps throughput to cell edge users. The studied 2x2 MIMO methods are not able to satisfy cell edge user performance for high load scenario. Surprisingly, also CSI is needed to obtain acceptable performance in the high load case. When CSI is available at the transmitter, MU-

MIMO technologies provide further energy efficiency enhancement in highly loaded network. 4x2 MU-MIMO with CSI and DTX obtains about 39 % power savings compared to 4x2 SU-MIMO with CAP and LTE compliant CQI and precoding. On the other hand, 4x2 MU-MIMO uses 10 % more power compared to 2x2 MU-MIMO in high load scenario. That is the required energy cost to ensure high capacity in the considered example scenario.

In this section energy efficiency of different MIMO modes in dense urban macro environment when each user was served with 1 Mbps throughput is considered. Based on the numerical examples, it can be concluded that the BS should adapt the number of used antennas in order to obtain energy savings. This means that the antenna muting for which further results and implementation issues are considered in Section 9.4 is a promising method to be implemented. Furthermore, the DTX scheduling provided better power savings than that the capacity adaptation based resource allocation. If CSI is available at the transmitter and general beamforming is used, further energy savings can be obtained compared to the system using LTE based CQI and PMI. In the case of high network load, the use of MU-MIMO can also decrease the BS power level when CSI is available. The results indicate that the 1x2 single antenna mode is suitable for low network load scenario. For medium network loads the 2x2 MIMO is the most suitable whereas at the high load case 4x2 MIMO is needed to guarantee the desired user throughput. Depending on the network load and antenna scheme, the DTX resource allocation provided power saving from 5 % to 37 % compared to CAP scheduling.

TABLE 6. Energy efficiency of MIMO schemes and resource allocation strategies in mean power/area (P/A) [kW/km^2] and cell edge user throughput.

	SIMO 1x2, CQI			**SU-MIMO 2x2, CQI**			**SU-MIMO 2x2, CSI**			**MU-MIMO 2x2, CSI**		
Load Mbps /km^2	**P/A, CAP** kW/km^2	**P/A, DTx** kW/km^2	**Cell edge** Mbps	**P/A, CAP** kW/km^2	**P/A, DTx** kW/km^2	**Cell edge** Mbps	**P/A, CAP** kW/km^2	**P/A, DTx** kW/km^2	**Cell edge** Mbps	**P/A, CAP** kW/km^2	**P/A, DTx** kW/km^2	**Cell edge** Mbps
10	0,71	0,52	1,0	0,96	0,64	1,0	0,84	0,58	1,0	0,85	0,58	1,0
30	1,12	0,86	0,92	1,35	0,94	0,99	1,2	0,81	1,0	1,23	0,77	1,0
60	1,45	1,23	0,78	1,76	1,38	0,87	1,52	1,08	1,0	1,52	1,1	0,96
120	1,87	1,76	0,36	2,2	2,02	0,27	1,9	1,64	0,78	1,9	1,57	0,75
	SU-MIMO 4x2, CQI			**SU-MIMO 4x2, CSI**			**MU-MIMO 4x2, CSI**					
30	2,06	1,57	1,0	1,84	1,21	1,0	1,84	1,19	1,0			
60	2,46	2,05	0,52	2,07	1,43	1,0	2,03	1,38	1,0			
120	2,83	2,69	0,20	2,39	1,94	0,94	2,26	1,73	0,97			

9.4. ANTENNA MUTING IN LTE

The idea is to activate an antenna only when motivated by traffic load and/or data rate but not reconfiguring the number of antennas in the cell. As shown in the previous section, from a power-savings perspective it is desirable to activate multiple power amplifiers only when motivated by traffic load and/or data rate. This is illustrated in FIGURE 67.

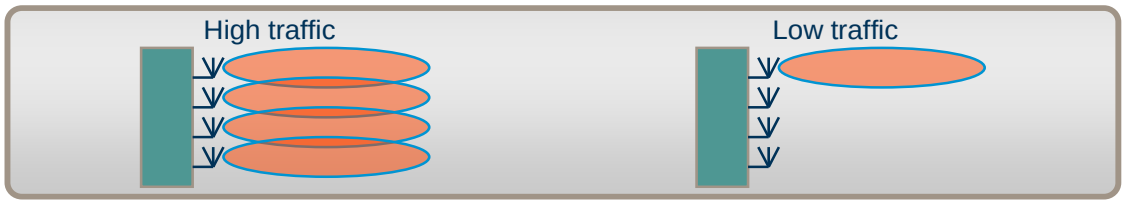

FIGURE 67. Adaptive multi-antenna transmission.

According to Rel-8 of the LTE specification [EARTH-D2.2], the number of antennas in a cell is static; therefore it is not possible to reconfigure the number of antennas without a cell re-configuration which is a slow process. In antenna muting method, the number of antennas is determined via blind decoding of the PBCH upon connection to the cell. The foundation for the concept is that control channels are designed for robustness and may be successfully decoded even when diversity is lost, coding rate decreased and output power reduced due to antenna muting, especially at low load situations.

Three alternatives exist for implementation of antenna muting which are shown in FIGURE 68. As is shown in FIGURE 68 a), in the first alternative the output power for signals on antenna ports 1 to 3 are simply set to zero which means that these signals will not be transmitted and thus will appear to the UEs as being in a deep, and long, fade. In alternative two presented in FIGURE 68 b), all signals are added together and then transmitted via one physical antenna which means that they will appear as fully correlated and finally, in FIGURE 68 c), an antenna muting configuration is shown which is a combination of the previous two alternatives in which signals intended for antenna port 0 and 1 are, for potentially improve mobility measurements, transmitted via one physical, antenna whereas signals on antenna ports 2 and 3 are not transmitted at all. When resource utilization reaches certain trigger level muted antenna ports are activated ensuring that high data rates and full output power can be reached.

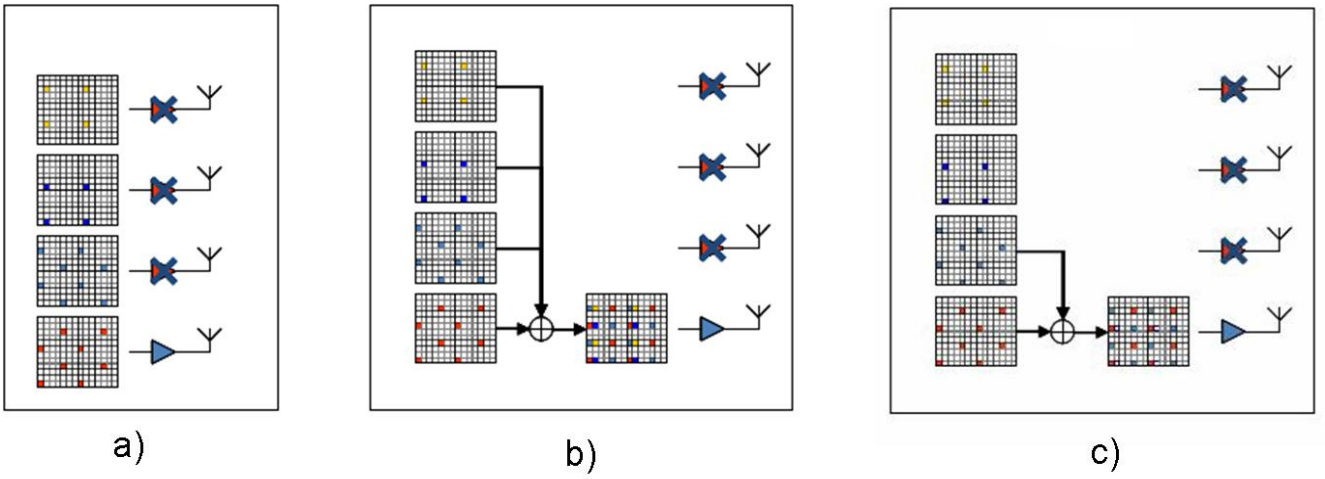

FIGURE 68. Antenna muting concept: a) Antenna ports 1-3 are muted, b) All signals are added and transmitted by one physical antenna, c) Signals on antenna ports 0 and 1 are added and transmitted by one physical antenna.

The concept has been evaluated according to scenario 1 in [EARTH-D2.2], for both 2 and 4 antenna ports and energy consumption per area unit calculated as a function of system throughput as shown in FIGURE 69. The legend "all active" is the reference scenario where all antenna ports are always active whereas "adaptive" is the scenario with antenna muting. As can be seen from the FIGURE 69 absolute savings are significant and largest savings of course appear at low load. As energy consumption increases with system throughput this will be even more significant for relative savings where up to 45% energy can be saved at load.

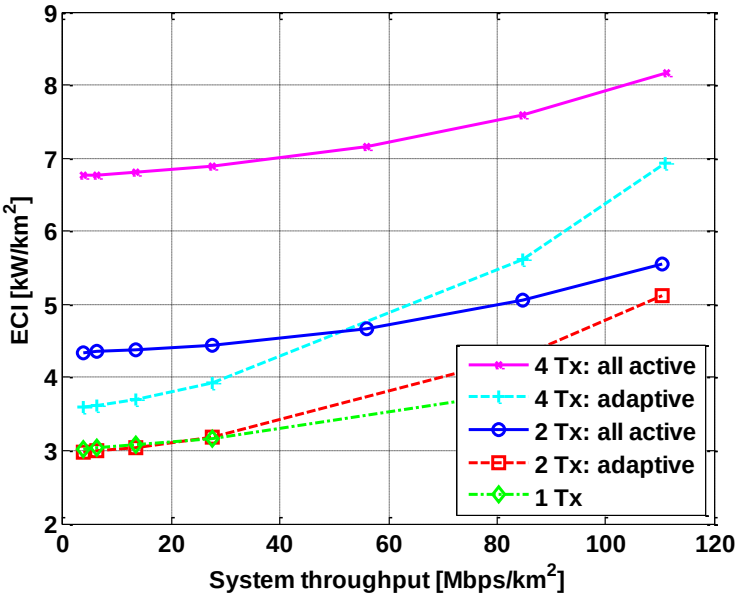

FIGURE 69. Energy consumption per area unit.

FIGURE 70 shows the resource utilization versus system throughput for different configurations. As can be seen, average physical resource block utilization increases with the offered load but we never reach 100%, not even for the one antenna case, but it is less for the 4Tx adaptive configuration.

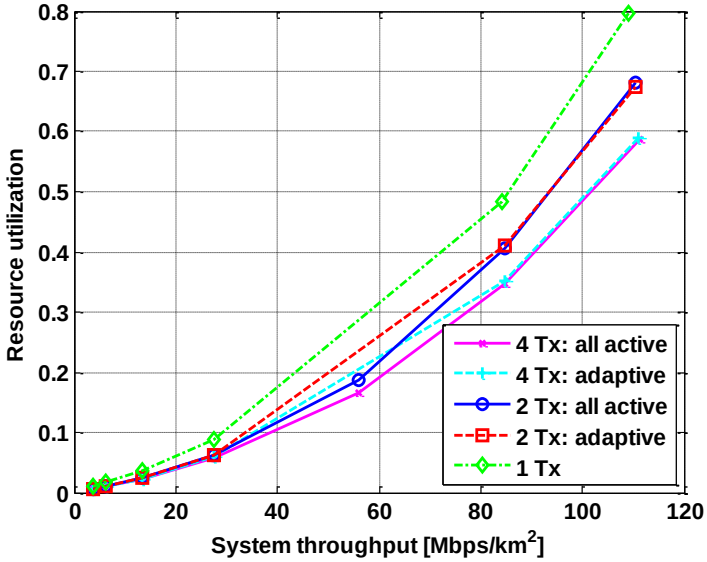

FIGURE 70. Resource utilization as function of system throughput.

10. CONCLUSION

This document has presented the latest results on energy savings for the energy efficiency enablers of Green Radios selected as the most promising tracks. They are based on refined definitions of the proposed solutions and performance evaluations which are done by simulations and even by experimental investigations.

In the first three chapters (2, 3, and 4), transceiver and antenna solutions at hardware level have been studied for energy efficiency improvements in macro- and small-cell BS. First, a signal load adaptive transceiver system (SLA-TRX), based on the combination of several functional blocks, has been proposed for macro-cell BS in order to reduce the power consumption of the PA which is the highest power consuming part in a macro cell BS and the power consumed by some to the small signal RF transceiver for load levels below the maximum. Based on the performance evaluation of the individual blocks, the power consumed by the whole SLA-TRX system has been evaluated for arbitrary signal loads and the results obtained with operating point optimization and deactivation of certain components show significant energy efficiency improvement in medium and low load situations. Operating point adjustment (OPA) leads to energy efficiency improvement up to 29% at low load, and component deactivation (CD) provides up to 54% power reduction.

Second, an energy flexible transceiver system for small-cell base-stations covering the BB processor, the RF transceiver, the PA and the antenna interface has been addressed. For the BB part, it has been shown that combining hardware optimization with flexible energy aware baseband signal processing algorithms brings an overall power reduction of 20% at low signal loads. For the RF transceiver part, a traffic load independent power efficiency improvement of 35% can be obtained by technology scaling and adequate architecture, and a traffic load dependent power efficiency improvement of 30% on average can be obtained by SiNAD adaptation and time/frequency duty-cycling. For the PA part, two approaches have been proposed. The first one, based on the PA solution proposed in the SLA-TRX system for macro-cell BS, brings power consumption reduction at medium and low signal loads (up to 55% for OPA and up to 80% for CD), whereas the second one, based on a tunable matching network, provides more than 30% energy efficiency improvement at medium and high signal loads. On the antenna, a duplexing antenna has been proposed to relax the transmit filter requirements and allow lower RF front-end insertion loss. The expected gain in terms of energy efficiency is higher than 50%.

Finally, printed antennas based on foam substrate have been proposed to improve the energy efficiency of antennas used in a BS and an energy efficiency improvement of about 15% over more conventional substrates have been estimated.

In the chapters 5, 6, and 7, energy reduction through adaptation of the transmission scheme and bandwidth to the traffic and channel conditions has been tackled. First, adaptability to system dynamics through adaptive modulation and coding rate that adapts the transmission scheme to the channel conditions has been proposed and simulation results show potential for energy efficiency improvement at BB level, rising up to 33% depending on the channel quality.

Then, different discontinuous transmission modes have been elaborated, providing 33% power reduction for MBSFN-based DTX and 53% for short DTX, based on the same CD performance as considered for micro DTX. Assuming that for MBSFN-based and for short DTX more components of a BS can be deactivated, as the duration of no signal transmission is longer, a higher amount of power reduction is expected.

In addition, different scheduling strategies taking into account power saving modes of the PA have been investigated. Promising energy savings have been obtained by combining bandwidth adaptation with micro DTX. Highest energy savings up to 20% and 28% can be achieved by using BW adaptation combined with micro DTX in a dense urban scenario and rural scenario, respectively, if only the improvements of the new hardware features of the PA are considered. Much higher energy savings up to 50% and 62% can be achieved in dense urban and rural scenarios, respectively, when considering not only the improvements by the PA but also the improvements of all other components of a cell, especially by using passive cooling. For all strategies higher

savings can be achieved in rural cells compared to dense urban cells, because the lower resource utilisation leaves more scheduling potential for energy savings.

In the last two chapters (8 and 9), multi-antenna techniques related to Beamforming and MIMO, usually seen as a way to provide increased system capacity, have been addressed from an energy efficiency point of view. Concerning beamforming, reconfigurable antenna systems have been identified as a way of improving the energy efficiency by taking care on the moving of “hotspots” in the cells. For hotspot probabilities between 30% and 70%, power savings around 10-15% have been estimated. By using active antennas, adaptive beamforming shows potential for further energy efficiency improvement, with an average estimated gain of 40%.

Concerning MIMO transmissions, different MIMO modes have been investigated. First, optimal number of antennas has been considered together with the down-scaling of power for picocell BS. For low load scenario, it has been shown that important energy gains can be achieved through the use of a single antenna and time-domain duty-cycling appears much better for energy savings than frequency-domain duty-cycling. Then, an energy efficient LTE compliant precoding for multi-user MIMO has been proposed, taking into account the characteristic of the PA in the precoding design. Simulation results show around 20% reduction of the PA power consumption. Power consumption of different number of transmit antennas, MIMO schemes and resource allocation methods has then been discussed. The obtained results indicate that the 1x2 single antenna mode is suitable for low to medium network load scenario. For medium to high network loads the 2x2 MIMO is needed whereas at the high load case 4x2 MIMO is needed to guarantee the desired user throughput. Depending on the network load and antenna scheme, the DTX resource allocation can provide power saving from 5% to 40% when compared to capacity adaptation scheduling. Finally, antenna muting related to the adaptation of the number of transmit antennas has been investigated showing up to 45% energy savings for different system throughput.

The presented solutions for the energy efficient operation of radio nodes are analyzed for specific deployment scenarios, operating conditions, optimization time scale, and traffic load. They serve together with the expected energy savings for the energy performance evaluations on network level as input to the activity “Integrated Solutions”, which provides the global results of the project.

11. REFERENCES

[BoDG11] Bories, S.; Dussopt, L.; Giry, A.; Delaveaud, C.; "Duplexer-less RF Front-end for LTE Pico-Cell using a Dual Polarization Antenna," *Wireless Conference 2011 - Sustainable Wireless Technologies (European Wireless), 11th European* , vol., no., pp.1-3, 27-29 April 2011

[CST11] www.cst.com

[DeDG12] C. Desset, B. Debaillie, V. Giannini, A. Fehske, G. Auer, H. Holtkamp, W. Wajda, D. Sabella, F. Richter, M.J. Gonzalez, I. Godor, P. Skillermark, M. Olsson, M. Imran, A. Ambrosy, O. Blume, "Flexible Power Modeling of LTE base stations," submitted to IEEE Wireless Communications and Networking Conference, 2012.

[DeWV09] B. Debaillie, P. Van Wesemael, G. Vandersteen, J. Craninckx, "Calibration of Direct-Conversion Transceivers," IEEE Journal of Selected Topics in Signal Processing, Vol. 3, pp. 488-498, 2009.

[DiBa07] G. Dietl and G. Bauch, "Linear precoding in the downlink of limited feedback multiuser MIMO systems," in Proceedings of the 2007 IEEE Global Telecommunications Conference (GLOBECOM 2007), November 2007, pp. 4359-4364.

[duplex] Anatech Electronics Inc. datasheet of the duplexer component Part Number: AM1900D325 available at: http://www.amcrf.com/products/large/datasheet/AM1900D325.pdf

[EARTH-D2.2] INFSO-ICT-247733 EARTH-Report D2.2, "Definition and Parameterization of Reference Systems and Scenarios"

[EARTH-D2.3] INFSO-ICT-247733 EARTH-Report D2.3, "Energy efficiency analysis of the reference systems, areas of improvements and target breakdown"

[EARTH-D4.1] INFSO-ICT-247733 EARTH-Report D4.1, "Most Promising Tracks of Green Radio Technologies"

[EARTH-D6.2a] INFSO-ICT-247733 EARTH Deliverable 6.2a, "Draft Integrated Solutions"

[EARTH-Leaf] EARTH project Summary leaflet, https://www.ict-earth.eu/

[EbG08] W. Eberle and M. Goffioul, "A scalable low-power digital communication network architecture and an automated design path for controlling the analog/RF part of SDR transceivers," *Conference on Design, Automation and Test in Europe*, pp. 710-715, Nov. 2008.

[ENS98] ENSEMBLE. "Design Review & 1D Array Synthesis", version 5.1, User´s Guide, Ansoft Corp., January 1998.

[FeBBWP10] D. Ferling, T. Bitzer, T. Bohn, D. Wiegner, and A. Pascht, "Power Efficient Transceivers to Enable Energy-Efficient Mobile Radio Systems" Bell Labs Tech. J., 15:2 (2010) pp. 59.

[FuMo08] Jia-Shiang Fu; Mortazawi, A., "Improving Power Amplifier Efficiency and Linearity Using a Dynamically Controlled Tunable Matching Network," Microwave Theory and Techniques, IEEE Transactions on , vol.56, no.12, pp.3239-3244, Dec. 2008

[GiFM10] Gianesello, F.; Boret, S.; Martineau, B.; Durand, C.; Pilard, R.; Gloria, D.; Rauber, B.; Raynaud, C.; , "Integration of multi-standard front end modules SOCs on high resistivity SOI RF CMOS technology," Radio Frequency Integrated Circuits Symposium (RFIC), 2010 IEEE , vol., no., pp.229-232, 23-25 May 2010

[HuBM09] Huang, C.; Buisman, K.; Marchetti, M.; Nanver, L.K.; Sarubbi, F.; Popadic, M.; Scholtes, T.; Schellevis, H.; Larson, L.E.; de Vreede, L.; , "Ultra Linear Low-Loss Varactor Diode Configurations for Adaptive RF Systems,"Microwave Theory and Techniques, IEEE Transactions on , vol.57, no.1, pp.205-215, Jan. 2009

[IsKBCY08] M. F. Iskander, W. Kim, J. Bell, N. Celik, and Z. Yun, “Antenna Array Technologies for Advanced Wireless Systems”, in Modern Antenna Handbook, edited by C. A. Balanis, Wiley, Danvers, 2008.

[JeKK09] Jinseong Jeong; Kimball, D.F.; Myoungbo Kwak; Draxler, P.; Chin Hsia; Steinbeiser, C.; Landon, T.; Krutko, O.; Larson, L.E.; Asbeck, P.M.; , "High-Efficiency WCDMA Envelope Tracking Base-Station Amplifier Implemented With GaAs HVHBTs," Solid-State Circuits, IEEE Journal of , vol.44, no.10, pp.2629-2639, Oct. 2009

[KDAT10] K. Kusume, G. Dietl, T. Abe, H. Taoka, S. Nagata, “System Level Performance of Downlink MU-MIMO Transmission for 3GPP LTE-Advanced,” in Proceedings of the 2010 IEEE 71st Vehicular Technology Conference (VTC 2010-Spring), May, 2010.

[Mont47] C. G. Montgomery, Technique of Microwave Measurements, McGraw-Hill, New York, 1947.

[NeLL06] Neo, W.C.E.; Yu Lin; Xiao-dong Liu; de Vreede, L.C.N.; Larson, L.E.; Spirito, M.; Pelk, M.J.; Buisman, K.; Akhnoukh, A.; Anton de Graauw; Nanver, L.K.; , "Adaptive Multi-Band Multi-Mode Power Amplifier Using Integrated Varactor-Based Tunable Matching Networks," Solid-State Circuits, IEEE Journal of , vol.41, no.9, pp.2166-2176, Sept. 2006

[PeNG08] Pelk, M.J.; Neo, W.C.; Gajadharsing, J.R.; Pengelly, R.S.; de Vreede, L.C.N.; , "A High-Efficiency 100-W GaN Three-Way Doherty Amplifier for Base-Station Applications," Microwave Theory and Techniques, IEEE Transactions on , vol.56, no.7, pp.1582-1591, July 2008

[QuPM09] Qureshi, J.H.; Pelk, M.J.; Marchetti, M.; Neo, W.C.E.; Gajadharsing, J.R.; van der Heijden, M.P.; de Vreede, L.C.N.; , "A 90-W Peak Power GaN Outphasing Amplifier With Optimum Input Signal Conditioning," Microwave Theory and Techniques, IEEE Transactions on , vol.57, no.8, pp.1925-1935, Aug. 2009

[SeTB09] S. Sesia, I. Toufik, and M. Baker, LTE, the UMTS Long Term Evolution: From Theory to Practice. John Wiley & Sons, 2009, pp. 262-263.

[Soi09] « Why SOI, why now? » in SOI Ind. Consort., 2009. [Online]. Available: http://www.soiconsortium.org/about-soi/why-soi.php

[TrBT07] M. Trivellato, F. Boccardi, and F. Tosato, “User selection schemes for MIMO broadcast channels with limited feedback,” in Proceedings of the 2007 IEEE 65th Vehicular Technology Conference (VTC 2007-Spring), April 2007, pp. 2089-2093.